STRESS/STRAIN RATIO EFFECTS ON FATIGUE RESPONSE OF A SCS-6/Ti-15-3 METAL MATRIX COMPOSITE AT ELEVATED TEMPERATURE

THESIS

Sean C. Jackson
Captain, USAF

AFIT/GAE/ENY/95D-14

DEPARTMENT OF THE AIR FORCE
AIR UNIVERSITY
AIR FORCE INSTITUTE OF TECHNOLOGY

Wright-Patterson Air Force Base, Ohio

AFIT/GAE/ENY/95D-14

STRESS/STRAIN RATIO EFFECTS ON FATIGUE RESPONSE OF A SCS-6/Ti-15-3 METAL MATRIX COMPOSITE AT ELEVATED TEMPERATURE

THESIS

Sean C. Jackson
Captain, USAF

AFIT/GAE/ENY/95D-14

AFIT/GAE/ENY/95D-14

STRESS/STRAIN RATIO EFFECTS ON FATIGUE RESPONSE OF A SCS-6/Ti-15-3 METAL MATRIX COMPOSITE AT ELEVATED TEMPERATURE

THESIS

Presented to the Faculty of the Graduate School of Engineering

of the Air Force Institute of Technology

Air University

In Partial Fulfillment of the

Requirements for the Degree in Aeronautical Engineering

Sean C. Jackson, B.S.A.E.

Captain, USAF

December 1995

Table of Contents

List of Figures

List of Tables

Table Page

Abstract

This study investigated the effects of stress/strain ratio and the loading control mode on the fatigue life and damage mechanisms of a unidirectional metal matrix composite (MMC) laminate. Fatigue tests were conducted using both the load control and strain control modes at 427°C. The trends in stress/strain response, stress vs. cycles to failure (N), strain vs. N, and modulus vs. N were measured for each case. A detailed post-mortem microscopic examination was conducted to identify damage mechanisms and failure modes. Further fatigue life comparisons were made to show the relationship between control mode and stress/strain ratio.

Strain control tests were performed for three different strain ratios ($R_\varepsilon = \varepsilon_{min}/\varepsilon_{max}$): -1, 0 and 0.5. Fatigue life comparisons showed that on a maximum strain basis, as R_ε is increased the fatigue life increases, while on a strain range basis the fatigue life decreases as R_ε is increased. Similar damage mechanisms were found between the tests conducted at $R_\varepsilon = -1$ and $R_\varepsilon = 0$ for a given maximum strain level. However, a comparison between tests conducted at $R_\varepsilon = 0$ and $R_\varepsilon = 0.5$ revealed increased matrix damage for tests conducted at $R_\varepsilon = 0.5$ at a given maximum strain level.

Load control tests were performed at a stress ratio (R_σ) of 0.5. This was combined with data of tests conducted at $R_\sigma = 0.1$ and $R_\sigma = -1$ from previous studies to make fatigue life and damage mechanism comparisons between load and strain control modes. When compared on a strain range basis, the control mode had no effect on fatigue life and

damage mechanisms at R = 0 and R = -1. However, at R = 0.5 the fatigue life and damage mechanisms were different for the two control modes. Strain control tests revealed more matrix damage and an increase in fatigue life at equivalent strain ranges in comparison to its counterpart from the load control mode. This was a result of matrix creep in the load control tests.

Additional tests were also completed at $R_\varepsilon = 0$ under the strain control mode for the cross-ply MMC laminate. These tests, coupled with the previously available studies, allowed for a fatigue life comparison between the cross-ply and unidirectional lay-ups under both the load and strain control mode at different stress/strain ratios. These comparisons showed no difference in the fatigue life when comparing tests conducted under the strain control mode when compared on a strain range basis at a strain ratio. The same trend was found for load control tests when compared on the basis of stress in the 0° plies for both laminates, at a stress ratio.

STRESS/STRAIN RATIO EFFECTS ON FATIGUE RESPONSE OF A SCS-6/Ti-15-3 METAL MATRIX COMPOSITE AT ELEVATED TEMPERATURE

1. Introduction

Recent advances in jet engine and aircraft technology have created the need for new, lightweight, high strength, temperature resistant materials. Programs such as the National Aerospace Plane (NASP) and High Temperature Engine Technology Program (HITEMP) require lightweight materials with good mechanical properties at high temperatures. Metal matrix composites (MMCs) use high strength, lightweight metal alloys combined with high strength ceramic fibers to create a high strength, lightweight, heat resistant material which meets these requirements.

Titanium based MMCs provide excellent high temperature characteristics along with high strength, high modulus, toughness and impact properties [29:3]; however, their composition leads to some unique damage mechanisms. First, after initial processing, the mismatch in the coefficient of thermal expansion (CTE) between the matrix and the fibers creates large residual stresses when the MMC is cooled. These residual stresses can result in damage to the as-received specimens and fatigue at the microscopic level during temperature changes.

The second area of concern is the fiber/matrix interphase region. The interphase region is located between the fiber and matrix and is created by the high reactivity of the titanium matrix with the carbon fiber. The properties of the interphase region are difficult

to predict and it is unstable when subjected to fatigue [24]. These unique characteristics of MMCs makes analytical modeling difficult and create the need for extensive fatigue testing to fully characterize the failure and damage mechanisms.

MMCs have the potential to be used in a number of different aerospace applications. For this reason the behavior of the material in a number of different environments and loading scenarios must be characterized. A significant amount of research has been conducted under monotonic, tension-tension and tension-compression fatigue loading conditions [1,5,8,12,13,14,15,21,24]. Monotonic tension tests revealed that specimen damage was dominated by matrix plasticity in the form of slip bands in the non-linear region of the stress-strain curve [14]. Testing of several different lay-ups also revealed that off-axis plies reduce the strength of the MMC [15]. Tension-tension and tension-compression cycling tests have shown that the fatigue life and damage mechanisms of MMCs are stress/strain dependent [1,5,12,13,16]. Previous studies have shown that fatigue life decreases as the maximum stress/strain increases which is consistent with conventional metal alloys. In high stress/strain regions failure is generally caused by fiber failure, while at lower stress/strain levels matrix cracking is the dominant mode. The fiber/matrix interphase region has also been shown to be a prime crack initiation site [17].

Even though a number of different fatigue studies have been performed for titanium MMCs, there are still areas that need to be explored. The majority of previous studies have been conducted under the load control mode. Most materials used in engineering applications are subjected to the strain control mode so the MMC's characterization in this area must be fully understood. Characterization of the MMC

under the strain control mode will also provide a basis for comparison with previous studies that have widely used the load control mode..

Previous studies have been confined to stress/strain ratios (R_σ or R_ε) of -1 or 0. Many components used in aerospace applications are subjected to high load/small amplitude loading histories. Figure 1 depicts a typical load profile for an aircraft turbine disk and shows that it is experiencing a significant amount of high load/small amplitude fatigue loading [19]. Therefore, the fatigue response of MMCs at high stress/strain ratios is also needed along with damage and failure mechanisms.

The purpose of this study was to investigate the fatigue behavior of a unidirectional MMC laminate at different stress/strain ratios under strain and load control at 427°C. The MMC was SCS-6/Ti-15-3 which consisted of a titanium alloy matrix,

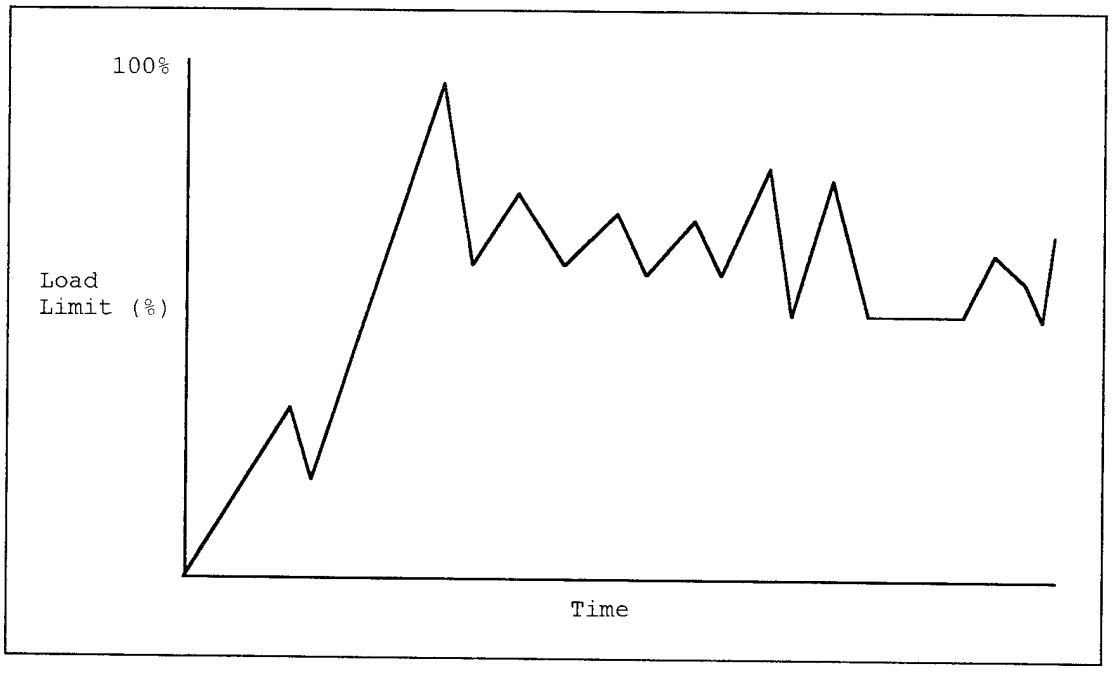

Figure 1. Turbine Blade Load History [19]

Ti-15-3, reinforced with silicon carbide fibers, SCS-6. For this purpose, several strain control tests at strain ratios of -1, 0 and 0.5 were performed. All strain control tests were run at a strain rate of 0.2%/s. Figures 2 - 4 show a graphical depiction of these three different loading conditions used for this study. These tests allowed for a comparison between fatigue life and damage mechanisms between different strain ratios. Previous studies have investigated the fatigue response of the SCS-6/Ti-15-3 MMC under the load control mode at stress ratios of -1 and 0.1 [8,12]; however, the fatigue response under this mode at $R_\sigma = 0.5$ is not available. Therefore, load control tests were also performed at a stress ratio of 0.5, at a frequency of 1 Hz, to cover a broad range of investigation. Fatigue life, failure mode and damage mechanisms were compared between the load and strain control modes.

Overall, ten tests were performed under the strain control mode and four under the load control mode for the unidirectional lay-up. Three additional strain control tests were performed at $R_\varepsilon = 0$ for a cross-ply, $[0/90]_{2S}$, lay-up. The purpose of these tests was to investigate the difference in fatigue behavior between the unidirectional and cross-ply lay-ups under varying stress and strain ratio conditions.

Fatigue life diagrams, i.e. ε-N and S-N curves, were established to compare the fatigue lives among control modes and stress/strain ratios. Fractography and microscopy were performed on selected specimens to reveal the damage and failure mechanisms at varying stress/strain levels. The fractography and microscopy were combined with the variation of stress/strain and moduli during cycling to establish the overall response

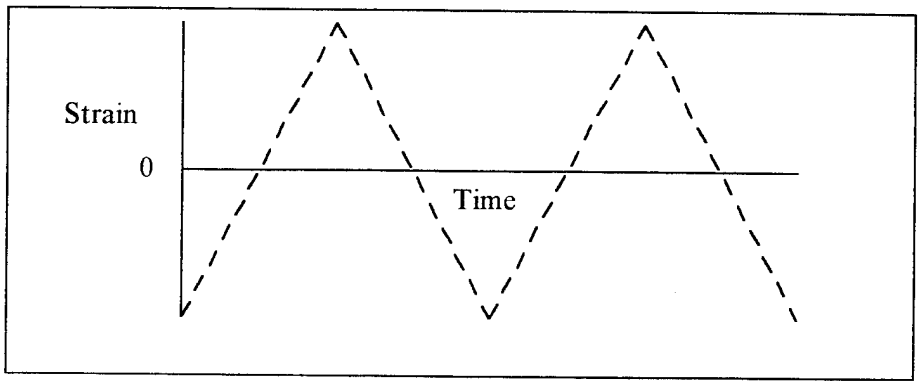

Figure 2. Tension-Compression Load History, $R_\varepsilon = -1$

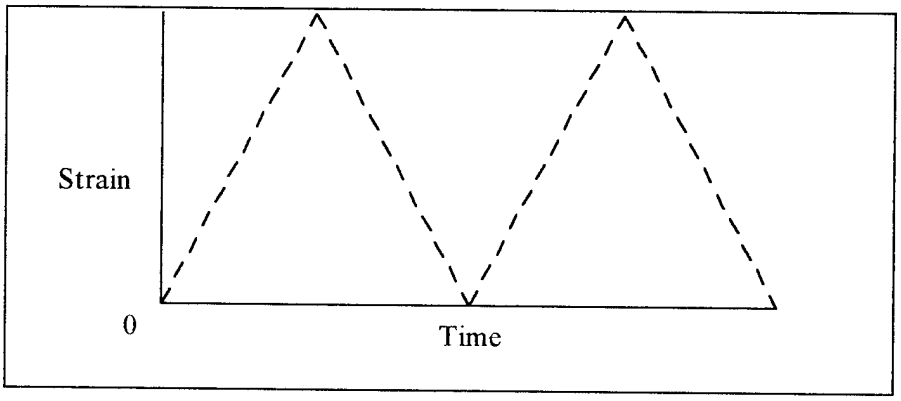

Figure 3. Tension-Tension Load History, $R_\varepsilon = 0$

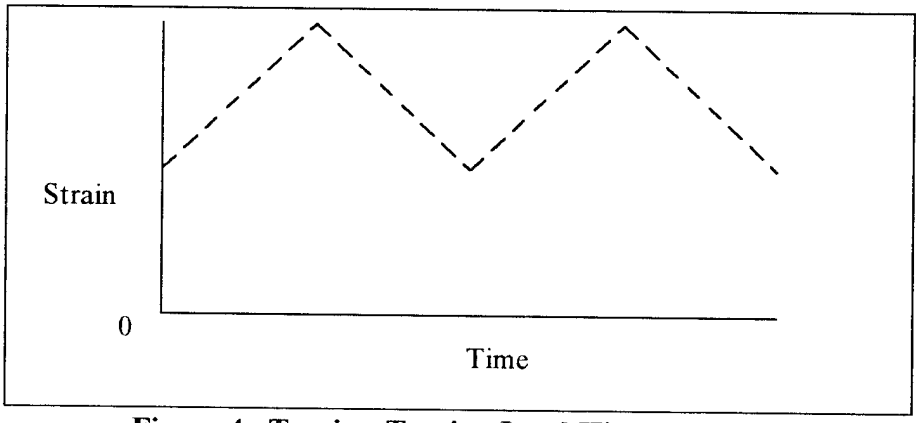

Figure 4. Tension-Tension Load History, $R_\varepsilon = 0.5$

between the damage and failure mechanisms at varying stress/strain ratios and differing control modes.

2. Background

The purpose of this chapter is to summarize previous studies that has been conducted on the SCS-6/Ti-15-3 MMC which was used in this study. Furthermore, this summary is divided between tension-tension and tension-compression cycling under load and strain control modes. Emphasis is placed on the fatigue life and damage mechanisms that were obtained in the previous studies. A summary of the trends in fatigue life and damage mechanisms is also presented. Although there have been several studies conducted, only the ones relevant to this study will be presented.

2.1 Tension-Tension Cycling

2.1.1 Load Control Mode

Johnson and Pollock investigated the tension-tension cycling behavior of three different lay-ups of the SCS-6/Ti-15-3 MMC at 650°C [20]. The load control tests were performed on a $[0]_8$, $[0/90]_{2S}$ and $[0/+45/-45/90]_S$ MMC using a stress ratio (R_σ) of 0.1. They concluded that the fatigue life of the MMC was governed by the cyclic stress in the 0° fibers. A plot of the 0° fiber stress versus fatigue life fell within a narrow band for all of the lay-ups tested. Fractography revealed that for high stress levels, damage was limited to fiber breakage and minimal matrix cracking. However, as the maximum stress was reduced matrix cracking was more extensive and little fiber fracture was observed. This trend was seen in all of the lay-ups tested.

Majumdar and Newaz investigated the tension-tension fatigue behavior of a unidirectional SCS-6/Ti-15-3 MMC at room temperature (RT) and elevated temperature (ET) (538°C) [17]. Even though the tests were performed under the load control mode, the strain range remained constant for nearly 90% of the fatigue life. This allowed strain range to be used as a correlating parameter in developing the fatigue life diagram.

At high strain ranges both room and elevated temperature tests exhibited fiber dominated failure mechanisms with no matrix cracking [17]. However, at room temperature extensive fiber-matrix debonding, which resulted in damage to the fibers, was observed. Fiber/matrix debonding can be caused by large interfacial shear stresses between the matrix and the fiber caused by the loading and unloading of the specimen at high strain levels. At elevated temperature, stress relaxation in the matrix due to creep led to a transfer of load to the fibers and eventual fracture.

At lower and intermediate strain ranges matrix cracking was found to be the dominant damage mechanism for both room and elevated temperature testing [17]. Matrix cracks generally initiated at Molyweave-ribbon and fiber/matrix interface regions. This molyweave used to hold the fibers in place during material processing acts as a precipitate or inclusion which is a prime crack initiation site. The fiber-matrix interface region is relatively weak when compared to the fiber and matrix, especially if debonding has occurred. This debonded region is also a prime crack initiation site. It was also observed that at lower and intermediate strain ranges at room temperature, the MMC had the same fatigue life to that of the matrix material alone, while at high strain ranges the MMC had a shorter life than the matrix material. At elevated temperature the MMC life

was significantly shorter than the matrix life. Figure 5 shows the three regions of the S-N diagram that Majumdar and Newaz proposed based on failure mechanisms [17]. The three regions were: Region 1 (fiber dominated), Region 2 (matrix dominated), Region 3 (fatigue limit).

Portner investigated the tension-tension fatigue behavior of a cross-ply SCS-6/Ti-15-3 MMC at 427°C [21]. All tests were conducted using a stress ratio of 0.1. Two different frequencies were used (0.02 and 2 Hz) to see if fatigue life and damage mechanisms were affected by frequency. Tests results showed that the low frequency tests had shorter fatigue lives than the high frequency tests. When compared on a time scale the opposite trend was found. The damage mechanisms for the two frequencies were also

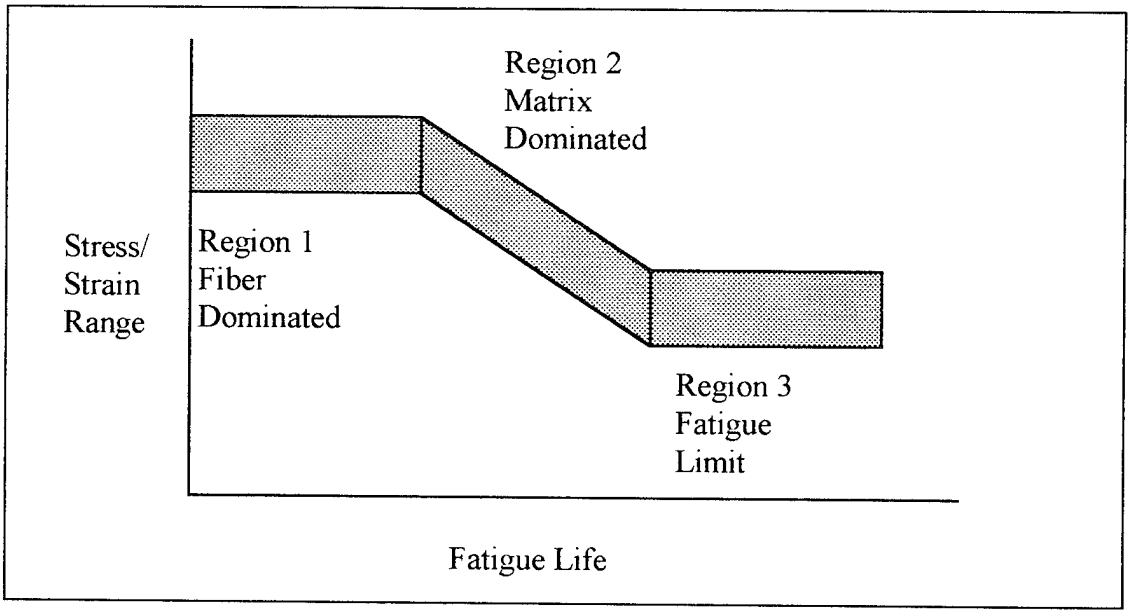

Figure 5. Three Regions on Fatigue Life Diagram [17]

found to be different. The low frequency tests were dominated by fiber failure while the high frequency tests showed more matrix dominated failure.

2.1.2 Strain Control Mode

Sanders conducted a fatigue study of the 0° and 90° lamina at elevated temperature (427°C) under the strain control mode [24]. Under the strain control mode, relaxation occurs which can cause the specimen to go into compression, leading to buckling of the thin MMC specimens available for testing. To prevent buckling, Sanders developed a hybrid strain control mode which increased the minimum strain whenever the minimum stress was negative. Microscopy and analytical modeling were used to characterize the damage progression and mechanisms.

The fatigue response of the 90° lay-up was dominated by the fiber-matrix interface damage [24]. The results were plotted on a ε-N diagram which was partitioned into four regions based on damage mechanism. Region I included the specimens which had a maximum strain greater than 0.35%. This region was dominated by matrix cracks. Region IIa included those specimens where the maximum strain was between 0.23% and 0.35%. This region was dominated by small matrix cracks, along with progression of the fiber-matrix interface damage. Region IIb included those specimens where the maximum strain was less than 0.23% and the failure was dominated by the fiber-matrix interface damage. Region III was the fatigue limit of the material where no fiber-matrix interface damage occurred and it is defined where the maximum strain is less than 0.05%.

The fatigue response of the 0° laminate comprised several different failure mechanisms and each of these was assigned a region on the ε-N diagram, which is illustrated in Figure 6 [24]. Region I was dominated by fiber fracture which occurs when the maximum strain is greater than 0.73%. Region II was dominated by matrix cracking and occurs when the maximum strain is between 0.73% and 0.3%. Region III was defined as the fatigue limit of the lamina and occurred when the maximum strain was below 0.3%. It is not shown in Figure 6. The limits of these regions are not well defined which results in many mixed mode failures in the boundary between two regions.

Figure 6 also illustrates changes in stress and modulus and their interrelationship with the damage mechanisms in the laminate during different portions of the fatigue life [24]. The damage and deformation mechanisms were divided into three stages.

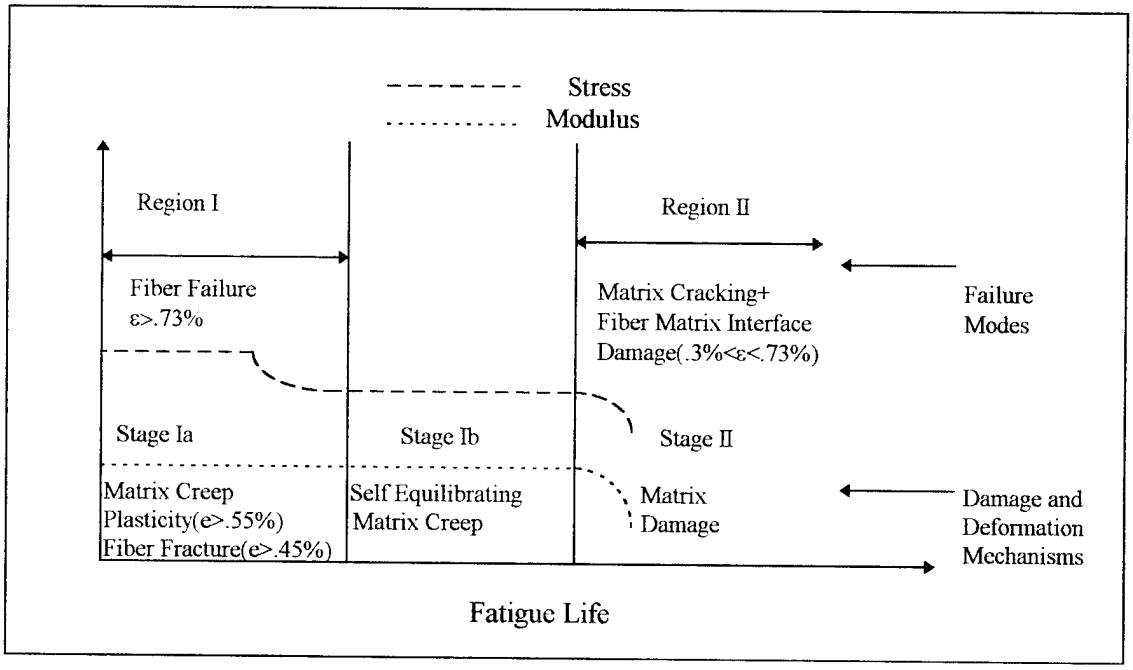

Figure 6. Damage and Failure Mechanism Diagram of 0° Laminate [24]

Stage Ia is dominated by matrix creep, plasticity and fiber fracture. Stage 1b consists of self equilibrating creep, along with an incubation period for cracks. Stage II consists of matrix damage.

2.2 Tension-Compression Cycling

2.2.1 Load Control Mode

Boyum conducted the fully-reversed load control tests of a cross-ply SCS-6/Ti-15-3 at 427°C [1]. Buckling was prevented by the use of an anti-buckling guide, along with specially designed dogbone specimens. Boyum divided the S-N diagram for the cross-ply lay-up under the load control mode into four regions based on failure mechanisms: fiber dominated (Region I), matrix and fiber failure (Region 2a), matrix cracking (Region 2b) and the fatigue limit of matrix (Region 3). A mixed mode region (2a) was added to account for the earlier initiation of matrix cracks caused by the presence of the 90° fibers. This is illustrated in Figure 7.

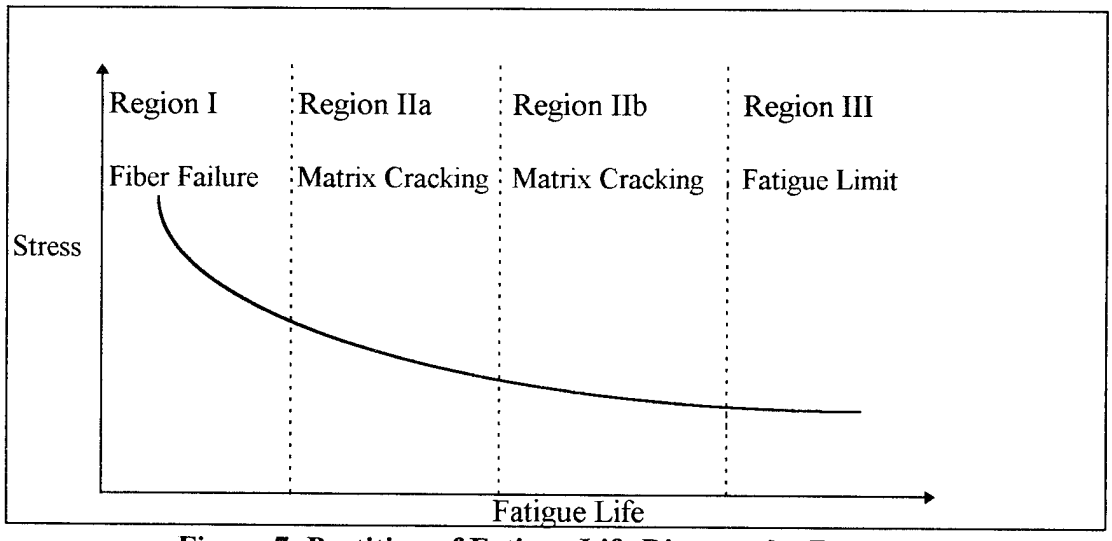

Figure 7. Partition of Fatigue Life Diagram by Boyum [1]

Boyum also compared the fatigue life for both tension-tension and tension-compression loading histories [1]. She found that the two different stress ratios resulted in distinct and separate curves on the S-N diagram. She also discovered that on a maximum stress basis the fully-reversed specimens had shorter fatigue lives than that of the tension-tension specimens. She concluded that this was due to the added damage and plasticity sites found only in the tension-compression specimens. The same specimens, when compared on a stress range basis, yielded opposite results. On a stress range basis the tension-tension specimens had shorter fatigue lives than the tension-compression ones. She hypothesized that fatigue life of the tension-tension specimens were shorter because the mean stress was greater than zero while the tension-compression specimens have zero mean stress.

Kraabel performed the fully reversed load control tests of the unidirectional SCS-6/Ti-15-3 at 427°C [12]. A buckling guide similar to that used by Boyum was used [1]. Kraabel partitioned his results into three groups based on the damage mechanisms. Group 1 was dominated by short matrix cracks which bridged only a few fibers and contained those specimens tested at a maximum stress above 675 MPa. At these higher stress levels a single crack becomes dominate and propagates very rapidly through the matrix, causing fiber failure and eventually specimen failure. Group 2 was dominated by matrix cracks with extensive fiber bridging and comprised specimens tested at a maximum stress between 425 MPa and 625 MPa. Group 3 was comprised of those specimens that were tested below the fatigue limit of the lamina.

The fatigue lives for the specimens were plotted on a S-N diagram using both maximum stress and strain or stress and strain range [12]. Comparison of tension-compression and tension-tension fatigue lives yielded two distinct regions on the S-N diagram. Similar to the cross-ply lay-up tested by Boyum [1], the fatigue life of the unidirectional lamina was greater for tension-tension versus tension-compression on a maximum stress or strain basis. However, on stress or strain range basis, the tension-compression specimens had a longer life than tension-tension. Kraabel hypothesized that the fatigue limit of the unidirectional lamina may be governed by strain range since both the tension-tension and tension-compression S-N curves converge at a strain range of 0.3%.

2.2.2 Strain Control Mode

Dennis conducted the fully reversed strain control tests of a cross-ply SCS-6/Ti-15-3 at 427°C [5]. Microscopic analysis revealed matrix cracking below a maximum strain of 0.73%. As the maximum strain was decreased the amount of matrix cracking increased leading to matrix dominated failure modes below a maximum strain of 0.5%. As in other studies [1,12,17,24], the ε-N diagram was divided into three regions based on the observed damage mechanisms. Region I was fiber dominated failure which occurred when maximum strains were above 0.75%. Region IIa consisted of fiber fracture along with matrix cracking which occurred at maximum strains between 0.45% and 0.75%. Region IIb was matrix dominated failure and occurred in specimens tested at maximum strains

between 0.05% and 0.3%. Region III was defined to be the fatigue limit of the material as was estimated to be below a maximum strain of 0.05%.

Dennis also compared the fatigue life under tension-compression loadings for the load and strain control modes [5]. He found that on a strain range basis the fatigue lives for both loadings was within a narrow band in the matrix dominated failure regions. He concluded that in the fiber dominated failure region matrix creep and plasticity may reduce the fatigue life under the load control mode relative to that under the strain control mode.

2.3 Summary of Findings from Previous Investigations

The previous research has highlighted several significant trends concerning the characterization of the SCS-6/Ti-15-3 MMC. The damage mechanisms for all types of fatigue tests are dependent on the stress/strain level. High stress/strain levels result in fiber fracture with matrix cracking occurring at low stress/strain levels. It has been shown that damage often initiates in the fiber/matrix interphase region. The relative weakness of this region compared to that of the fiber and matrix makes it a prime crack initiation site. The specimen edges, along with molyweave sites are other areas where damage originates. Figure 8 shows a graphical representation of the different types of damage mechanisms observed in MMC's.

Using the observed damage mechanisms shown in Figure 8, several previous investigations [1,5,12,17,24] have partitioned the S-N diagram into three regions:

- Region I: fiber dominated failure
- Region II: matrix dominated failure
- Region III: fatigue limit of composite

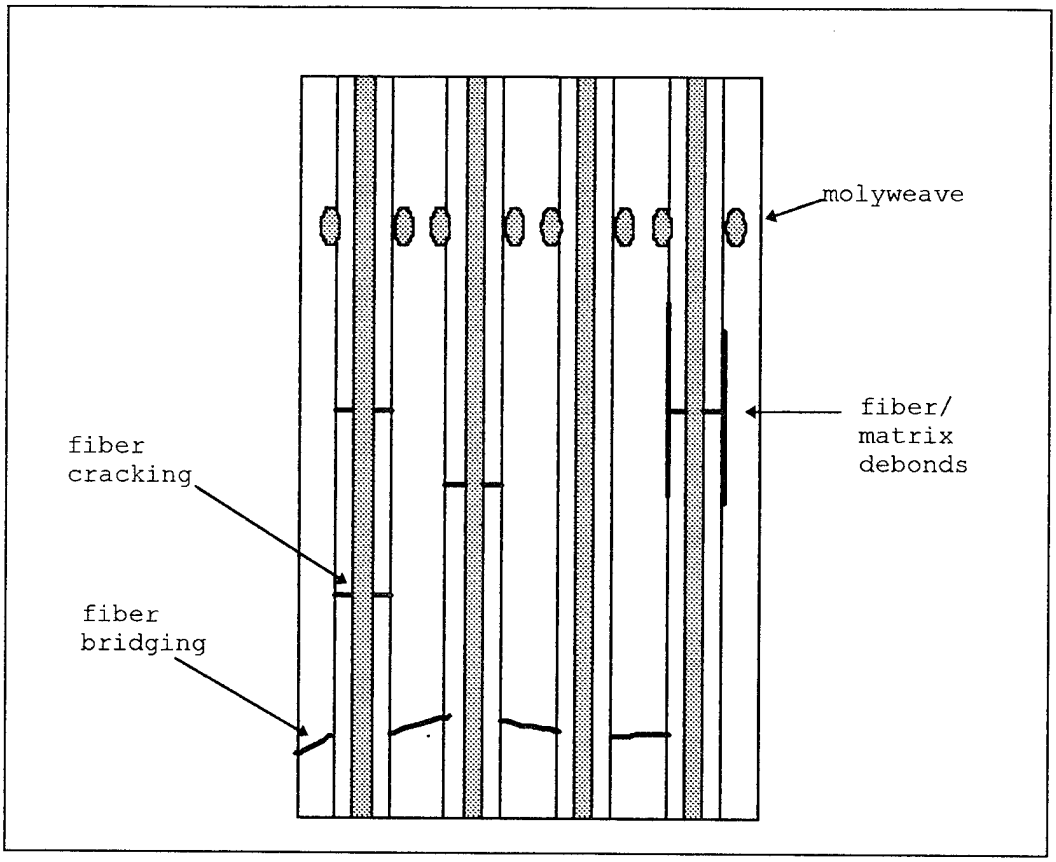

Figure 8. Fiber/Matrix Damage Mechanisms

Furthermore, several studies have divided Region II into two regions to show that at higher stress/strain levels a combination of fiber and matrix damage is present [1,5,12].

Some recent studies have attempted to compare the fatigue lives for different stress/strain ratios for the unidirectional and cross-ply lay-ups [1,5,12]. These results show that each of the tests conducted at different stress/strain ratios comprise distinct regions of the S-N diagram and do not collapse onto each other. However, these tests have been limited to two stress/strain ratios of -1 and 0, and no comprehensive study has been

performed for the unidirectional lay-up that investigates the effects of stress/strain ratio and control mode effects on fatigue life and damage mechanisms.

The purpose of this investigation was to investigate the stress/strain ratio effects on a unidirectional, SCS-6/Ti-15-3, lay-up under both the load and strain control modes. Fatigue tests were conducted to establish a fatigue life comparison among the different stress/strain ratios and control modes. Microscopy was performed on selected specimens to analyze the various damage and failure mechanisms. This information was then used to establish the comprehensive interrelationship between fatigue life and damage and failure mechanisms at different stress/strain ratios and for two control modes.

3. Experiments

The purpose of this chapter is to give a detailed description of the MMC, test equipment and procedures that were used in this study. The MMC composition, along with the specimen preparation steps are described. The test equipment, including the AFIT buckling guide, are also discussed. Finally, the experimental procedures that are required to perform tension-compression and tension-tension testing along with the post-test specimen preparation are described.

3.1 Material Description

An 8-ply unidirectional, $[0]_8$, and a cross-ply, $[0/90]_{2S}$, lay-up were investigated in this study. A schematic of the unidirectional and cross-ply lay-ups are shown in Figures 9 and 10. The MMC was composed of silicon carbide fibers (SCS-6) with a titanium metal matrix (Ti-15-3). The exact composition of the matrix material is: Ti-15V-3Cr-3Al-3Sn. The fibers have a nominal diameter of 0.142 mm and are composed of an inner core enclosed in bulk SiC with alternating layers of silicon and carbon. Table 1 lists the fiber and matrix properties. The fiber volume fraction for the plate was 36%.

Table 1. Fiber and Matrix Properties

	Fiber	Matrix (RT)	Matrix (427°C)
Modulus (GPa)	440	90	80
α (10^{-6} mm/mm/C)	4.86	10	10
ν	0.25	0.36	0.36
σ_{vs} (MPa)	--	800	525

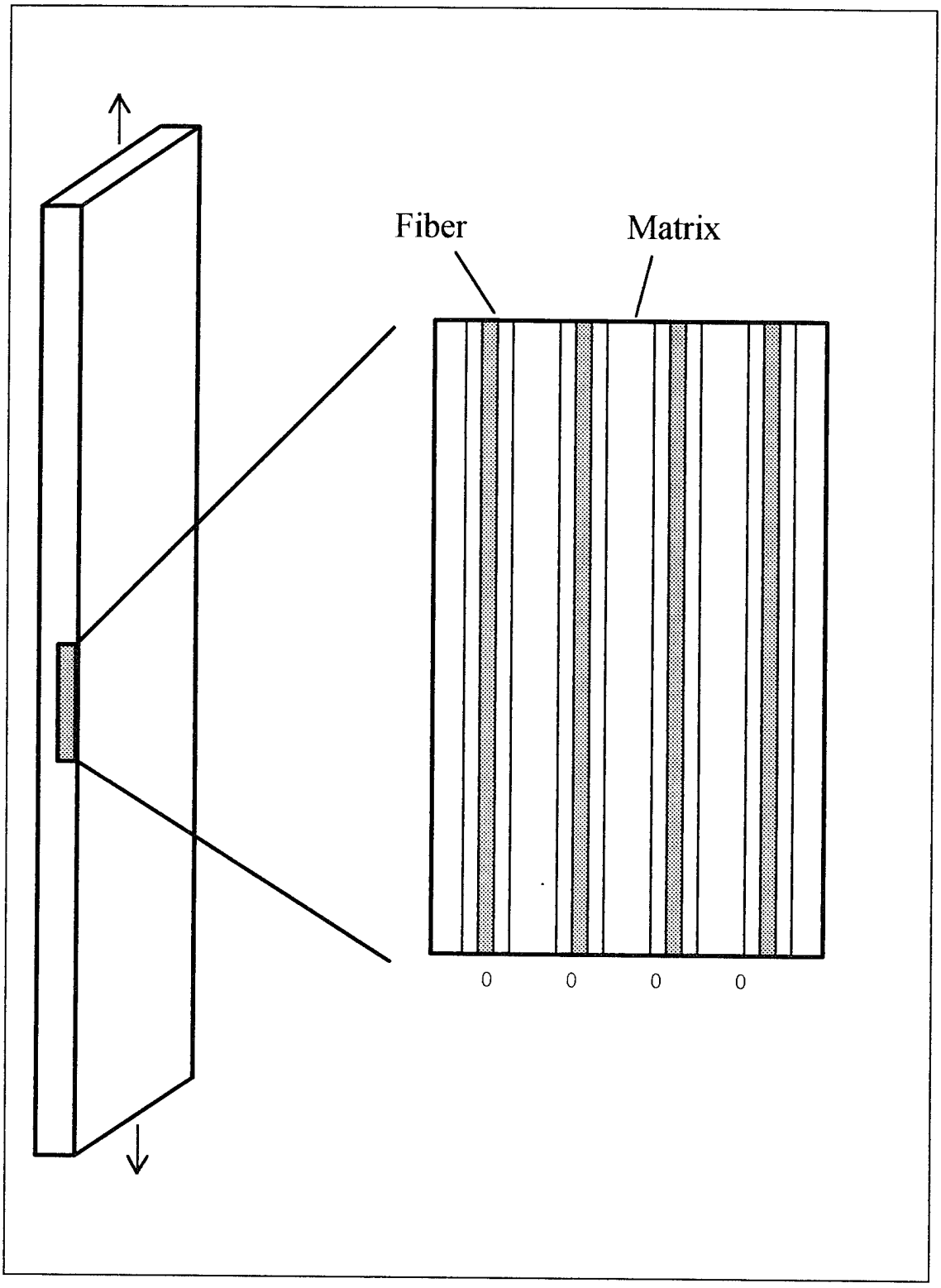

Figure 9. Unidirectional Lay-up

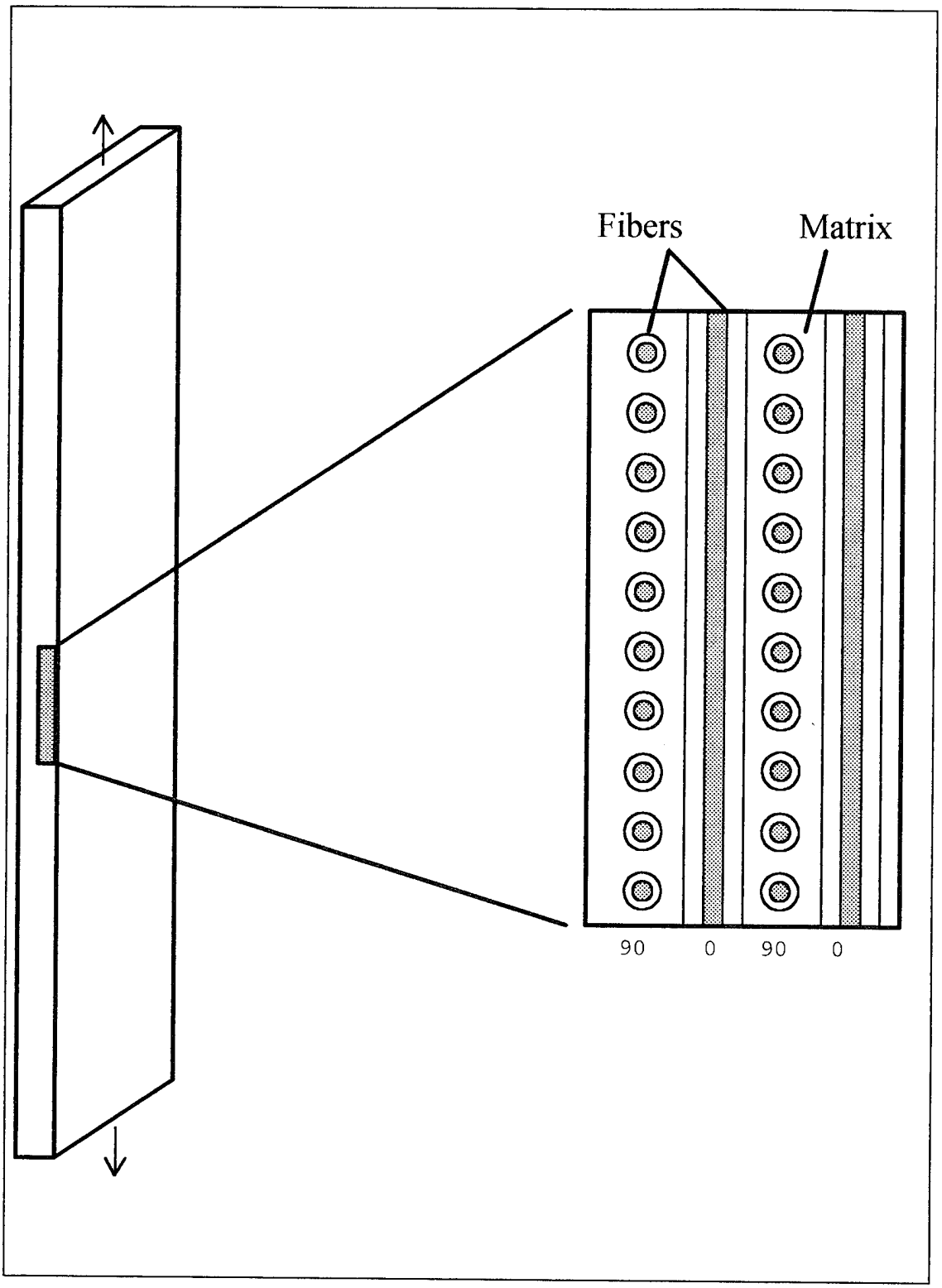

Figure 10. Cross-Ply Lay-up

The 305 mm x 305 mm x 1.55 mm plate employed in this study was manufactured by Textron Specialty Materials Incorporated using a Hot ISO static Pressing (HIP) method. Each plate is manufactured by arranging the silicon carbide fiber mats which are held in place by a molybendum woven weave, along with alternating layers of titanium foil matrix. This process is known as the foil fiber foil method. The exact time-temperature-pressure profile used to consolidate the plates is proprietary.

3.2 Specimen Design and Preparation

Previous studies on the unidirectional lay-up have shown that the dogbone specimen shape helps to precipitate failure in the gage section for tension-tension as well as tension-compression testing [12,17]. For that reason, dogbone specimens were used in all tests conducted for this study.

The goal in designing a dogbone specimen is to reduce the cross-sectional area in the gage section of the specimen while keeping the shoulder radius as large as possible. A large shoulder radius minimizes the shear stresses in the shoulder region and therefore reduces the risk of failure in that region [17:5]. Several recent studies have used dogbone specimens with excellent results [1,4,12]. A similar geometry was used in this study.

Figure 11 shows the dogbone specimen design. The dogbone specimens were made by first cutting rectangular strips 5.37 cm long by 1.27 cm wide using a diamond encrusted blade. Each specimen was individually placed on a computer controlled milling machine where the specimens were machined to the exact specifications. The dogbone design for the $[0/90]_{2S}$ lay-up was the same except the width in the heat zone was

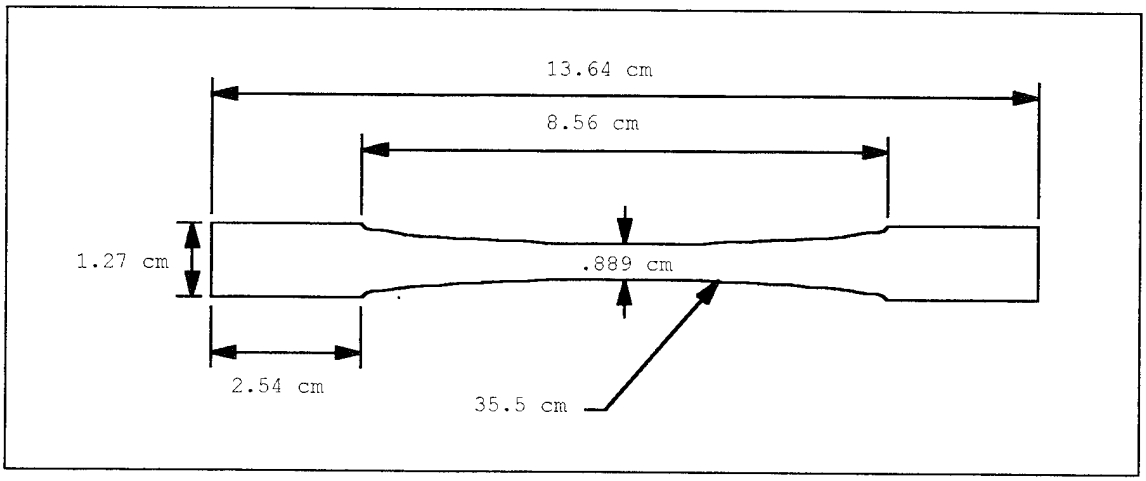

Figure 11. Dogbone Specimen Geometry

reduced to 0.51 cm to accommodate a different buckling guide.

Mall and Schubbe conducted thermomechanical testing of a $[0/90]_{2S}$, SCS-6/Ti-15-3 MMC from 149°C to 427°C [27]. The specimens were not heat treated and showed as much as a 20% increase in the modulus during fatigue testing. This change in modulus has been observed in other studies of the SCS-6/Ti-15-3 MMC [21]. In an attempt to minimize this change in modulus during fatigue testing, several researchers have heat treated the MMC prior to testing. A commonly used heat-treatment for this material is to wrap the specimens in tantalum foil and heat treat for 24 hours at 700°C in an argon atmosphere. Lerch and Saltzman showed that this heat treatment stabilizes the microstructure without significantly altering the mechanical response of the specimen [15].

The final step in specimen preparation was to debur the specimen edges. The purpose of this step is to remove any imperfections induced during the machining process. Any imperfections can lead to stress concentrations in that area and cause premature

failure of the specimen. The specimens were deburred using three different grades of grit sandpaper. Each edge of the specimen was sanded with 180, 240 and 400 grit sandpaper successively until the edges were flat and all visible flaws were removed.

3.3 Buckling Guide Description

The need to perform compression testing of the available 8 ply MMC led to the design of an anti-buckling guide. The purpose of the guide is to allow the specimen to experience compressive stresses without excessive buckling. Boyum developed the original AFIT buckling guide which was successful for fatigue tests of thin MMC laminates [1]. This study used a modified buckling guide which was first used by Kraabel and Dennis [5,12]. Figure 12 shows the buckling guide design used in this study. It consisted of two pieces: a top main piece and the fork slider. The specimen is placed in the buckling guide and the buckling guide is clamped to the specimen by tightening the screws on either end of the guide. A small gap is left between the fork slider and the top piece to allow for specimen displacement. Before every test a small amount of graphite powder was placed on the fork slider to allow for frictionless displacement.

3.4 Test Equipment

Figure 13 shows the test setup. All tests were performed on an MTS 22-kip screw-driven load cell with two water-cooled hydraulic grips. Strain was measured using a quartz rod extensiometer (MTS model 632.50004) with a 1.23 cm gage length. Two air

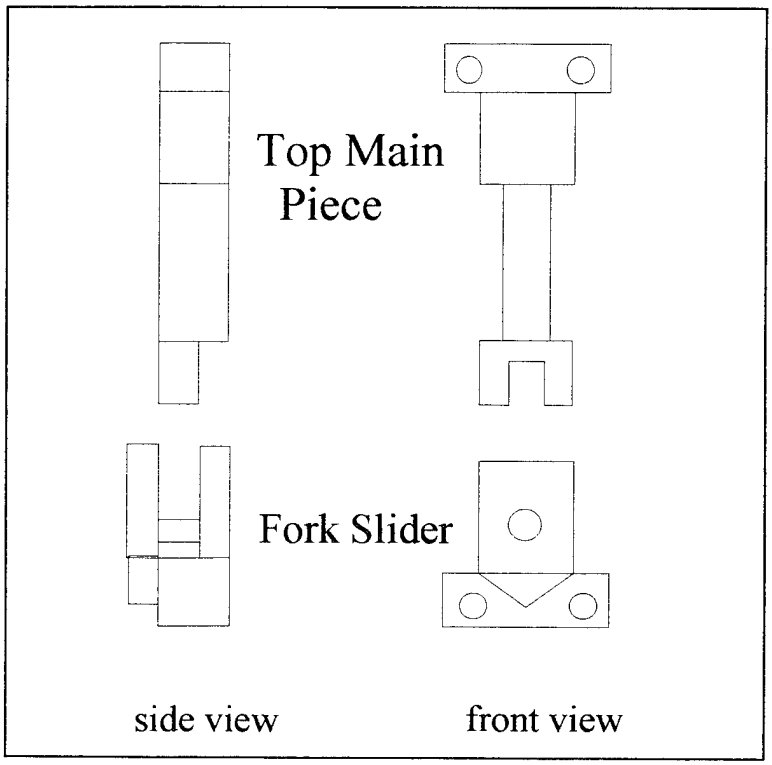

Figure 12. AFIT Buckling Guide

and water cooled lamps were used to heat the specimens. Each lamp consisted of two 1 kW, tungsten filament bulbs. The lamps were controlled by an independent Microcon controller. The Microcon receives feedback from each of the two Chromel-Alumel (type K) thermocouples spot welded on either side of the buckling guide. Finally, data acquisition was performed on a 486DX2-50 Mhz PC computer combined with an analog to digital converter board.

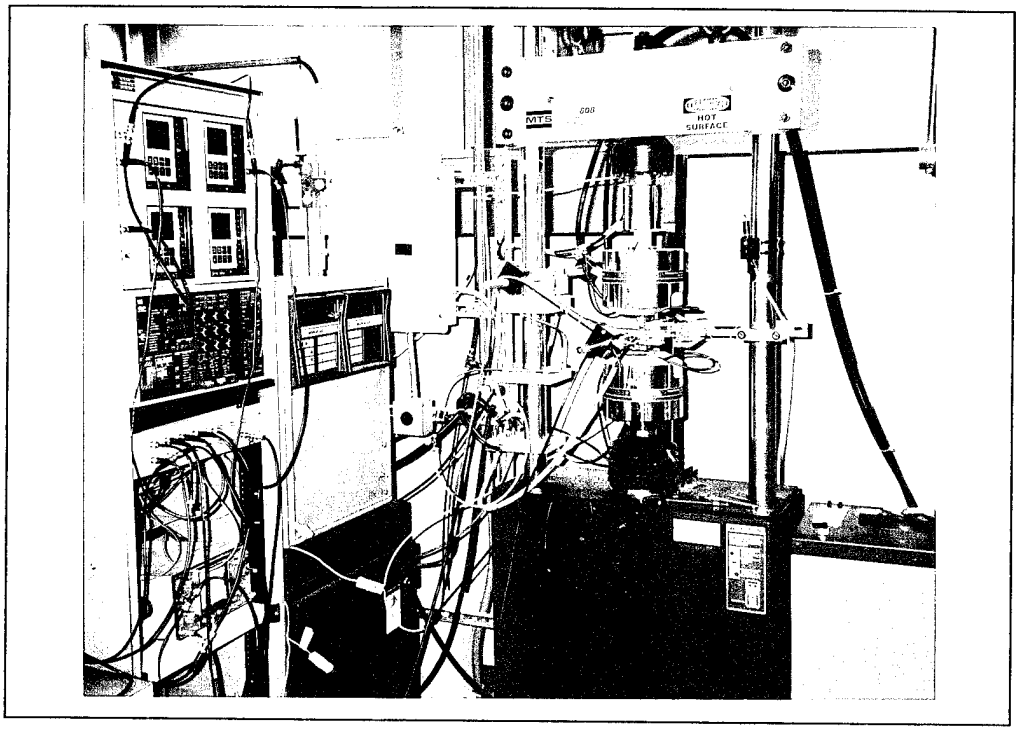

Figure 13. Test Equipment

3.5 Experimental Procedures

Table 2 shows the test matrix for this study. For the tests conducted at $R_\varepsilon = 0$ and $R_\varepsilon = -1$ the first step was to place the specimen in the buckling guide. It was important to

Table 2. Test Matrix

Laminate	Stress/Strain Ratio	Strain Control Mode (# of tests performed)	Load Control Mode (# of tests performed)
Unidirectional	R = -1	3	--
Unidirectional	R = 0	3	--
Unidirectional	R = 0.5	4	4
Cross-Ply	R = 0	3	--

ensure that the specimen was correctly aligned in the buckling guide. Once the proper alignment was obtained, the screws were tightened and the specimen/buckling guide was placed in the load cell. Figure 14 shows the specimen and buckling guide in the test stand. In order to prevent buckling, a level was used to ensure that the specimen was vertically aligned in the load cell. The extensometer rods were then placed on the edge of specimen and the extensometer was zeroed to ensure correct strain measurements.

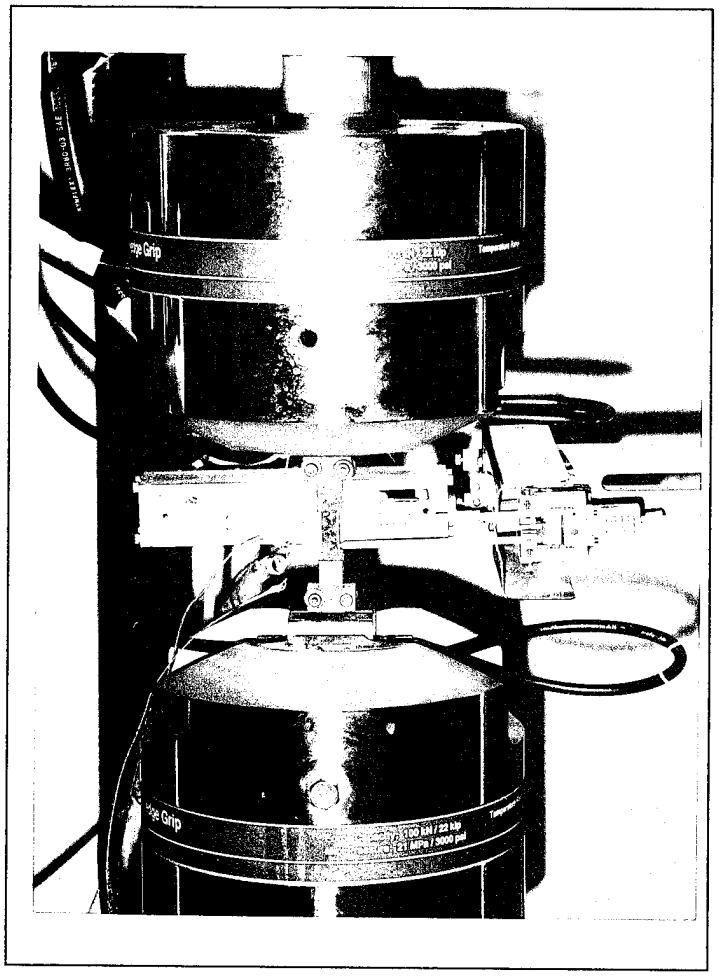

Figure 14. Specimen and Buckling Guide in Test Stand

The next step was to weld thermocouples onto the buckling guide. The thermocouples were not welded to the specimen because the present buckling guide does not allow it. Kraabel showed that the specimen reached 427°C, the same temperature as that of the buckling guide, in approximately 40 minutes so this same procedure was used [12]. Once the specimen reached the required equilibrium temperature (427°C) the first cycle was run manually. This provides the initial modulus of the material and also checks to see if excessive buckling is present. Buckling is represented by a region of nonlinearity in the compressive region of the stress-strain curve. Figure 15 shows an example where excessive buckling was present. If buckling is evident then the specimen is removed and realigned in the buckling guide and the above process is repeated. Once a suitable stress/strain curve was obtained, the test was started.

The tests conducted at R= 0.5 under both load and strain control did not require the buckling guide. The thermocouples were welded directly to the specimen for each of these tests. These specimens were then heated to the required temperature of 427°C and the initial cycle was performed manually to obtain the initial modulus. Once the initial modulus was determined the tests were started.

3.6 Post Failure Analysis

After failure, each of the fractured specimens was examined visually for any trends or defects. All of the specimens were then photographed to show the entire fracture pattern. The next step was to examine the fracture surface of the specimen. The fracture surface of each specimen was removed using a diamond encrusted blade. The fracture

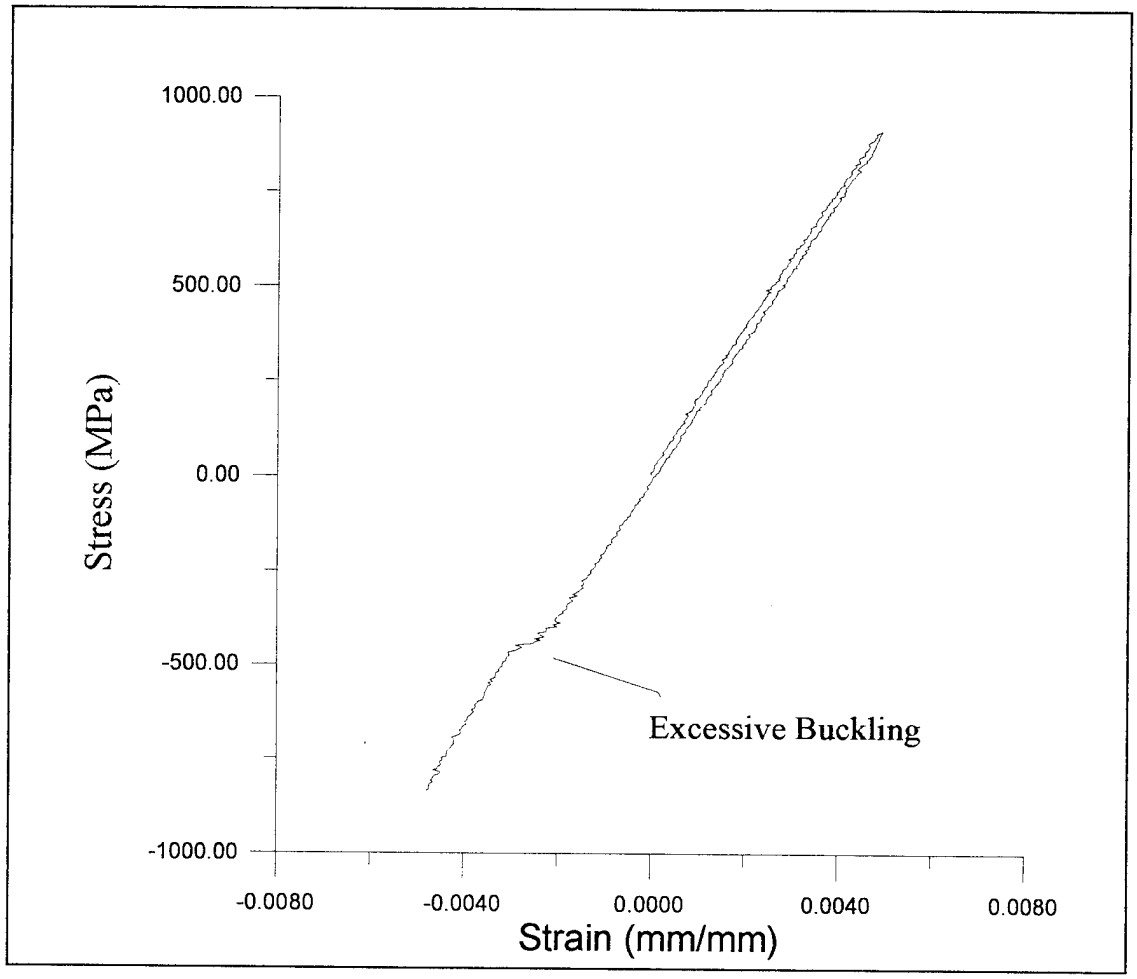

Figure 15. Excessive Buckling

surface was then mounted on a special circular mount with silver conductive paint and examined using a scanning electron microscope. Photographs were taken of each of the fracture surfaces to show the damage and failure mechanisms.

After viewing the fracture surface, the specimens were sectioned to reveal fiber and matrix damage. One section parallel to the loading direction was cut from each of the

specimens. The location of the section along with the fracture surface cut are shown in Figure 16. The section parallel to the loading direction was mounted in Buehler Konductomet, a black conductive mounting compound, and polished. Polishing was completed by using successively finer diamond slurry paste. The sectioned specimens were initially polished with 45 μm paste until the fibers were visible. Successively smaller pastes (9, 6, 3, 1 μm) were then used until the majority of the scratches were removed. The sectioned specimens were then placed in a Beuhler Vibromet which

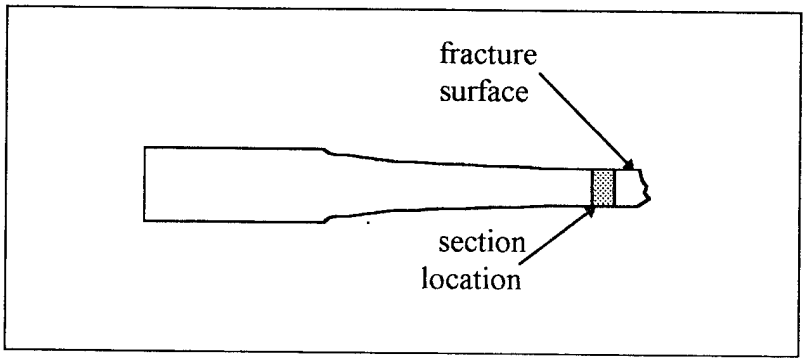

Figure 16. Specimen Sectioning and Fracture Surface

automatically polishes the specimens at 1 μ for 24 hours. This same process is then repeated with 1/2 μ. The last step was to final polish the specimens in a Mastermet acidic solution for four hours which removes any final blemishes and cleans the sectioned surface. The polished sectioned specimens were then viewed under magnification to determine the damage mechanisms present in the fibers and matrix.

4. Results and Discussion

In this chapter the macro-mechanical and microscopy results will be presented for the unidirectional, $[0]_8$, SCS-6/Ti-15-3 specimens tested in this study. The macro-mechanical discussion will include stress, strain and modulus histories during cycling. The microscopy section will investigate the failure and damage mechanisms of the specimens. The macro-mechanical response and damage/failure mechanisms will be compared among control modes and the stress/strain ratios to determine their effects.

4.1 Macro-Mechanical Evaluation

4.1.1 Strain Control Mode

4.1.1.1 Tension-Compression ($R_\varepsilon = -1$)

Three tests were conducted for the tension-compression portion of this study. The maximum strain, strain range, initial modulus, cycles to failure and the dominant failure modes for the three tests are given in Table 3.

Table 3. Tension-Compression ($R_\varepsilon = -1$) Macro-Mechanical Results

Max Strain(%)	Strain Range(%)	Initial Modulus(GPa)	Cycles to Failure	Failure Mode
0.5	1	187.4	6,382	ff,mc
0.4	0.8	203.2	15,995	fb,mc
0.325	0.65	192.5	113,710	fb,mc

mc = matrix cracking, ff = fiber failure, fb = fiber bridging

Figure 17 shows the compression (E_c) and tensile (E_t) modulus histories for the test conducted at a maximum strain of 0.325%. Figure 17 reveals that the compressive

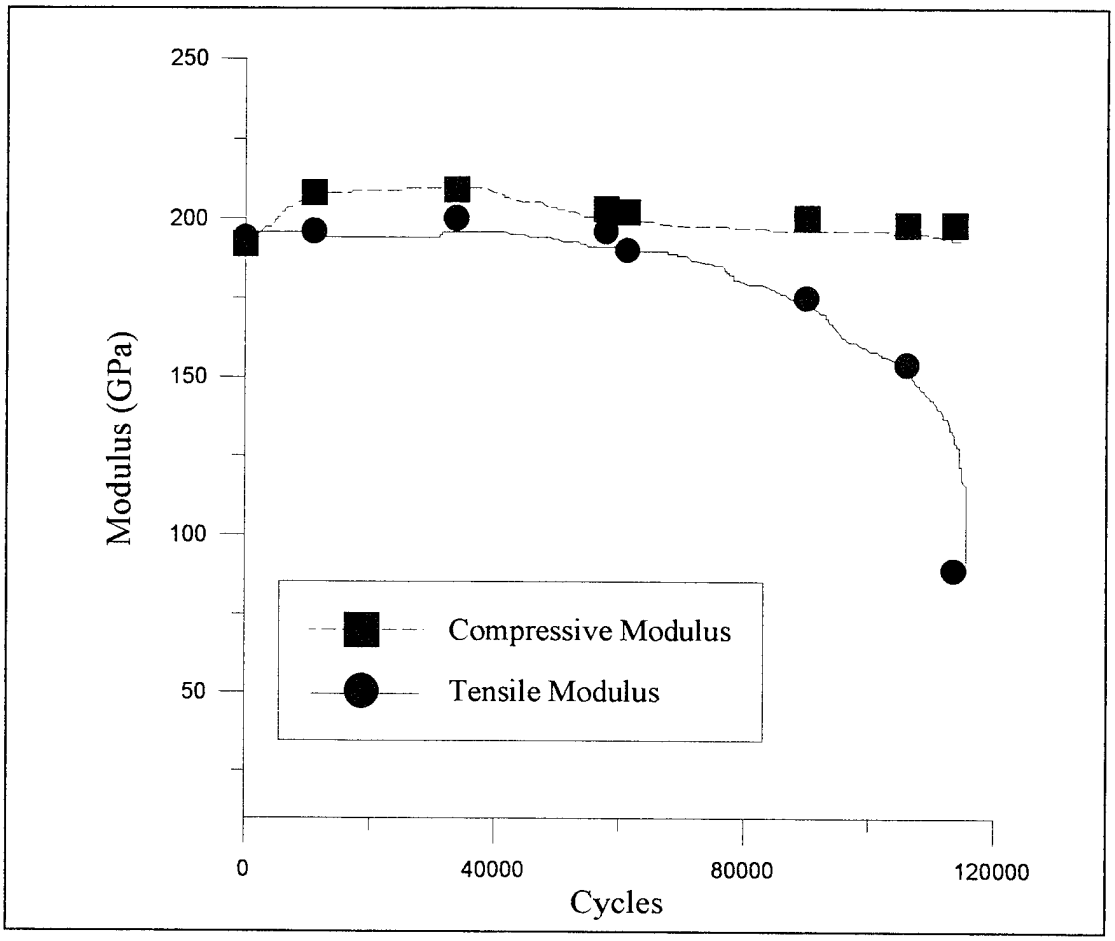

Figure 17. $\varepsilon_{max} = 0.325\%$: Tensile and Compressive Modulus History ($R_\varepsilon = -1$)

modulus is greater than the tensile modulus after the first cycle. This same behavior was reported by Dennis in tension-compression testing of a cross-ply SCS-6/Ti-15-3 lay-up [5]. This stiffening of the material may be caused by the closure of any matrix cracks during the compressive portion of the loading cycle. The large drop in tensile modulus during the later part of cycling as shown in Figure 17 is indicative of matrix damage which will be discussed later. However, the compressive modulus remains relatively unchanged after its initial increase, which implies that the development of matrix cracks only affects

the tensile modulus. For this reason, modulus comparisons for other tests conducted under tension-compression fatigue conditions will be based on the tensile modulus only.

The normalized modulus history for all three tension-compression tests is shown in Figures 18a and 18b. The normalized modulus is calculated by dividing the current modulus by the initial modulus. Similarly, the normalized fatigue life is calculated by dividing the current cycle by the fatigue life of the specimen. Significant reduction in the modulus is generally a sign of damage in the specimen. Previous studies have shown that fiber cracking generally does not result in modulus degradation unless the crack opening displacement is on the order of two to three fiber diameters [18:13]. Therefore, any reduction in modulus is generally a sign that matrix damage has occurred. This will be

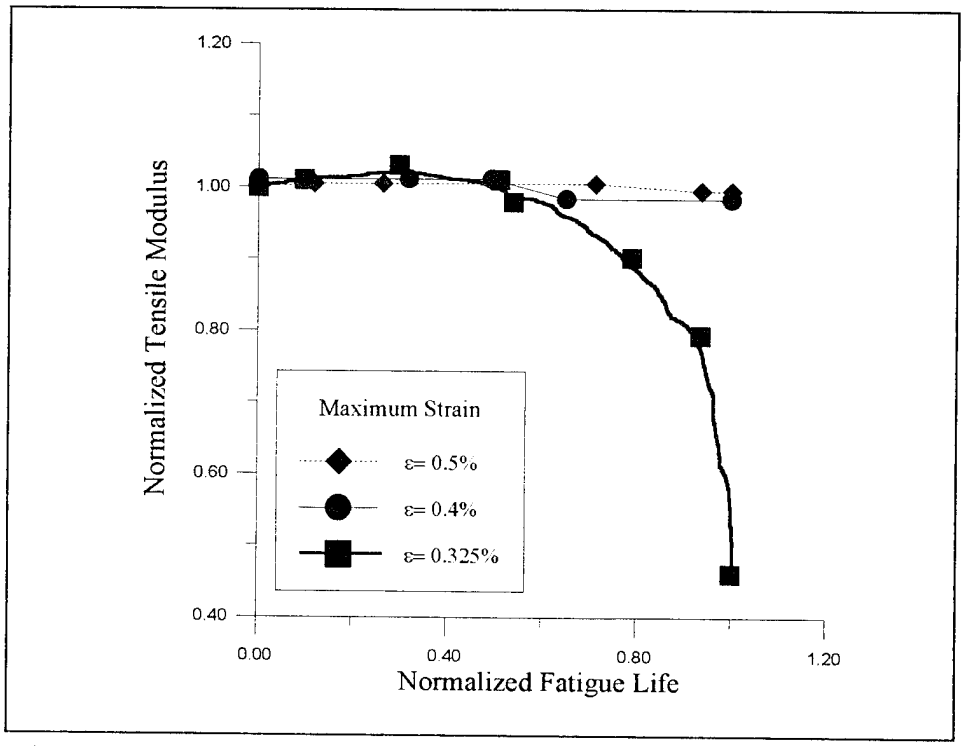

Figure 18a. Tension-Compression (R_ε = -1) Tensile Modulus Histories: Normalized Fatigue Life

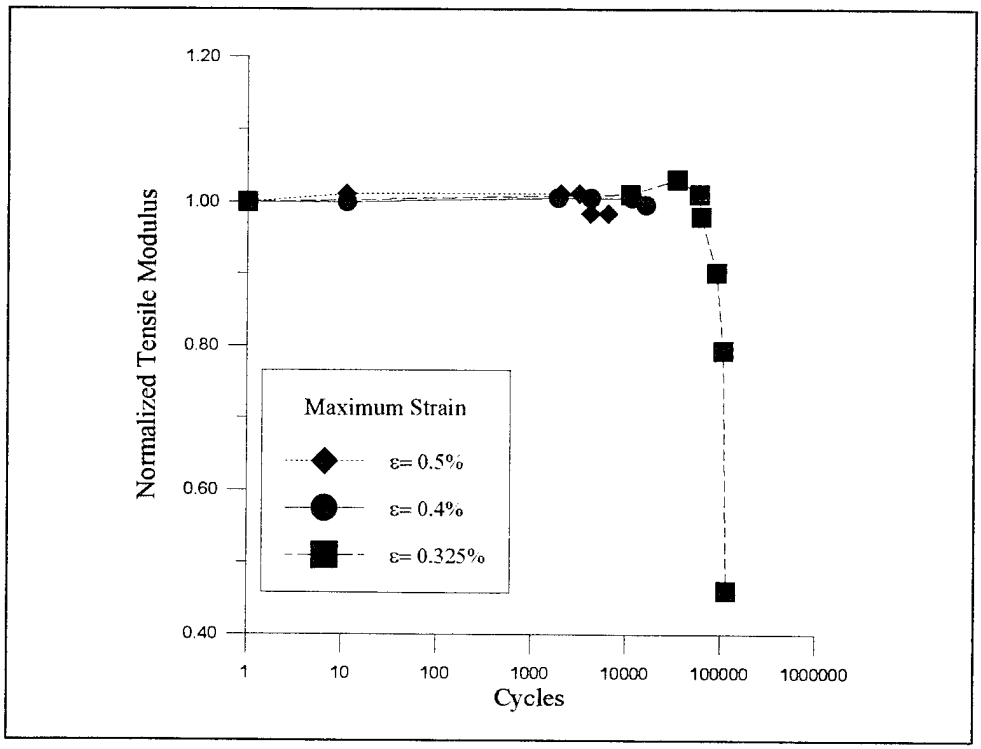

Figure 18b. Tension-Compression (R_ε = -1) Modulus History: Cycles

verified later when discussing the microscopic observations.

The normalized modulus histories for the tests conducted at a maximum strain of 0.5% and 0.4% show very little degradation throughout the entire fatigue life indicating that little matrix damage occurred prior to failure (see Figure 18). Microscopic analysis of the test conducted at a maximum strain of 0.5% showed very little matrix damage; however, the test conducted at a maximum strain of 0.4% did reveal an increased amount of matrix damage, though it was not enough to significantly alter the modulus.

The modulus history for the test conducted at a maximum strain of 0.325% showed two distinct trends (see Figure 18). Over the first half of the fatigue life the

modulus remained relatively constant. Then, the modulus started to decrease steadily until failure. The large drop in modulus was caused by extensive matrix cracking; therefore, the difference in modulus trends between this test and the other two is caused by the density of matrix cracks.

Figure 19 shows the stress-strain history for the test conducted at a maximum strain of 0.325%. A large change in the slope of the tensile portion of the loading cycle for this test was observed during the later half of the life. This decrease in slope along with the increase in hystersis is a sign that matrix damage occurred. Figure 19 also shows that the slope of the compressive portion of the stress-strain curves remains relatively constant. This stress-strain response reinforces the trends that were found in the compressive and tensile modulus histories shown in Figure 17.

The trends in the maximum and minimum stresses during cycling also provide insight into the fatigue response of the material. The stress histories for the tests conducted at $R_\varepsilon = -1$ are shown in Figures 20a and 20b. The maximum and minimum stress for the tests conducted at a maximum strain of 0.5% and 0.4% remained relatively constant throughout the entire fatigue life. The test conducted at a maximum strain of 0.325% experienced a large drop in maximum stress over the second half of its fatigue life. The microscopic analysis will show that the decrease in maximum stress was caused by matrix damage. In summary the modulus and stress histories (see Figures 18 and 20) indicate that the amount of matrix damage increases as the maximum strain decreases for tension-compression tests.

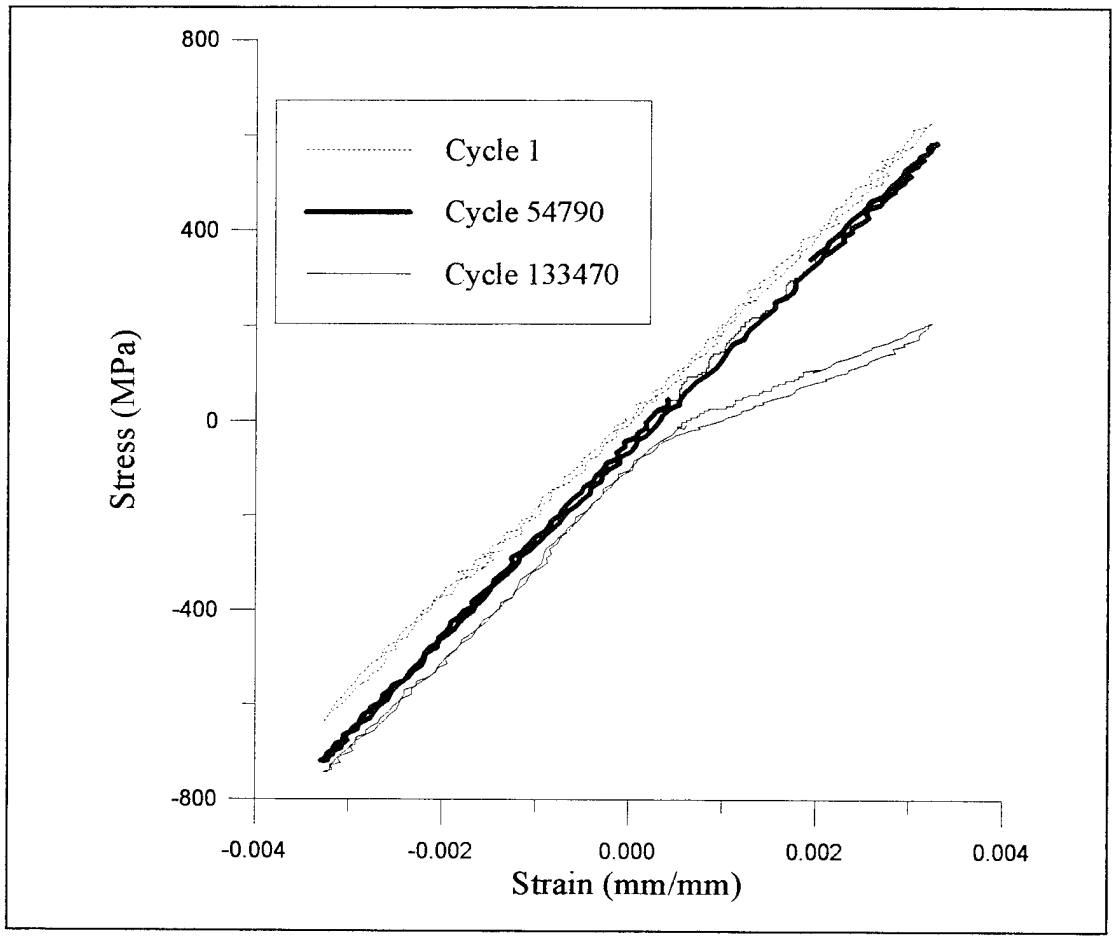

Figure 19. ε_{max} = 0.325%: Tension-Compression (R_ε = -1) Stress/Strain History

4.1.1.2 Tension-Tension (R_ε = 0)

Three tests were conducted for the tension-tension case (R_ε = 0) under the strain control mode. The maximum strain, strain range, initial modulus, cycles to failure and the dominant failure modes are given in Table 4. The trends in normalized modulus for each of the three tests are shown in Figures 21a and 21b. The tensile modulus for each of these tests showed little reduction prior to specimen failure. The modulus response suggests

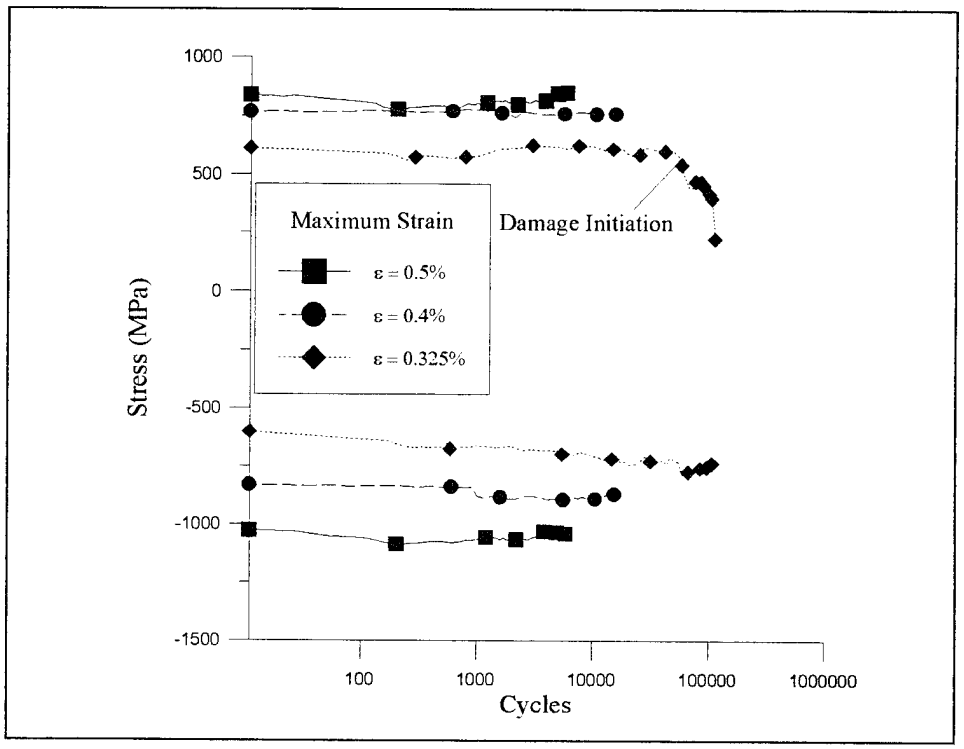

Figure 20a. Tension-Compression (R_ε = -1) Stress Histories: Cycles

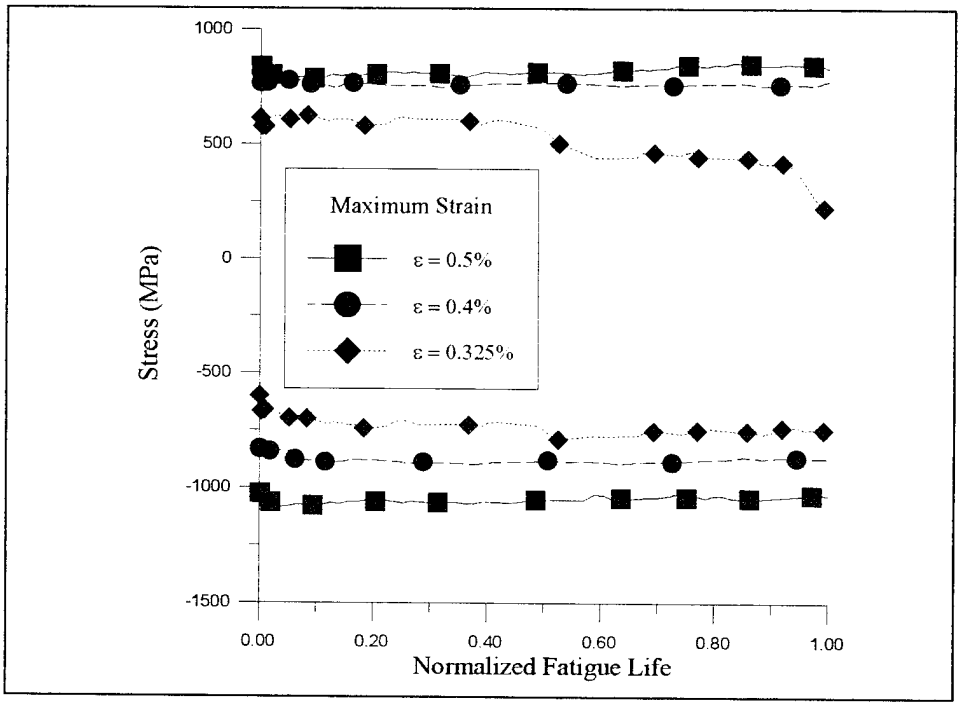

Figure 20b. Tension-Compression (R_ε = -1) Stress Histories: Normalized Fatigue Life

Table 4. Tension-Tension ($R_\varepsilon = 0$) Macro-Mechanical Results

Max Strain(%)	Strain Range(%)	Initial Modulus(GPa)	Cycles to Failure	Failure Mode
0.6	0.6	182	16,106	ff
0.5	0.5	196	33,095	ff
0.4	0.4	186	100,717	ff,mc

mc = matrix cracking, ff = fiber failure

fiber dominated failure for each of these tests. The microscopic analysis will show that the tests conducted at maximum strain of 0.6% and 0.5% were dominated by fiber failure. However, the test conducted at a maximum strain of 0.4% did contain some matrix cracking, although the density of matrix cracks was not sufficient to significantly reduce the modulus.

A comparison between the trends in modulus for the tests conducted at a maximum strain of 0.5% and 0.4%, for $R_\varepsilon = 0$ and $R_\varepsilon = -1$, show similar trends. In each case the modulus showed little degradation before specimen failure (see Figures 18 and 21). The microscopic analysis will also show that each of these tests at the same maximum strain level had similar damage mechanisms. This indicates that the type of fatigue damage is dependent on the maximum strain value when comparing specimens tested at $R_\varepsilon = 0$ and $R_\varepsilon = -1$.

The trends in the maximum and minimum stresses for the three tests conducted under the strain control mode at $R_\varepsilon = 0$ are shown in Figures 22a and 22b. The stress

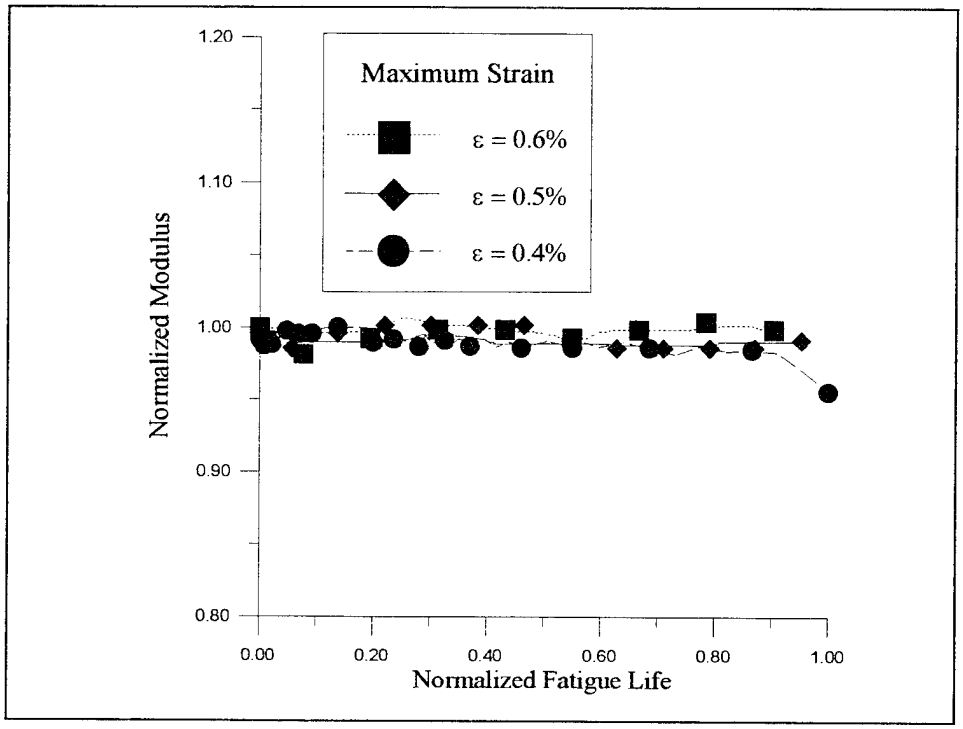

Figure 21a. Tension-Tension ($R_\varepsilon = 0$) Modulus Histories: Normalized Fatigue Life

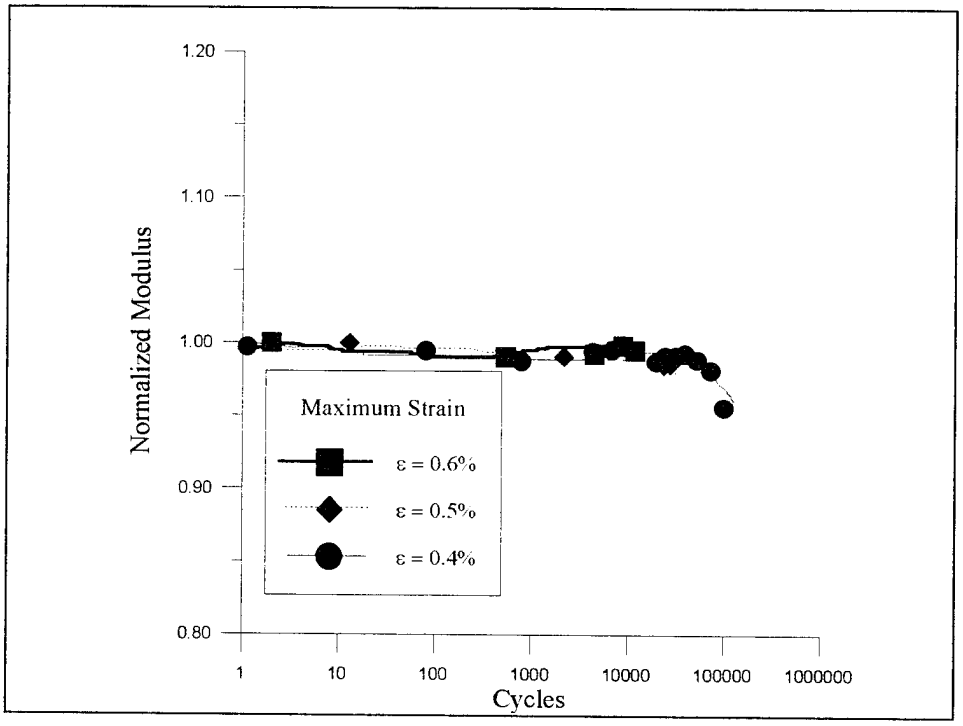

Figure 21b. Tension-Tension ($R_\varepsilon = 0$) Modulus Histories: Cycles

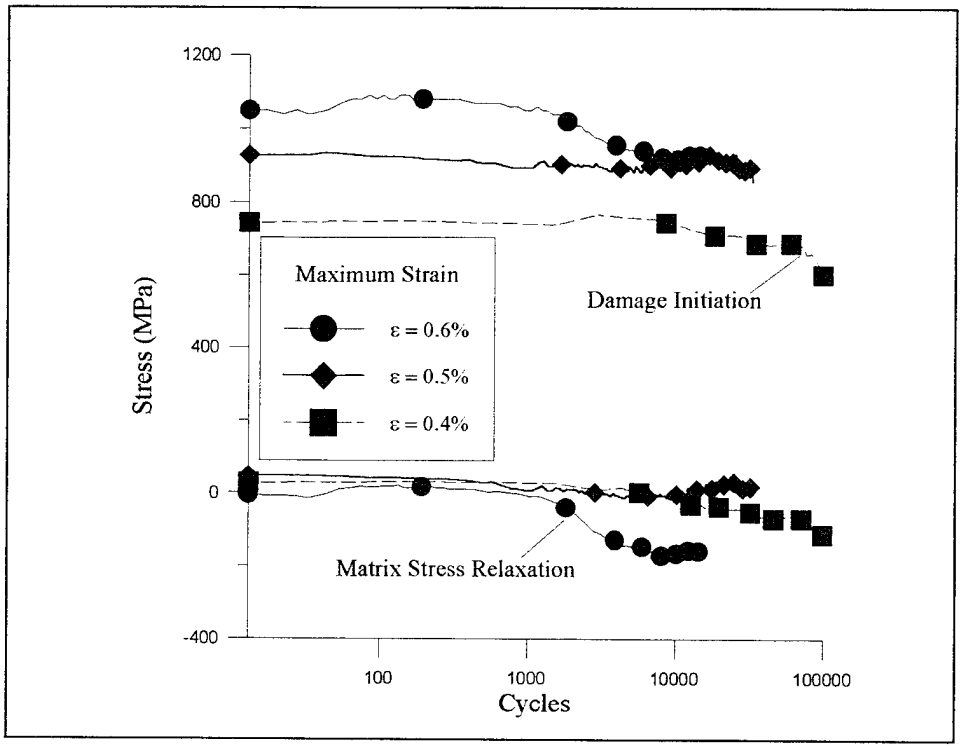

Figure 22a. Tension-Tension ($R_\varepsilon = 0$) Stress Histories: Cycles

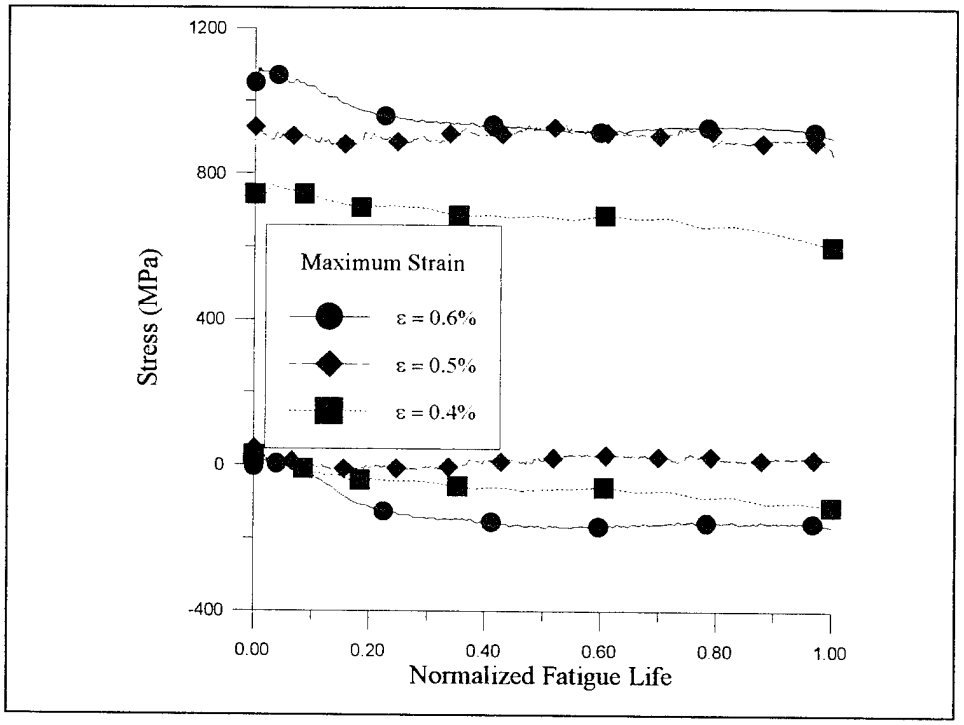

Figure 22b. Tension-Tension ($R_\varepsilon = 0$) Stress Histories: Normalized Fatigue Life

histories for the three tests can be divided into three stages. In Stage I the maximum and minimum stresses remain constant for approximately 1,000 cycles. Stage II is represented by a decrease in both the maximum and minimum stresses. In all three tests the stress stabilized by approximately 40% of the fatigue life. This decrease in stress is not accompanied by any modulus degradation or change in stress range. This suggests that the reduction in stress in this stage is a result of stress relaxation of the matrix material [25]. Once the stress stabilized it remained constant until failure for the tests conducted at a maximum strain of 0.6% and 0.5%. However, the maximum stress for the test conducted at a maximum strain of 0.4% decreased near the end of the fatigue life. It will be shown later that this decrease in maximum stress was due to matrix damage. The stress histories indicate that the two high strain tests were dominated by fiber failure while the test conducted at a maximum strain of 0.4% sustained some matrix damage.

4.1.1.3 Tension-Tension ($R_\varepsilon = 0.5$)

Four tests were conducted for the tension-tension ($R_\varepsilon = 0.5$) case under the strain control mode. The maximum strain, strain range, initial modulus, cycles to failure and the dominant failure modes are given in Table 5.

Table 5. Tension-Tension ($R_\varepsilon = 0.5$) Macro-Mechanical Results

Max Strain(%)	Strain Range(%)	Initial Modulus (GPa)	Cycles to Failure	Failure Mode
0.75	0.375	177.1	20,900*	ff,mc
0.75	0.375	170.5	54,170	ff,mc
0.7	0.35	179.8	29,287	ff,mc
0.6	0.3	179.5	136,147	ff,mc

mc = matrix cracking, ff = fiber failure, * did not fail

The trends in normalized modulus for the four tests conducted at $R_\varepsilon = 0.5$ are shown in Figures 23a and 23b. The modulus for two tests conducted at a maximum strain of 0.75% remained unchanged for approximately 4,000 cycles then degraded until failure. This large drop in modulus indicates significant damage to the specimen. The first test conducted at a maximum strain of 0.75% was interrupted after 20,900 cycles due to the large decrease in both stress and modulus. Previous studies under the strain control mode have used a criterion that a large simultaneous drop in modulus and stress is equivalent to a specimen failure [8,24]. For this study a simultaneous drop in both modulus and stress greater than 30% was considered a failure. The second specimen tested at a maximum stress of 0.75% failed in two pieces. The microscopic analysis will reveal that matrix cracking was present in both of these tests. The larger decrease in modulus for the interrupted test conducted at a maximum strain of 0.75% may have been caused by a material imperfection which caused the large matrix crack to develop (see Figure 49).

Previous tests conducted at $R_\varepsilon = 0$ under the strain control mode showed that for maximum strains above 0.73% the failure was dominated by fiber failure [24]. In this study the tests conducted at a maximum of strain of 0.75% at $R_\varepsilon = 0.5$, revealed matrix and fiber damage. These results indicate that maximum strain does not only govern fatigue damage when comparing tests conducted at $R_\varepsilon = 0.5$ and $R_\varepsilon = 0$.

The modulus for the tests conducted at a maximum strain of 0.7% and 0.6% showed different trends than the previous case. The modulus for the test conducted at a maximum strain of 0.7% revealed little degradation while the test conducted at a

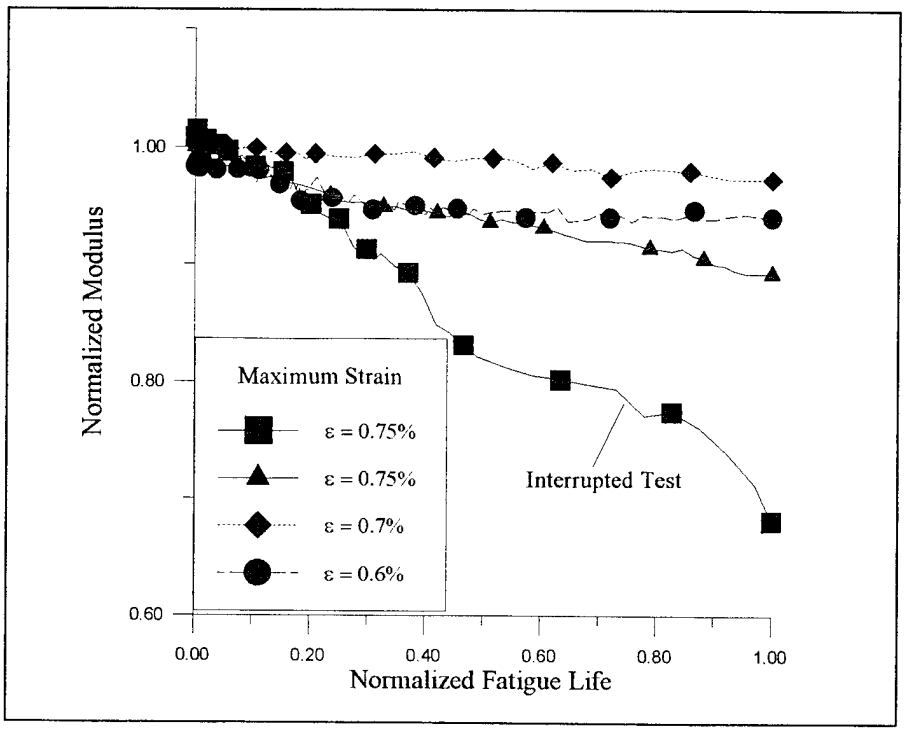

Figure 23a. Tension-Tension (R_ε = 0.5) Modulus Histories: Normalized Fatigue Life

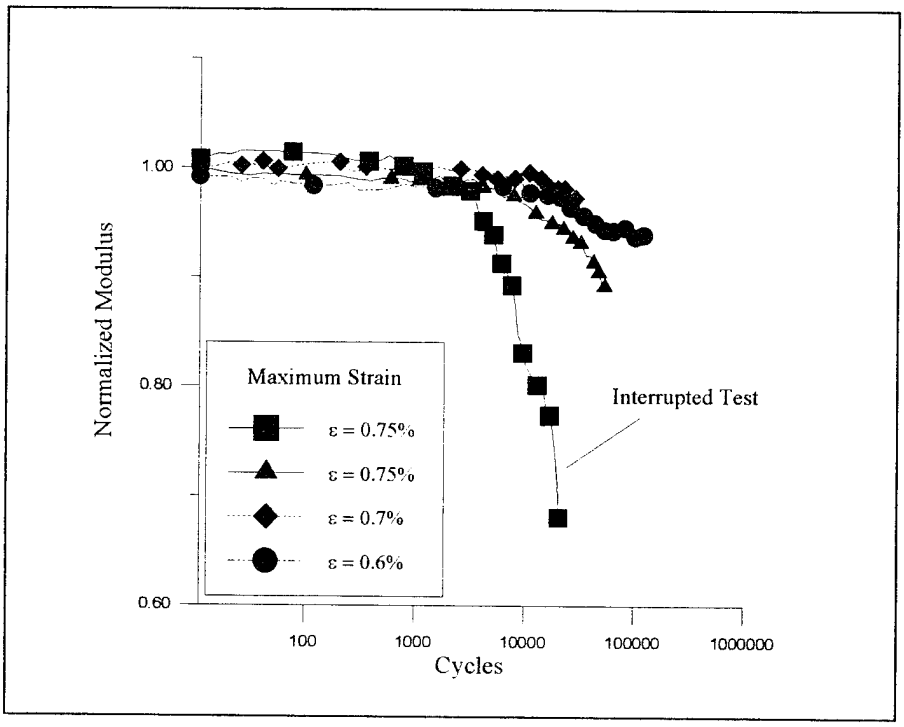

Figure 23b. Tension-Tension (R_ε = 0.5) Modulus Histories: Cycles

maximum strain of 0.6% showed some modulus degradation. Microscopic analysis will show that both specimens contained a mixture of fiber and matrix damage.

Figure 24 shows a comparison between modulus histories for tests conducted at a maximum strain of 0.6% at $R_\varepsilon = 0$ and $R_\varepsilon = 0.5$. The modulus history for the test conducted at $R_\varepsilon = 0$ showed little degradation throughout its fatigue life while the test conducted at $R_\varepsilon = 0.5$ contained some modulus degradation. The microscopic analysis will show that matrix cracking occurred in the test conducted at $R_\varepsilon = 0.5$ while none was

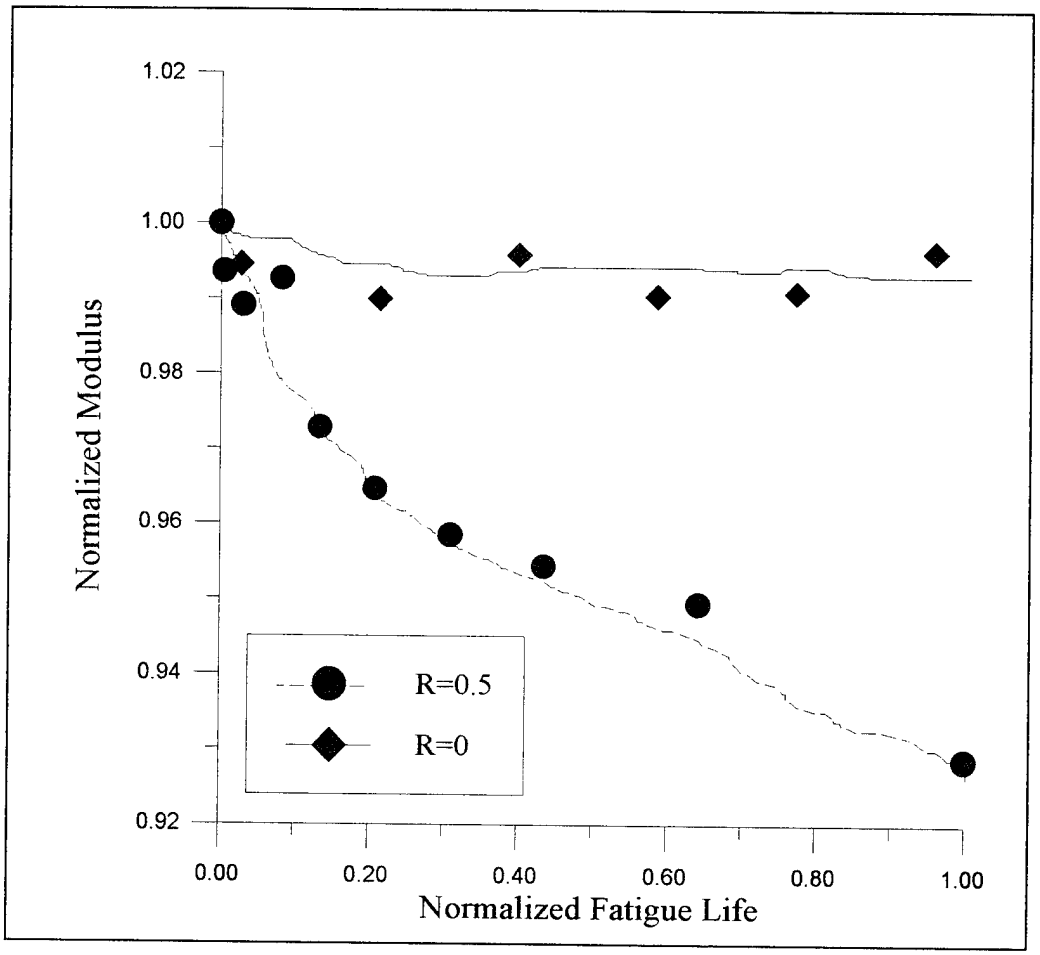

Figure 24. $\varepsilon_{max} = 0.6\%$: Modulus Comparison Between $R_\varepsilon = 0$ and $R_\varepsilon = 0.5$

found in the test conducted at $R_\varepsilon = 0$. The matrix damage found at $R_\varepsilon = 0.5$ is a result of the increased fatigue life due to the lower strain range when compared to the test conducted at $R_\varepsilon = 0$. Fatigue life analysis (Chapter 5) will show that on a maximum strain basis fatigue life increases as R_ε increases. For the test conducted at $R_\varepsilon = 0$ the higher strain range (0.6%) results in a shorter fatigue life (16,106 cycles) with fiber failure being the dominant failure mode. In the test conducted at $R_\varepsilon = 0$ the matrix cracks do not have time to develop. At $R_\varepsilon = 0.5$, the reduced strain range (0.3%) increases fatigue life (136,147 cycles) and allows matrix cracks to develop and propagate. This comparison shows that the damage mode is influenced by both maximum strain and strain range.

Figure 25 shows the stress/strain curves for the interrupted test conducted at a maximum strain of 0.75%. The first cycle shows evidence of matrix plasticity. Sanders showed that matrix plasticity generally occurs on the first cycle for a unidirectional lay-up when the strain is above 0.55% [24]. The decreasing slope of the stress/strain curves (a sign of matrix damage) is clearly evident in Figure 25.

The trends in maximum and minimum stresses for each of the tests are shown in Figures 26a and 26b. For each test, the maximum and minimum stress reduction does not begin until approximately 1,000 cycles. Comparing the modulus and stress trends, the reduction is initially caused by matrix relaxation; however, after 5,000 cycles the modulus in the interrupted test conducted at a maximum strain of 0.75% degrades rapidly which

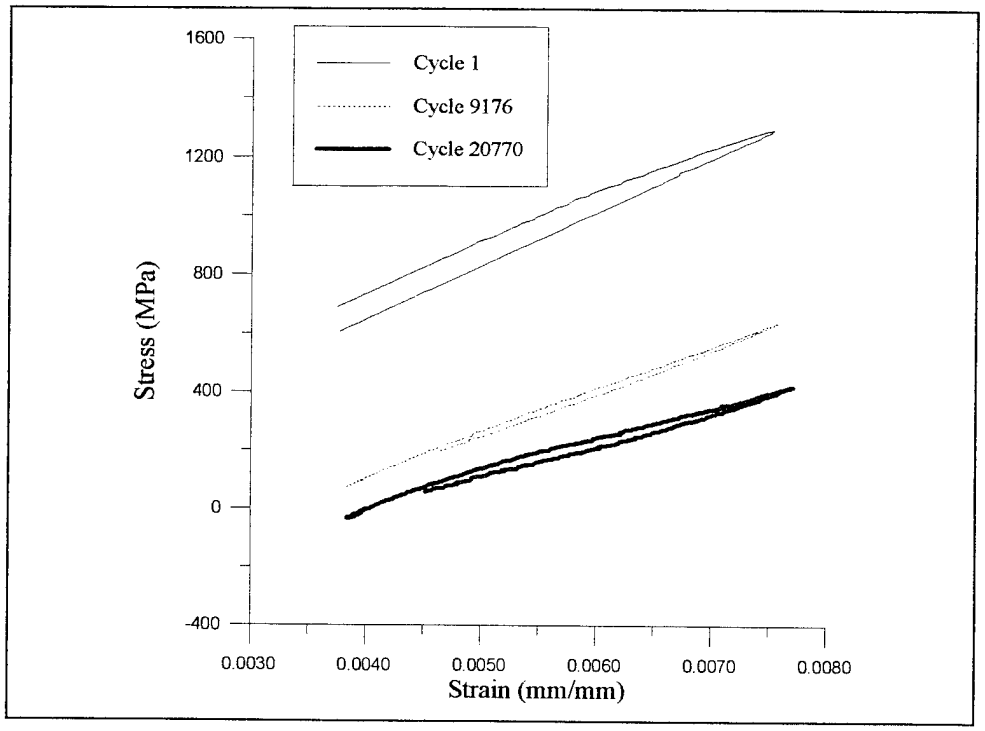

Figure 25. ε_{max} = 0.75%: Tension-Tension (R_ε = 0.5) Stress/Strain History

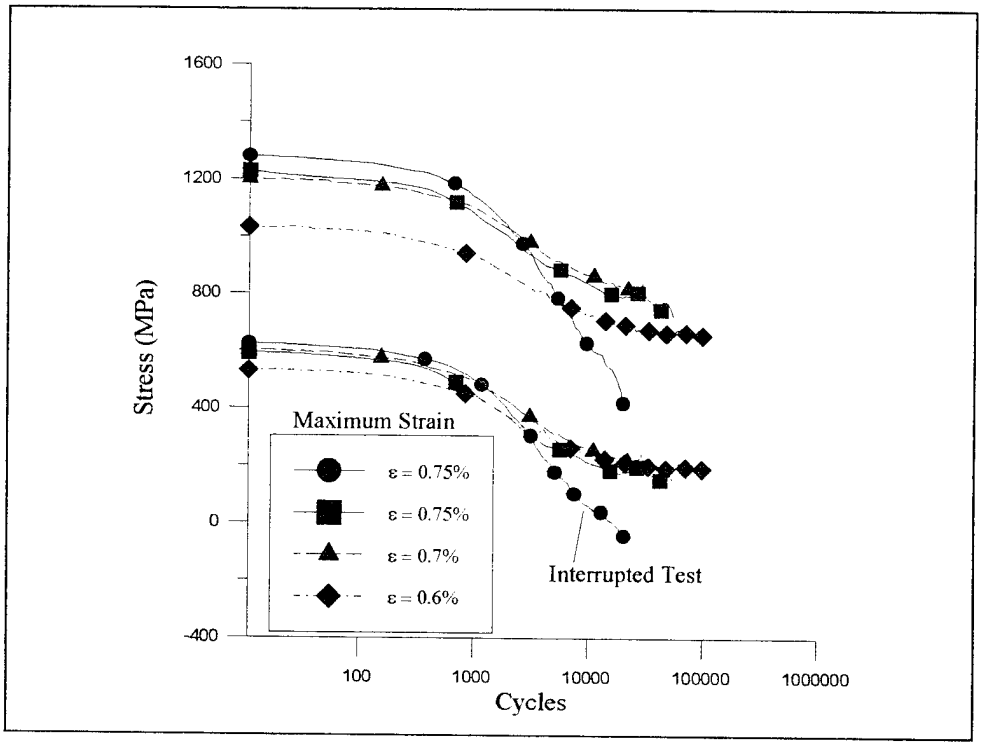

Figure 26a. Tension-Tension (R_ε = 0.5) Stress Histories: Cycles

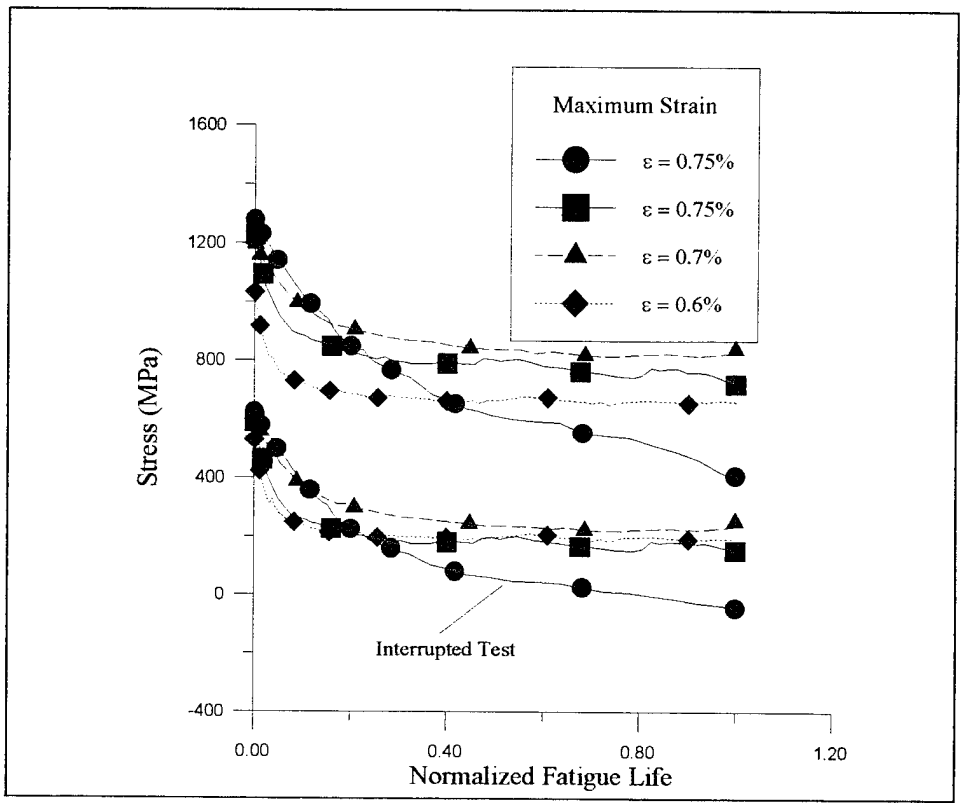

Figure 26b. Tension-Tension ($R_\varepsilon = 0.5$) Stress Histories: Normalized Fatigue Life

indicates that the continued stress reduction is caused by matrix damage. The maximum and minimum stresses for the repeated test at a maximum strain of 0.75% stabilized and then declined near the end of the fatigue life due to matrix damage. The difference in stress histories for the two tests conducted at a maximum strain of 0.75% suggests increased matrix damage in the interrupted test which is supported by the modulus histories shown in Figure 23. The maximum and minimum stresses for the tests conducted at a maximum strain of 0.6% and 0.7% stabilized and remained constant until failure.

Figure 27 shows a comparison of the normalized maximum stress histories for the tests conducted at a maximum strain of 0.6% at $R_\varepsilon = 0$ and $R_\varepsilon = 0.5$. Figure 27 reveals the increased stress relaxation that occurs in the test conducted at $R_\varepsilon = 0.5$. The increased stress relaxation can be explained by examining the response of the matrix stresses. Figure 28 shows the matrix stress histories for the tests conducted at $R_\varepsilon = 0.5$ and $R_\varepsilon = 0$. These were calculated using the Concentric Cylinder Model (CCM) program developed by Sanders [24]. This figure shows that the maximum and minimum matrix stresses relax until they experience the fully reversed tension-compression state. This was defined by Sanders as the self-equilibrating creep [24]. As strain ratio is increased, the corresponding decrease in strain range results in increased matrix stress relaxation to achieve self-equilibrating creep at $R_\varepsilon = 0.5$.

Figure 28 also shows that the test conducted at $R_\varepsilon = 0.5$ experiences a higher mean matrix stress than the test conducted at $R_\varepsilon = 0$. The mean matrix stress is higher at $R_\varepsilon = 0.5$ for the longer period of cycling. The increased mean matrix stress may also cause the increased matrix damage when comparing tests conducted at $R_\varepsilon = 0.5$ and $R_\varepsilon = 0$ (see Figure 24).

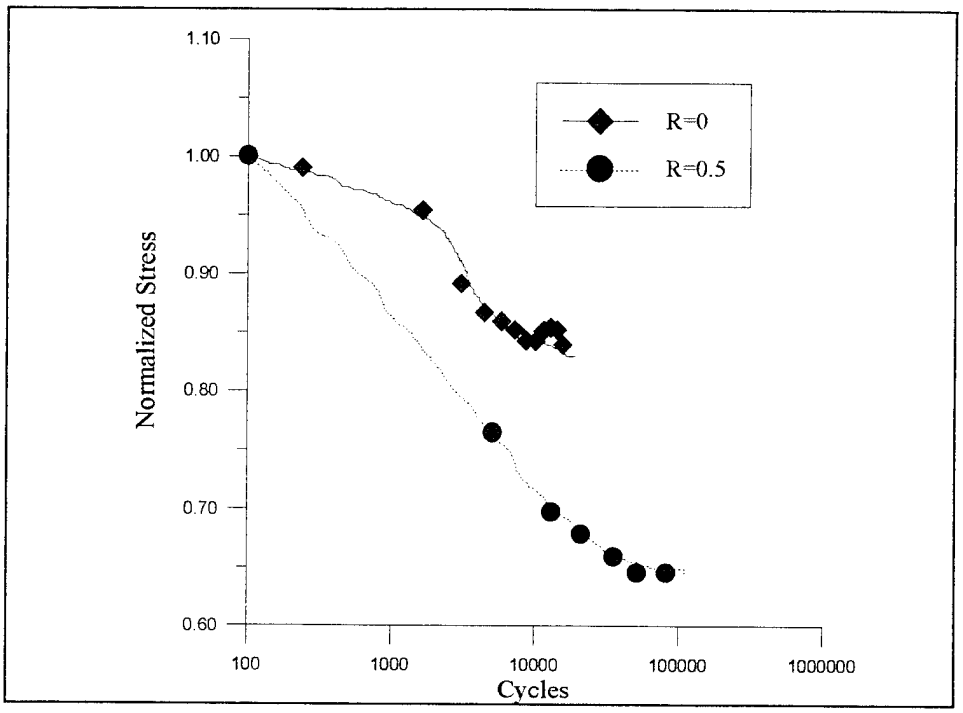

Figure 27. ε_{max} = 0.6%: Maximum Stress History Comparison at R_ε = 0 and R_ε = 0.5

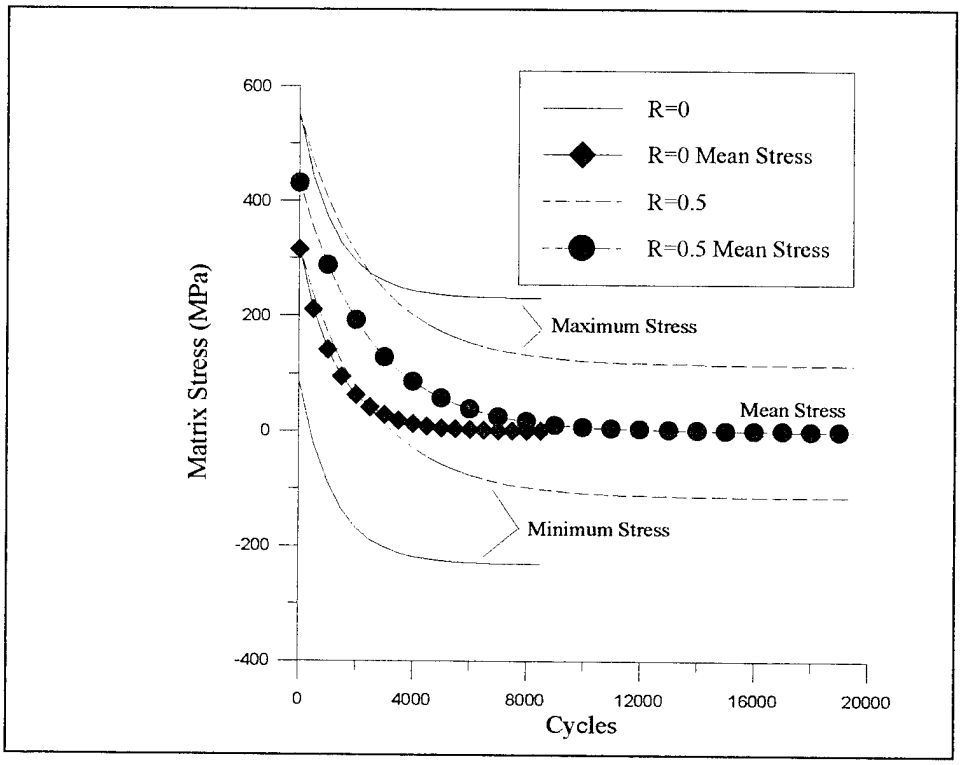

Figure 28. ε_{max} = 0.6%: R_ε = 0 and R_ε = 0.5 Matrix Stress History

4.1.2 Load Control Mode

4.1.2.1 Tension-Tension ($R_\sigma = 0.5$)

Four tests were conducted for the tension-tension ($R_\sigma = 0.5$) case under the load control mode. The maximum stress, strain range, initial modulus, cycles to failure and failure modes are given in Table 6. The strain range given in Table 6 was calculated at the half fatigue life of the specimens.

Table 6. Tension-Tension ($R_\sigma = 0.5$) Macro-Mechanical Results

Max Stress(%)	Strain Range(%)	Initial Modulus (GPa)	Cycles to Failure	Failure Mode
1300	0.33	185	7,950	ff
1150	0.30	190	8,600	ff
1000	0.27	200	123,700	mc,fb
900	0.24	192	127,525	mc,fb

fb = fiber bridging, ff = fiber failure, mc = matrix cracking

The modulus and strain histories during cycling for the four tests can be divided into two groups based on their damage mechanisms, as shown in Figures 29 and 32. Group 1 was dominated by fiber failure while Group 2 combined a mixture of matrix cracking and fiber failure. The tests conducted at a maximum stress of 1300 MPa and 1150 MPa comprise Group 1 while the tests conducted at a maximum stress of 1000 MPa and 900 MPa comprise Group 2.

The normalized modulus histories for each of the tests are shown in Figure 29a and 29b. The moduli for the specimens in Group 1 remained constant for the entire

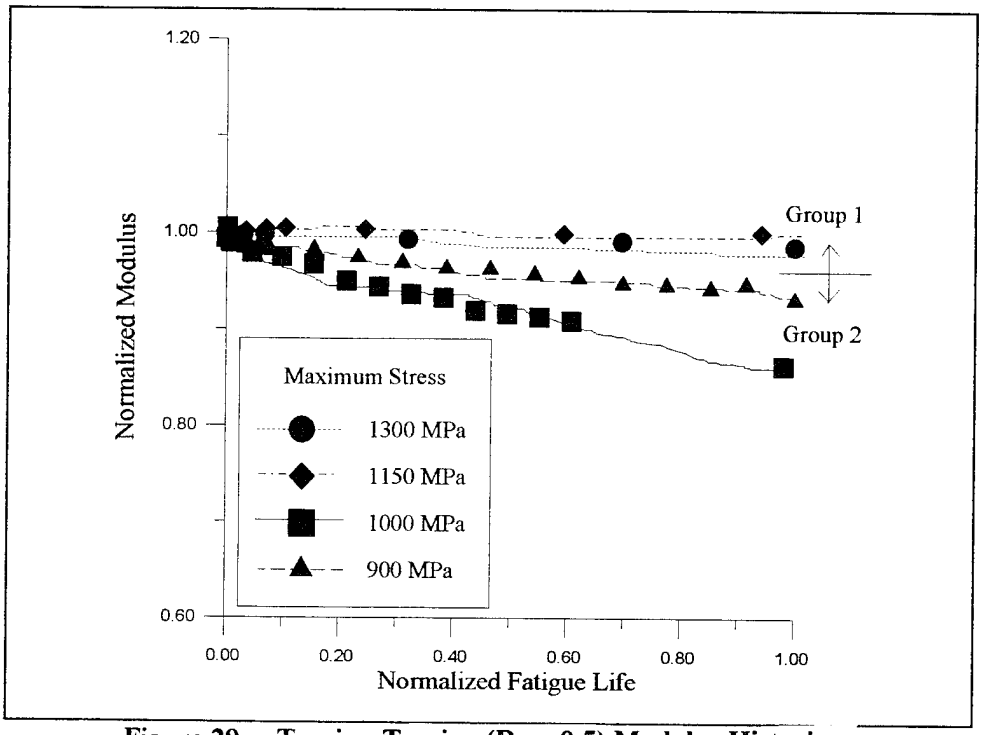

Figure 29a. Tension-Tension (R_σ = 0.5) Modulus Histories: Normalized Fatigue Life

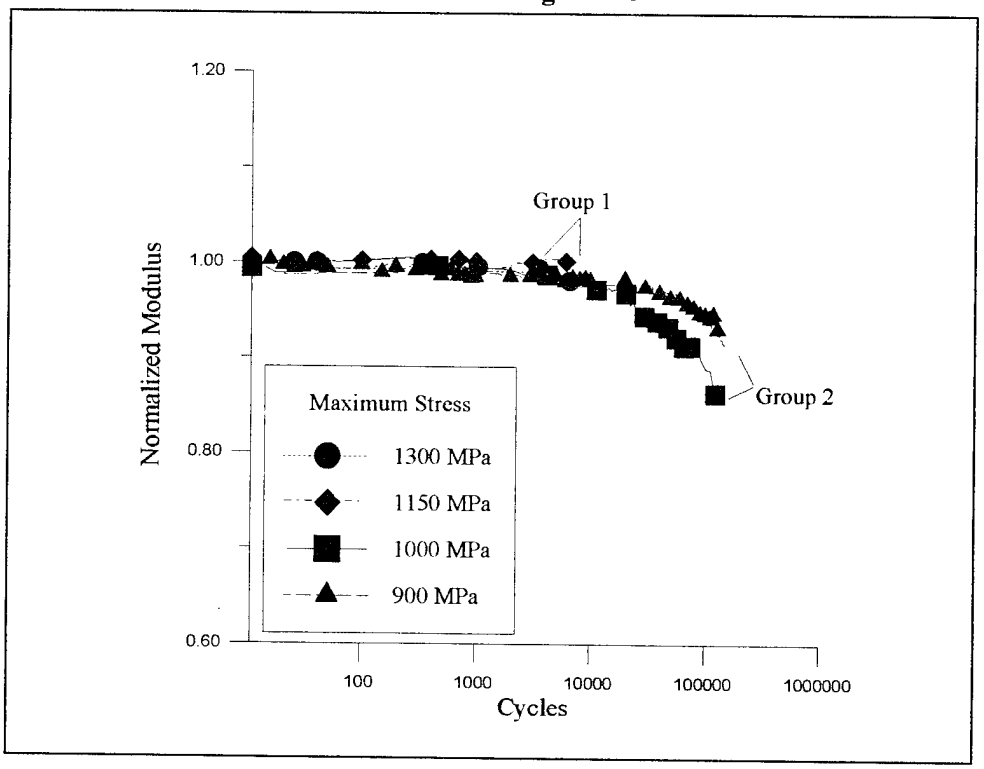

Figure 29b. Tension-Tension (R_σ = 0.5) Modulus Histories: Cycles

fatigue life which indicates that the specimens were dominated by fiber failure. Group 2 is defined by a slow decrease in modulus starting at approximately 10% of the fatigue life. This type of modulus behavior suggests that matrix damage began occurring at 10% of the fatigue life and accumulated until failure. The microscopic analysis will show that the decrease in modulus was caused by matrix cracking. These moduli histories show that the specimens that comprise Group 1 spend most of their fatigue life in the matrix crack initiation phase, while the specimens that comprise Group 2 spend most of their fatigue life in the matrix crack propagation phase.

Figure 30 shows a modulus comparison between the test conducted at a maximum stress of 1150 MPa and the strain control test conducted at the same strain ratio and strain range ($\varepsilon_{max} = 0.6\%$). This figure shows that modulus degradation occurs in the test conducted under strain control but not under load control. The difference in damage mechanisms is a result of matrix creep in the load control test. Under the load control mode, matrix creep transfers load to the fibers leading to fiber failure which will not affect the modulus [18].

Figure 31 shows a direct comparison between two tension-tension tests, both conducted at a maximum stress of 1000 MPa under the load control mode with R_σ of 0.1 from the previous study [12] and 0.5 of the present study. The test conducted at $R_\sigma = 0.1$ shows no modulus degradation while the test conducted at $R_\sigma = 0.5$ reveals gradual modulus degradation throughout the specimen fatigue life. Microscopic analysis showed that the test conducted at $R_\sigma = 0.5$ contained fiber and matrix cracking while the test

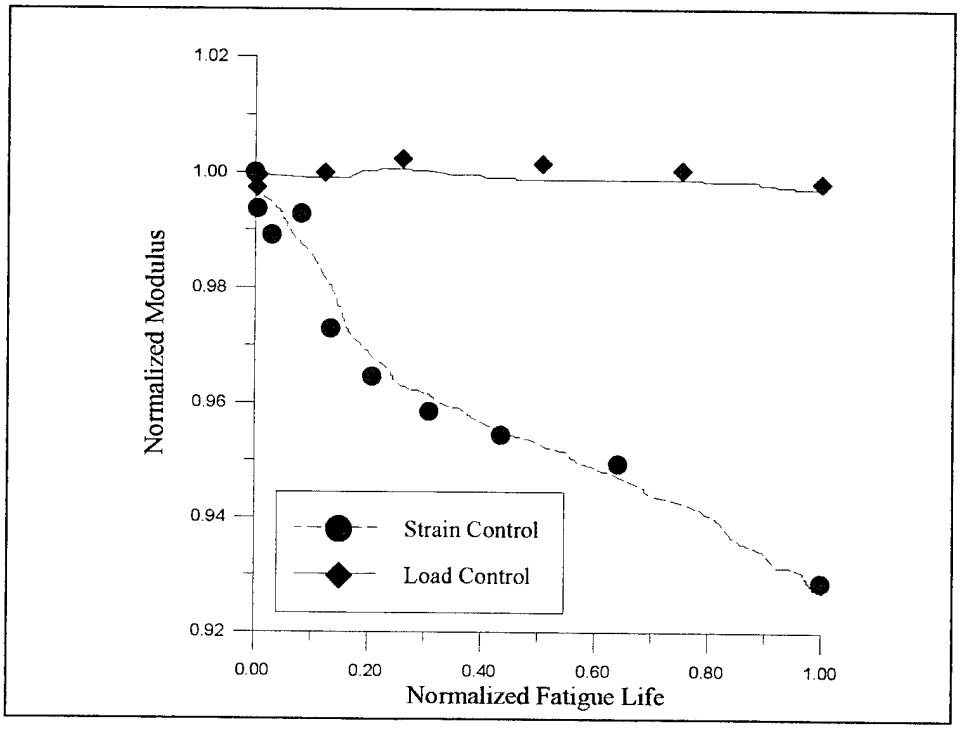

Figure 30. R = 0.5, ε_{range} = 0.3%: Modulus Histories

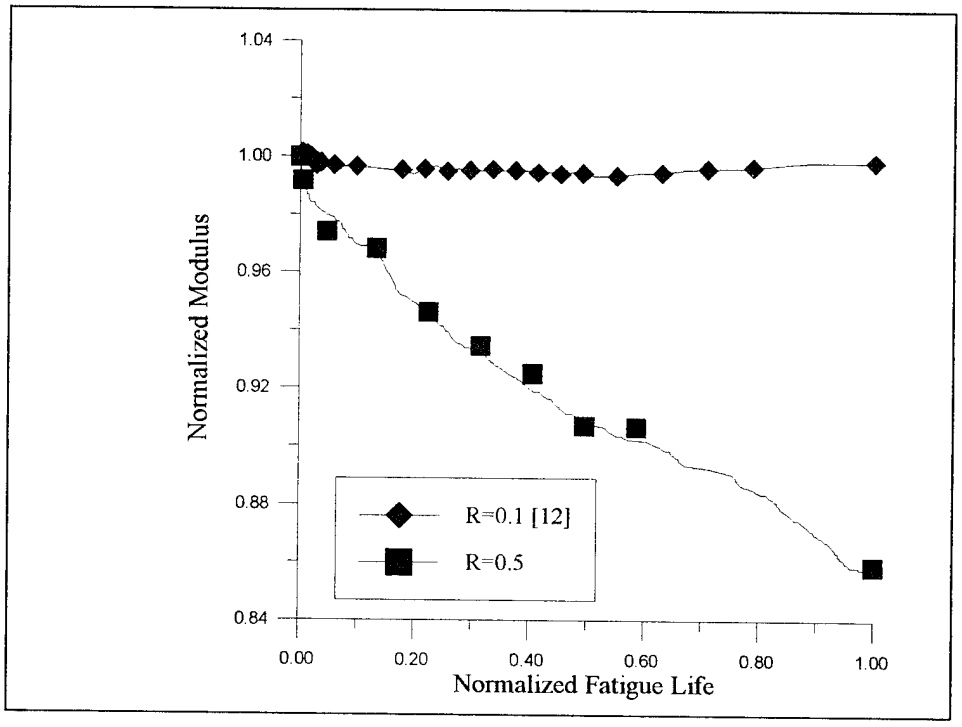

Figure 31. σ_{max} = 1000 MPa: R_σ = 0.1 and R_σ = 0.5 Modulus Comparison (Load Control)

conducted at $R_\sigma = 0.1$ was dominated by fiber failure [12]. The matrix damage found at $R_\sigma = 0.5$ is a result of the increased fatigue life due to the lower stress range when compared to the test conducted at $R_\sigma = 0.1$. The fatigue life analysis (Chapter 5) will show that on a maximum stress basis, fatigue life increases as R_σ increases. For the test conducted at $R_\sigma = 0.1$ the higher stress range (910 MPa) results in a shorter fatigue life (18,000 cycles) with fiber failure being the dominant failure mode. In the test conducted at $R_\sigma = 0.1$ the matrix cracks to do not have time to develop. At $R_\sigma = 0.5$, the reduced stress range (500 MPa) increases fatigue life (123,700 cycles) and allows matrix cracks to develop and propagate. The increased mean matrix stresses for the test conducted at $R_\sigma = 0.5$ may also contribute to the increased matrix damage. These results are similar to those obtained in comparisons made between tests conducted at $R_\varepsilon = 0$ and $R_\varepsilon = 0.5$ under the strain control mode discussed in section 4.1.1.3.

Figures 32 and 33 show the maximum and minimum strain and strain range histories for each of the four tests conducted under the load control mode at $R_\sigma = 0.5$. The strain remained constant for each of the two groups, as defined previously, for the first 1,000 cycles. At approximately 1,000 cycles the strain began to increase for specimens in each group. This increase in strain was caused by matrix creep. For the specimens that comprise Group 1, the strain continued to increase until failure with the strain range remaining relatively constant until just before specimen failure. An increase in strain range would indicate damage in the specimen and would result in a reduction in

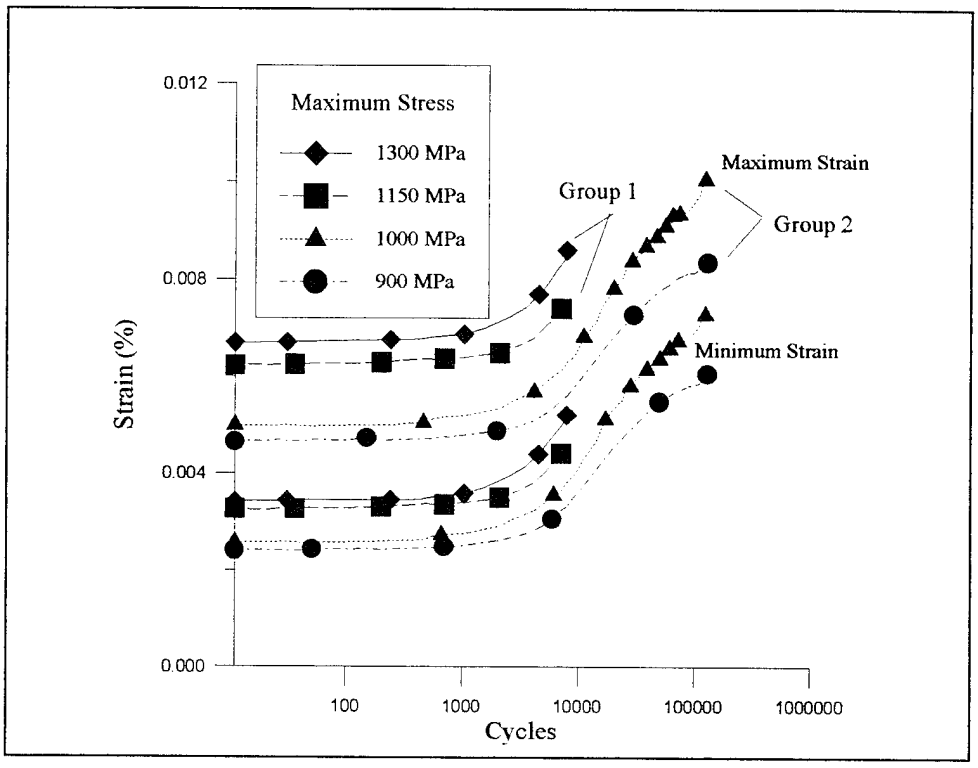

Figure 32a. Tension-Tension ($R_\sigma = 0.5$) Stress Histories: Cycles

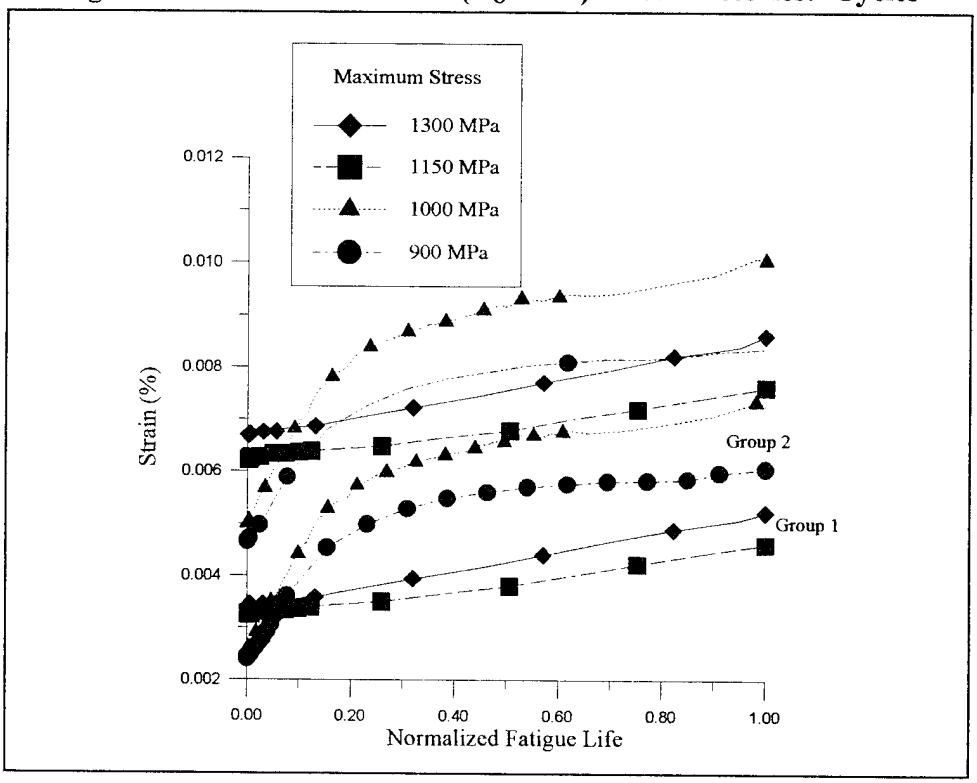

Figure 32b. Tension-Tension ($R_\sigma = 0.5$) Stress Histories: Normalized Fatigue Life

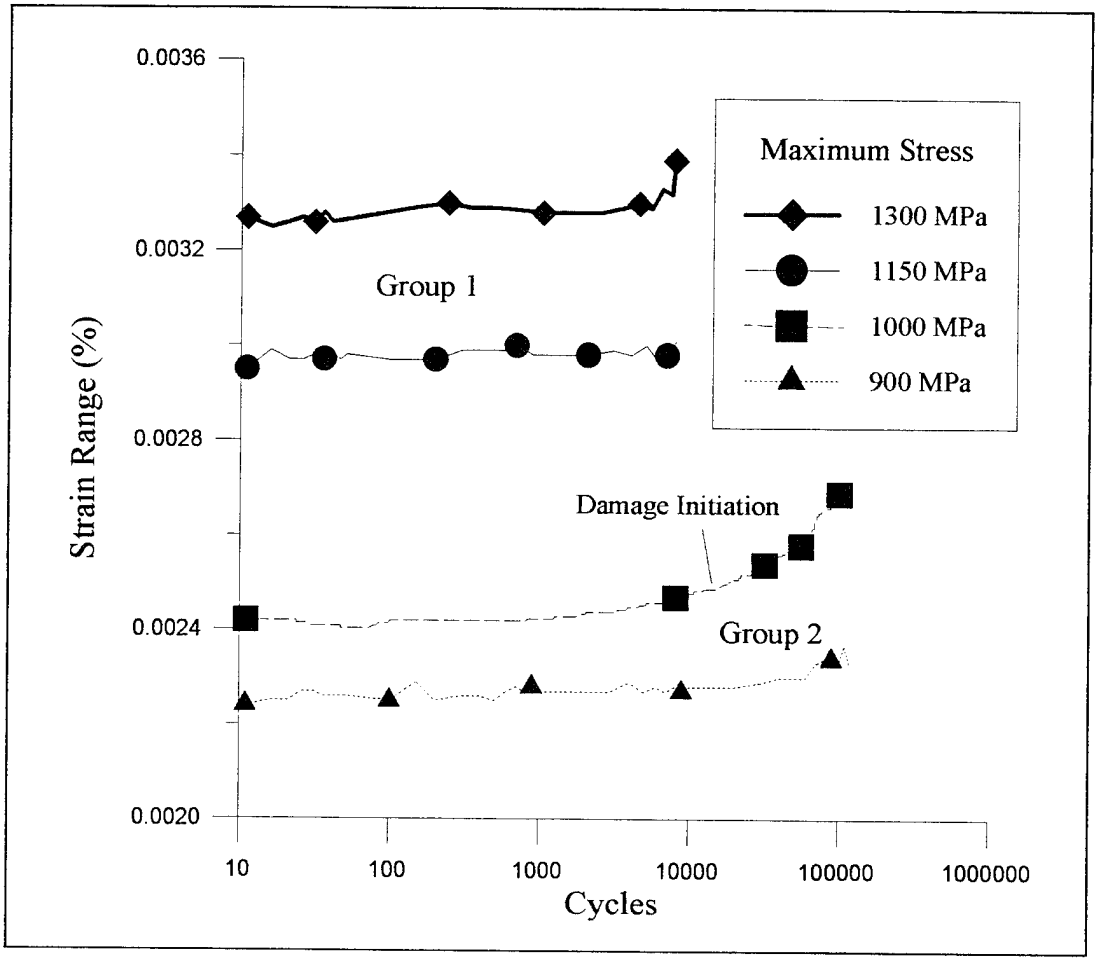

Figure 33. Tension-Tension ($R_\sigma = 0.5$) Strain Range Histories

modulus. The specimens that comprise Group 2 experienced matrix creep for the first 10% of their fatigue life then the strain range (see Figure 33) began to increase leading to a decrease in modulus. The increase in strain range and decrease in modulus for the specimens that comprise Group 2 is caused by damage in the matrix.

4.2 Microscopic Evaluation

4.2.1 Strain Control Mode

4.2.1.1 Tension-Compression ($R_\varepsilon = -1$)

The test conducted at a maximum strain of 0.5% showed evidence of fiber cracking along with a few short matrix cracks. Figure 34 shows a portion of the fracture surface where regions of matrix necking and fiber pullout were discovered. This indicates that the fibers failed first, followed by matrix yielding which was caused by tensile overload. A close-up of the necked region, Figure 35, reveals areas of ductile void coalescence represented by dimples, which were caused by tensile overload in the matrix. Figure 36 shows a region on the fracture where fiber failure occurred along the same plane as the molyweave.

The fracture surface also revealed flat regions which are indicative of matrix cracking. These flat regions represent areas where matrix cracks developed and fibers failed behind the advancing crack tip. The flat portions of the matrix were confined to the specimen edges which indicates that the majority of matrix cracks started from the edge of the specimen.

Figure 37 shows the sectioned specimen along the longitudinal direction, tested at a maximum strain of 0.5%. The sectioned specimen revealed both fiber and matrix cracking. Matrix cracking was limited to short cracks that initiated from the debonded fiber/matrix interface region. Figure 38 illustrates fiber/matrix debonding which is represented by the dark regions between the fiber and matrix. This figure depicts how

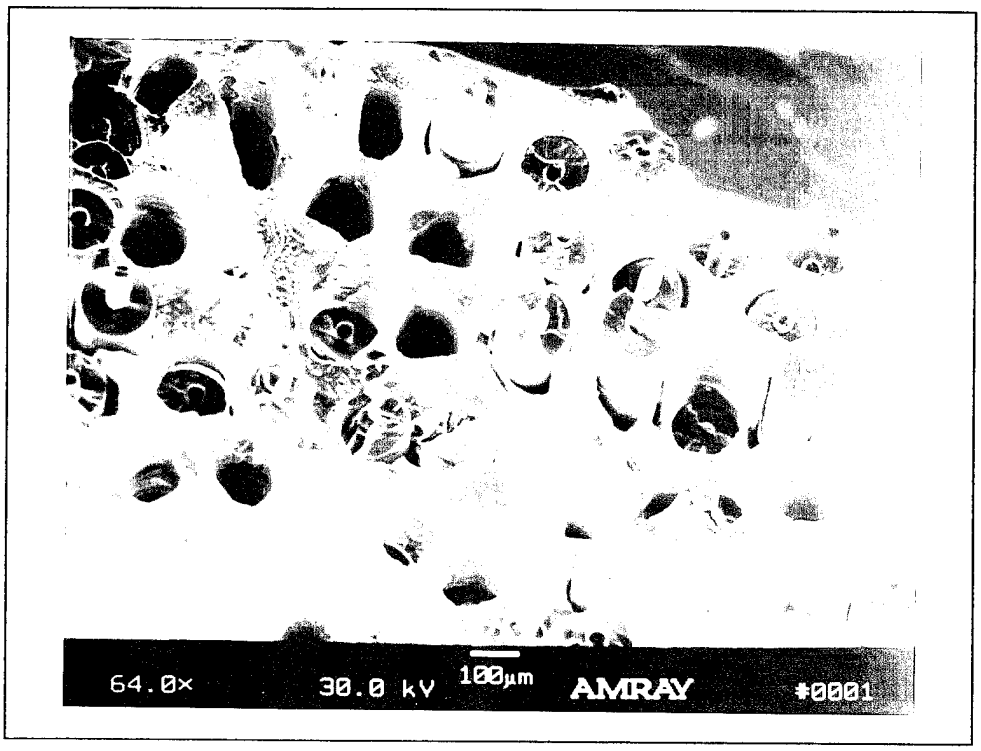

Figure 34. Tension-Compression ($R_\varepsilon = -1$) $\varepsilon_{max} = 0.5\%$: Fracture Surface

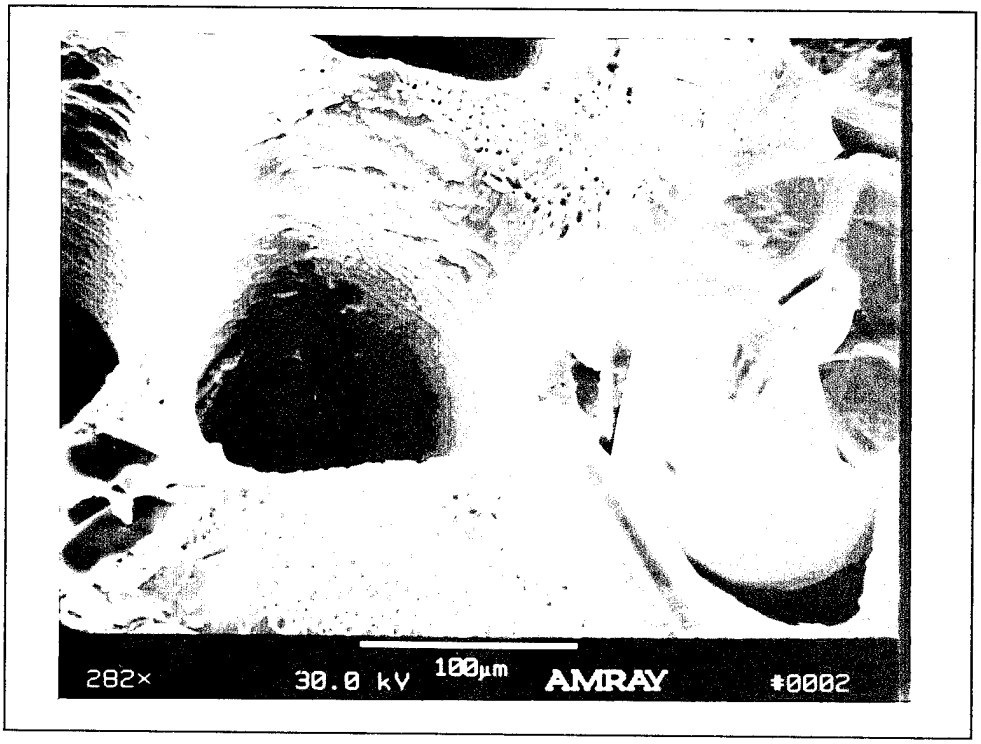

Figure 35. Tension-Compression ($R_\varepsilon = -1$) $\varepsilon_{max} = 0.5\%$: Ductile Void Coalescence

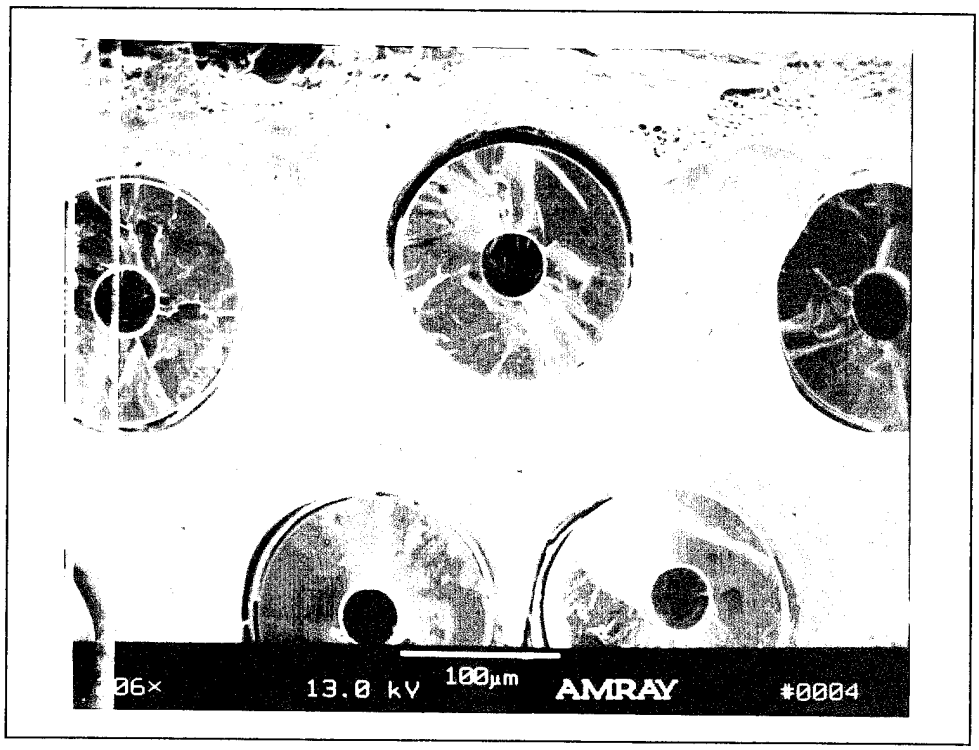

Figure 36. Tension-Compression ($R_\varepsilon = -1$) $\varepsilon_{max} = 0.5\%$: Fiber Fracture Near Molyweave Sites

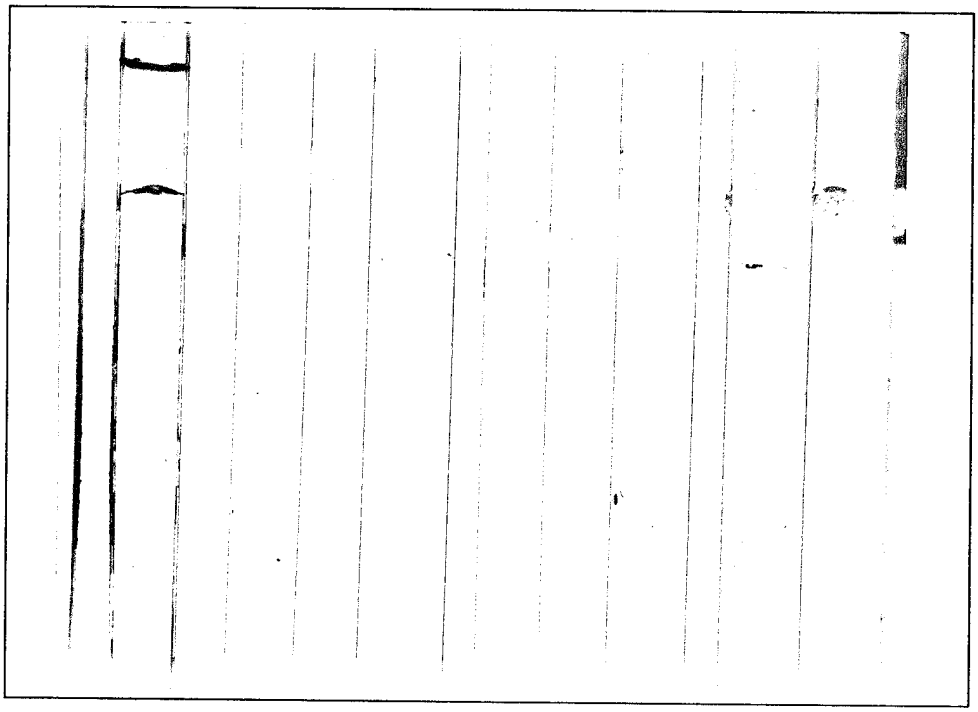

Figure 37. Tension-Compression ($R_\varepsilon = -1$) $\varepsilon_{max} = 0.5\%$: 0^o Fiber Cracks and Short Matrix Cracks (50X)

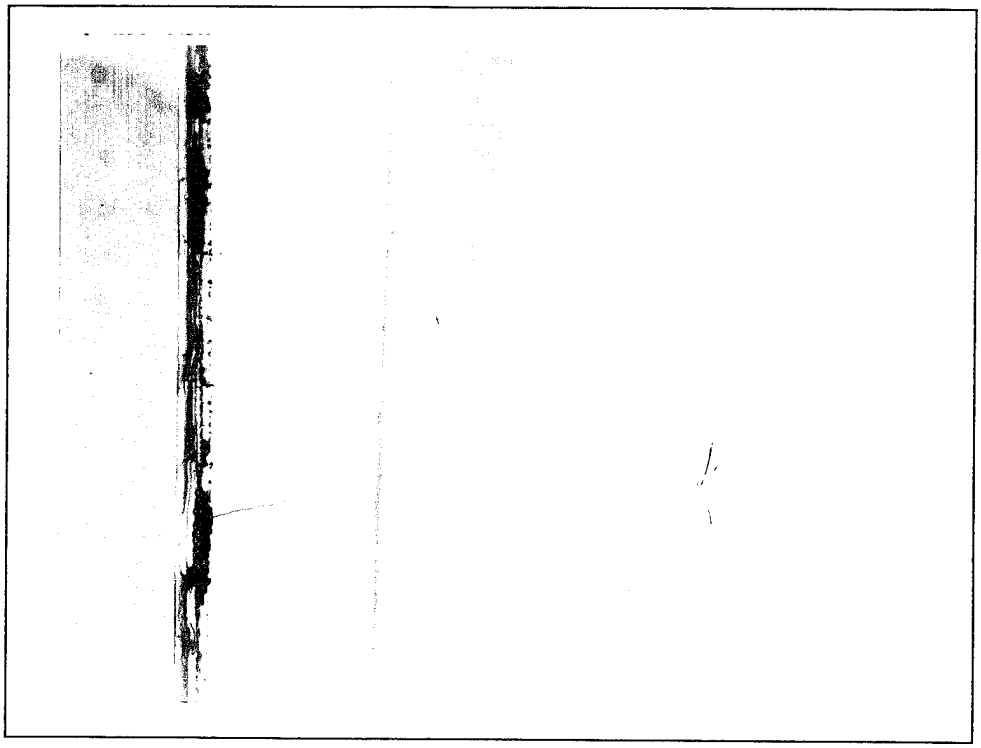

Figure 38. Tension-Compression ($R_\varepsilon = -1$) $\varepsilon_{max} = 0.5\%$: Fiber/Matrix Interface Damage (400X)

matrix cracks initiate from the debonded fiber/matrix interface region. The limited matrix cracking for the test conducted at a maximum strain of 0.5% explains the lack of modulus degradation that was shown in the modulus history (see Figure 18).

The tests conducted at a maximum strain of 0.4% and 0.325% both exhibited more matrix damage than the test conducted at a maximum strain of 0.5%. Each of the fracture surfaces was dominated by flat surfaces, which are indicative of matrix dominated failure; however, regions of fiber pullout and matrix necking were also present. Figure 39 shows a flat portion located on the specimen edge for the test conducted at a maximum strain of 0.325%. This flat shiny portion is evidence of brittle cleavage occurring in the material. Brittle cleavage is caused by the breaking of atomic bonds of the material and is generally

caused by crack propagation through the matrix [2]. Figure 40 shows fatigue striations on the fracture surface for the test conducted at a maximum strain of 0.325%. This figure shows advancing matrix cracks with fatigue striations growing in a number of different directions. Fatigue striations were also found on the fracture surface of the test conducted at a maximum strain of 0.4%.

Figures 41 and 42 show the sectioned specimens along the longitudinal direction for both tests conducted at a maximum strain of 0.4% and 0.325%. Both figures reveal matrix cracking along with fiber bridging. Fiber bridging occurs when a matrix crack reaches a fiber and propagates around the fiber into the matrix again. The disruption of the fiber/matrix interface region leads to fiber/matrix debonding. Matrix cracks originated from the specimen edge and the debonded fiber/matrix interface region for both these strain levels. The matrix crack density for the test conducted at a maximum strain of 0.325% was much higher than either of the other two tests and explains the large drop in modulus shown in Figure 18. The extensive matrix damage in the test conducted at a maximum strain of 0.325% also explains the large reduction in maximum stress over the final half of the fatigue life shown in Figure 20.

The tension-compression strain control tests exhibited similar failure and damage mechanisms when compared to the corresponding tests conducted under the load control mode. Kraabel reported matrix dominated failure below a strain range of 0.85% [12], while matrix dominated failure was seen in this study below a strain range of 0.8%. This indicates that damage and failure mechanisms of the MMC are independent of control mode under tension-compression loadings.

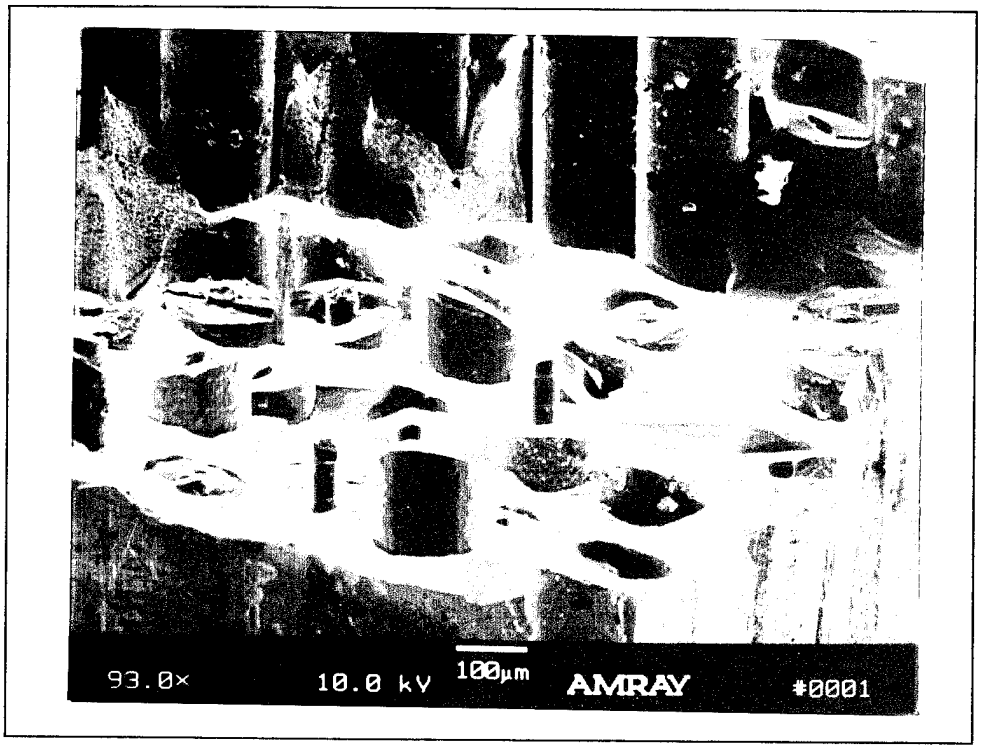

Figure 39. Tension-Compression ($R_\varepsilon = -1$) $\varepsilon_{max} = 0.325\%$: Flat Portion of Fracture Surface

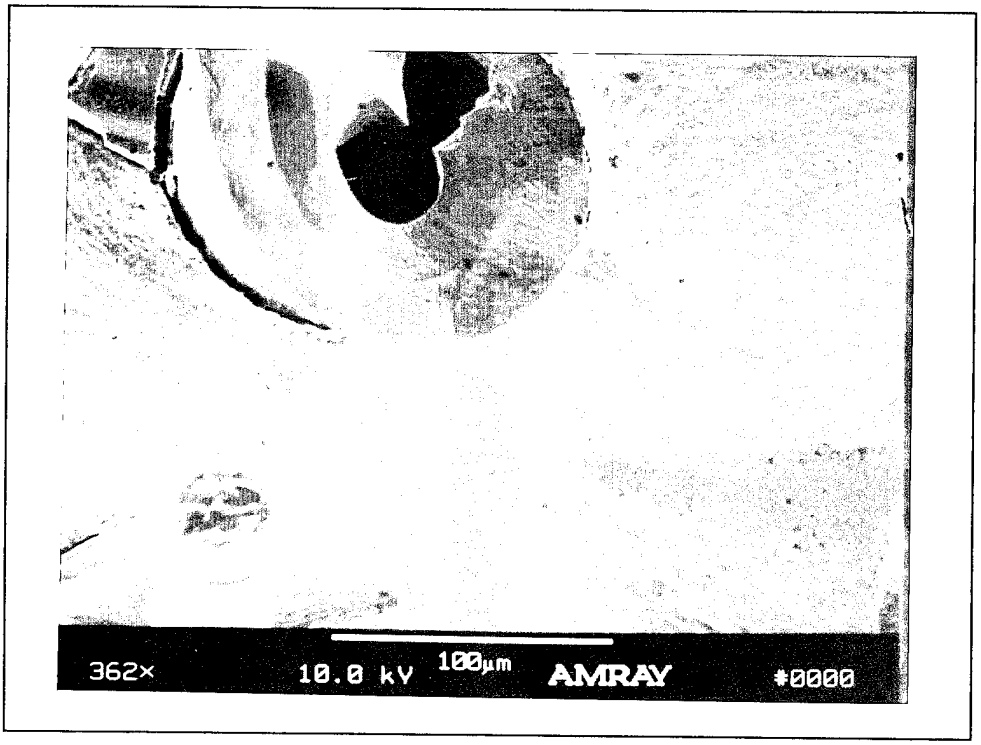

Figure 40. Tension-Compression ($R_\varepsilon = -1$) $\varepsilon_{max} = 0.325\%$: Matrix Cracks and Fatigue Striations

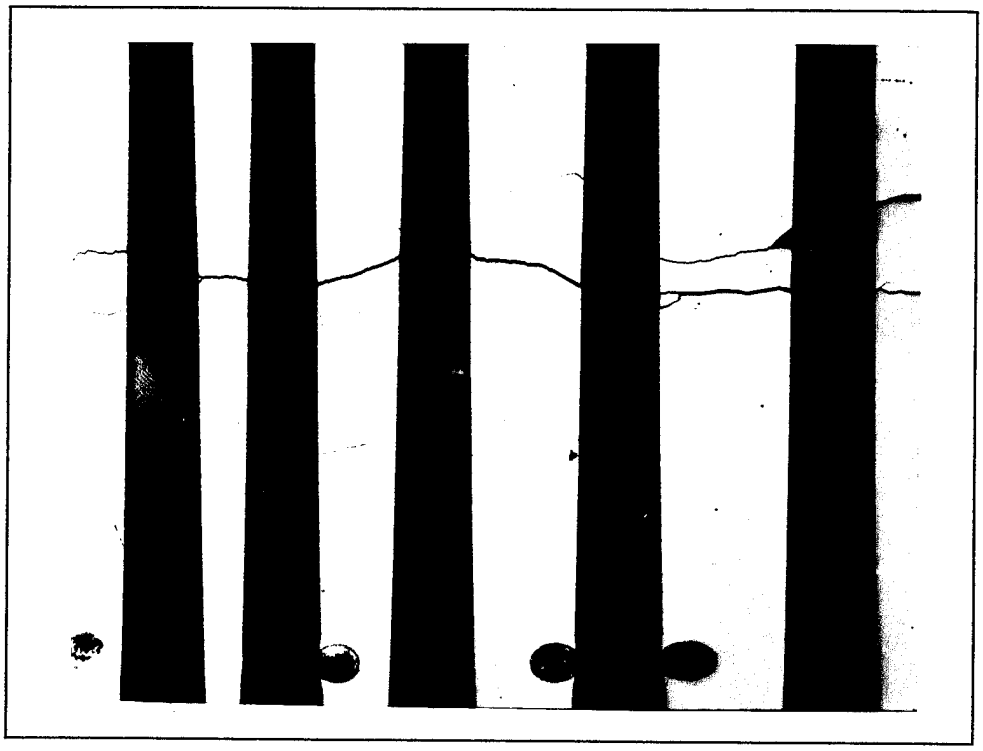

Figure 41. Tension-Compression ($R_\varepsilon = -1$) $\varepsilon_{max} = 0.4\%$: Matrix Cracks and Fiber Bridging (100X)

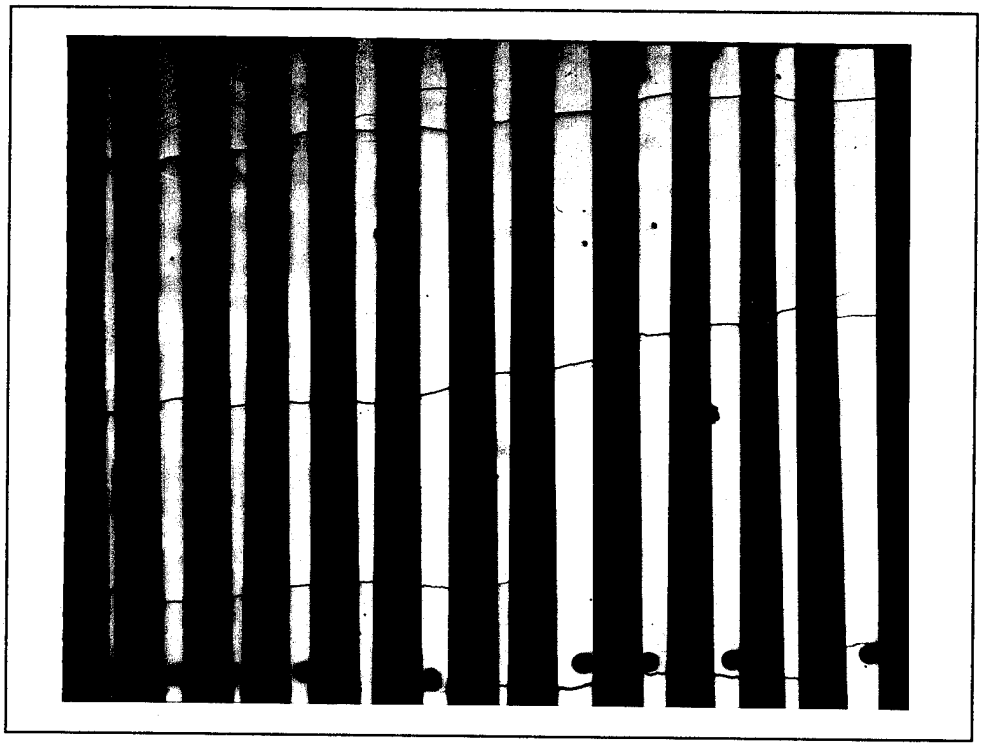

Figure 42. Tension-Compression ($R_\varepsilon = -1$) $\varepsilon_{max} = 0.325\%$: Extensive Fiber Bridging (50X)

4.2.1.2 Tension-Tension ($R_\varepsilon = 0$)

The tests conducted at a maximum strain of 0.6% and 0.5% both exhibited fiber dominated failure. The fracture surfaces, along with the sectioned specimens revealed fiber pullout and fiber cracking respectively. Figure 43 shows a portion of the fracture surface for the test conducted at a maximum strain of 0.6% which consists of fiber pullout resulting in matrix necking. The fracture surfaces of both of these tests were dominated by regions of fiber pullout.

Figures 44 and 45 show the sectioned regions of both specimens, along the longitudinal direction. The sectioned specimens revealed fiber cracking in both tests with no visible matrix cracks. Both sectioned specimens revealed similar fiber crack densities. Regions of fiber/matrix debonding were also present; however, the debonded regions were not matrix crack initiation sites. The lack of matrix damage explains the absence of any degradation in the modulus for both of these tests (see Figure 21).

Figure 46 shows the sectioned specimen along the longitudinal direction for the test conducted at a maximum strain of 0.4%. The sectioned specimen revealed short matrix cracks and areas of fiber cracking. Figure 46 reveals fiber cracks that led to debonding of the fiber/matrix interface region. These debonded regions did serve as matrix crack initiation sites which was not the case with the other two tests at higher maximum strain levels. The matrix damage that was shown in Figure 46 explains the reduction in maximum stress near the end of the fatigue life for this specimen (see Figure 22).

Figure 43. Tension-Tension ($R_\varepsilon = 0$) $\varepsilon_{max} = 0.6\%$: Fiber Pullout on Fracture Surface

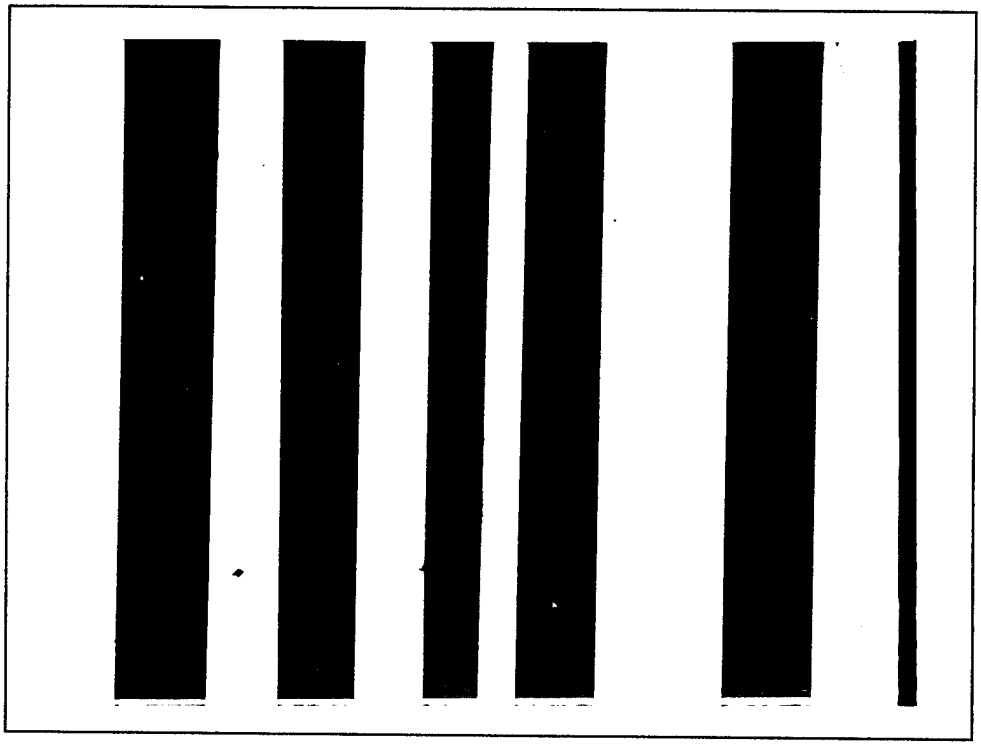

Figure 44. Tension-Tension ($R_\varepsilon = 0$) $\varepsilon_{max} = 0.6\%$: 0° Fiber Cracks (100X)

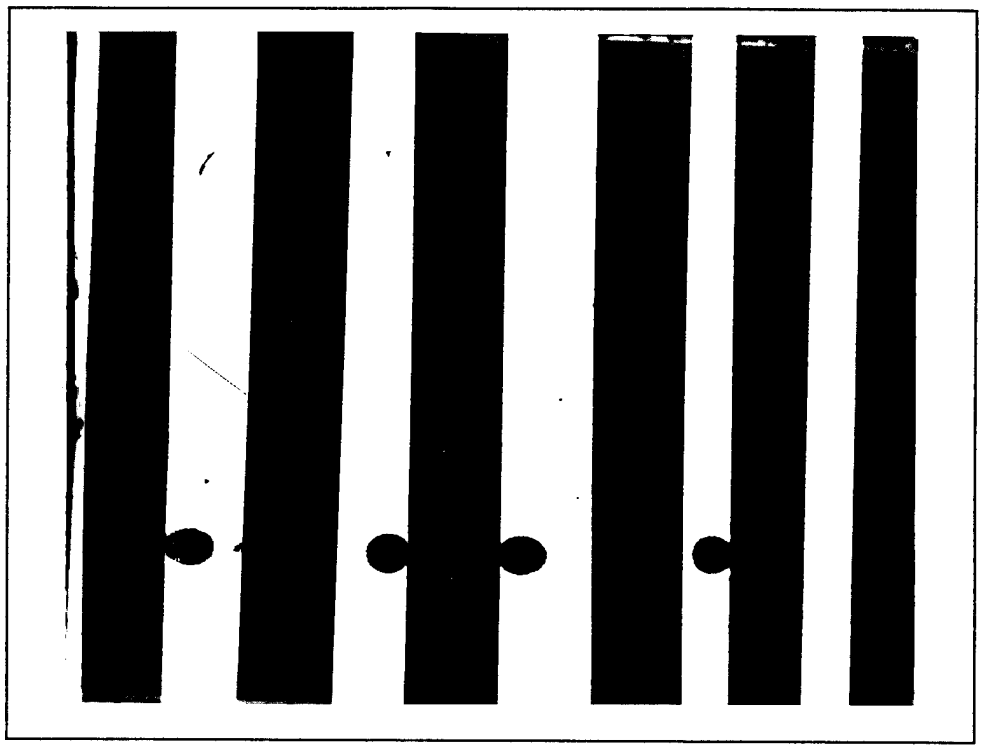

Figure 45. Tension-Tension ($R_\varepsilon = 0$) $\varepsilon_{max} = 0.5\%$: 0° Fiber Cracks (100X)

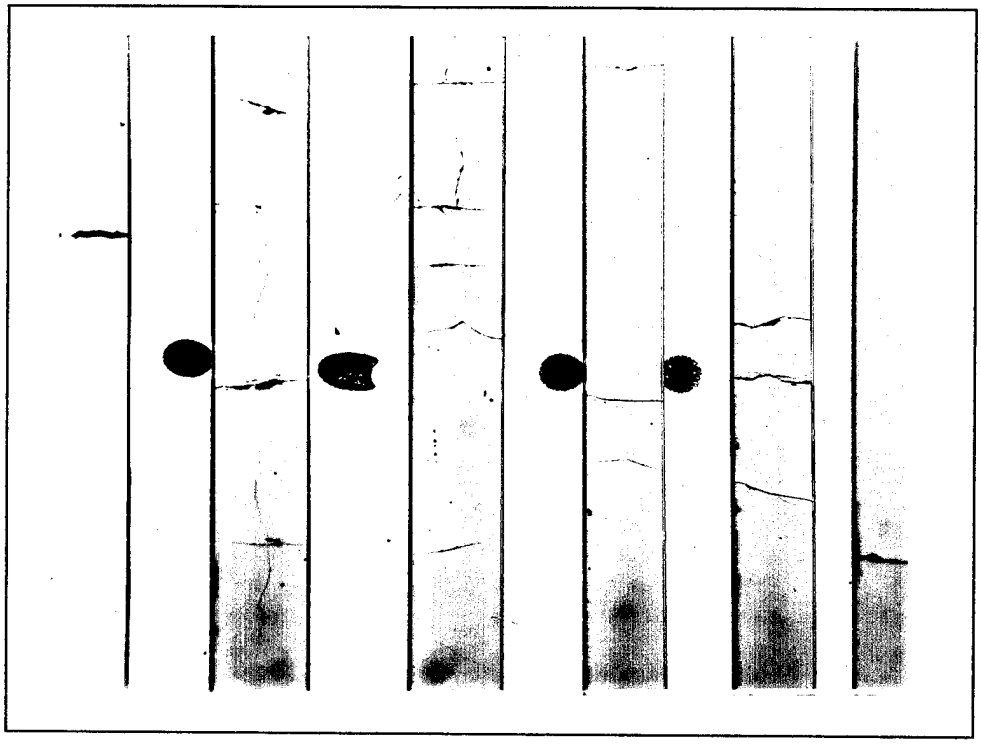

Figure 46. Tension-Tension ($R_\varepsilon = 0$) $\varepsilon_{max} = 0.4\%$: 0° Fiber Cracks and Short Matrix Cracks (100X)

A comparison with the test conducted at a maximum strain of 0.4% at $R_\varepsilon = -1$ reveals similar damage mechanisms. Both tests revealed matrix cracking; however, the density of matrix cracks was greater for the test conducted at $R_\varepsilon = -1$ (see Figures 41 and 46). The increased matrix crack density is a result of the larger strain range at $R_\varepsilon = -1$ and the reduced maximum matrix stress and matrix stress range at $R_\varepsilon = 0$.

A comparison with load control tests conducted at $R_\sigma = 0.1$ revealed similar damage mechanisms. Majumadar and Lerch reported that failure was fiber dominated above a strain range of 0.5% and matrix dominated below that strain range [16]. This corresponds with the damage mechanisms and failure trends for the strain control tests conducted at $R_\varepsilon = 0$ in this study. This suggests that the damage and failure mechanisms for this MMC are independent of control mode for tension-tension $R_\varepsilon = 0$ loadings.

4.2.1.3 Tension-Tension ($R_\varepsilon = 0.5$)

The tests conducted at a maximum strain of 0.7% and 0.6% both exhibited fiber dominated failure mechanisms; however, some matrix cracking was present. Figure 47 shows the fracture surface for the test conducted at a maximum strain of 0.7%. Both fracture surfaces contained regions of fiber pullout and matrix ductility, although flat portions containing fatigue striations were found on both fracture surfaces. Figure 48 shows a region of the fracture surface for the test conducted at a maximum strain of 0.6%, where matrix cracking, along with fatigue striations are visible.

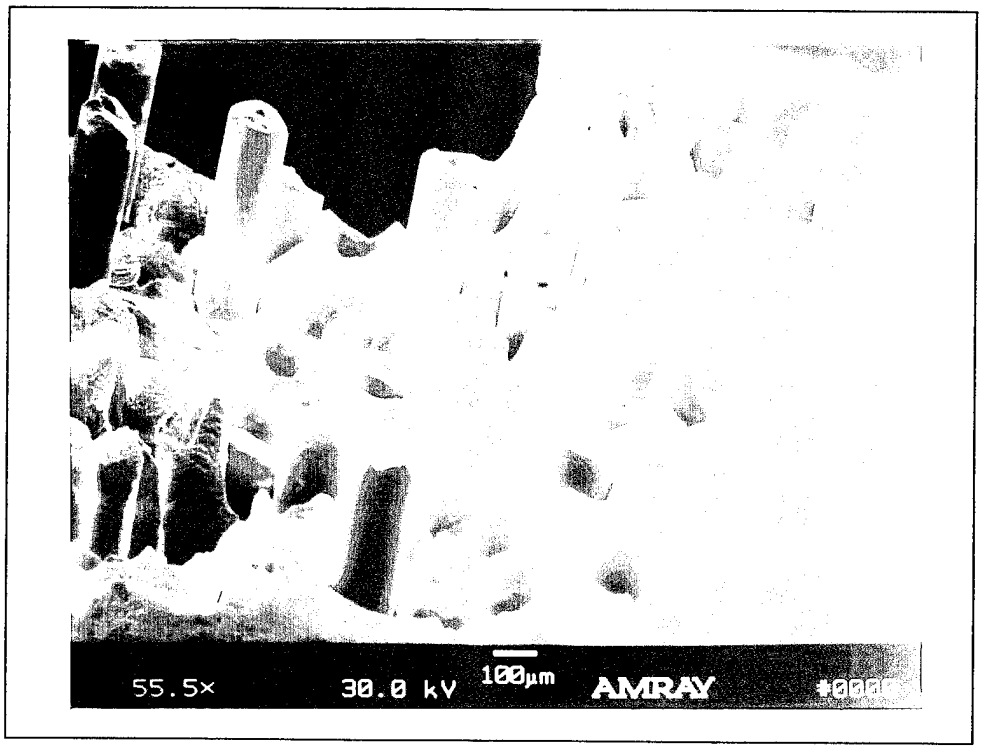

Figure 47. Tension-Tension ($R_\varepsilon = 0.5$) $\varepsilon_{max} = 0.7\%$: Fiber Pullout on Fracture Surface

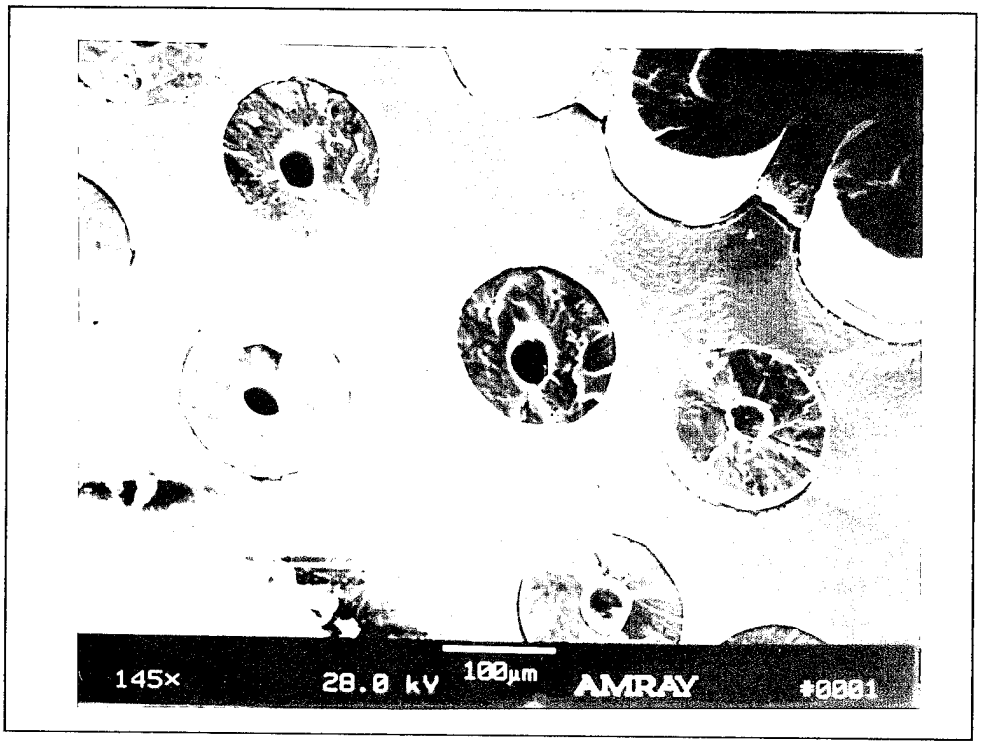

Figure 48. Tension-Tension ($R_\varepsilon = 0.5$) $\varepsilon_{max} = 0.6\%$: Matrix Cracking and Fatigue Striations

The sectioned specimen along the longitudinal direction for both tests conducted at a maximum strain of 0.75% revealed fiber cracking with matrix cracks. Figure 49 shows the outside view of the large crack that developed in the interrupted test. The crack extends approximately half way across the specimen and explains the large drop in modulus from Figure 23. Figure 50 shows the sectioned specimen with the single matrix crack described above. Additional matrix cracking, along with fiber cracks are also visible in Figure 50. The short matrix cracks originated from the debonded fiber/matrix interface region while the dominant matrix crack originated along the same plane as the molyweave. The dominant matrix crack propagated through the matrix, causing fibers to break behind the advancing crack tip. Figure 51 shows the sectioned specimen from the second test conducted at the same maximum strain level. Like the first test, it reveals matrix cracks that bridged several fibers. The matrix damage found in both tests conducted at a maximum strain of 0.75% reveals that the reduction in modulus and maximum stress shown in Figures 23 and 26 was caused by matrix cracking.

The strain control tests conducted at $R_\varepsilon = 0.5$ revealed more matrix damage when compared to the tests conducted at $R_\varepsilon = 0$. The test conducted at a maximum strain of 0.6% at $R_\varepsilon = 0$ was dominated by fiber failure (see Figures 43 and 44) while the same maximum strain level at $R_\varepsilon = 0.5$ revealed matrix cracking (see Figure 48). This indicates that the increased fatigue life for tests conducted at $R_\varepsilon = 0.5$ when compared to tests conducted at $R_\varepsilon = 0$ results in the development of matrix cracks as discussed previously in section 4.1.1.3. The increased mean matrix stress during the early portions of the fatigue

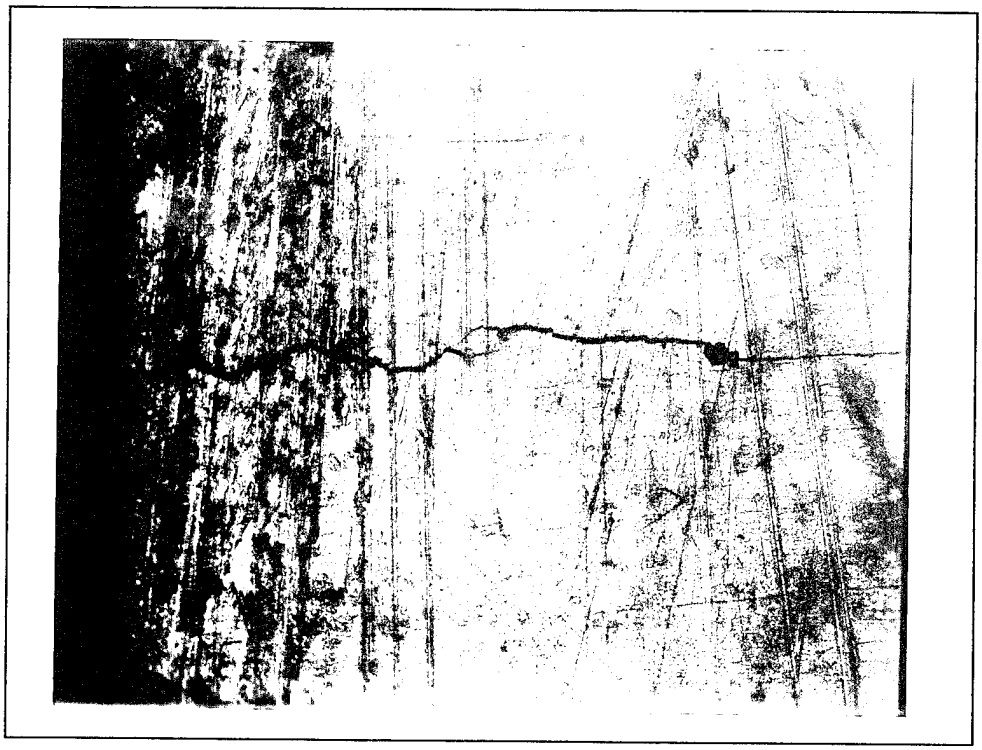

Figure 49. Tension-Tension ($R_\varepsilon = 0.5$) $\varepsilon_{max} = 0.75\%$: Large Specimen Crack (2X)

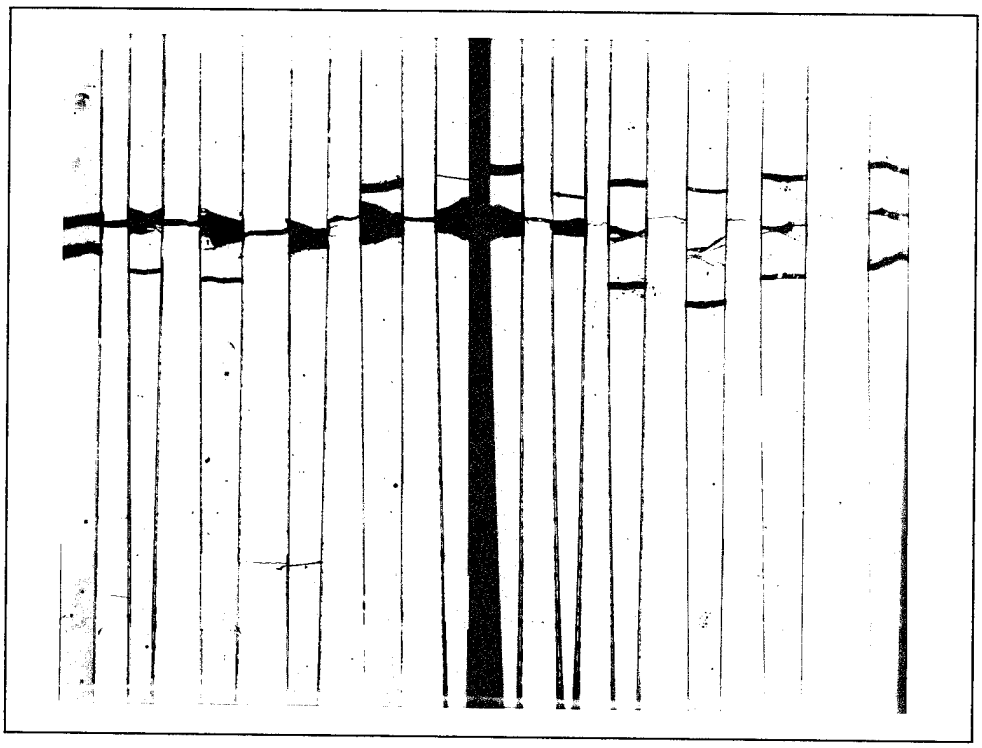

Figure 50. Tension-Tension ($R_\varepsilon = 0.5$) $\varepsilon_{max} = 0.75\%$: Fiber Bridging and Fiber Cracking (50X)

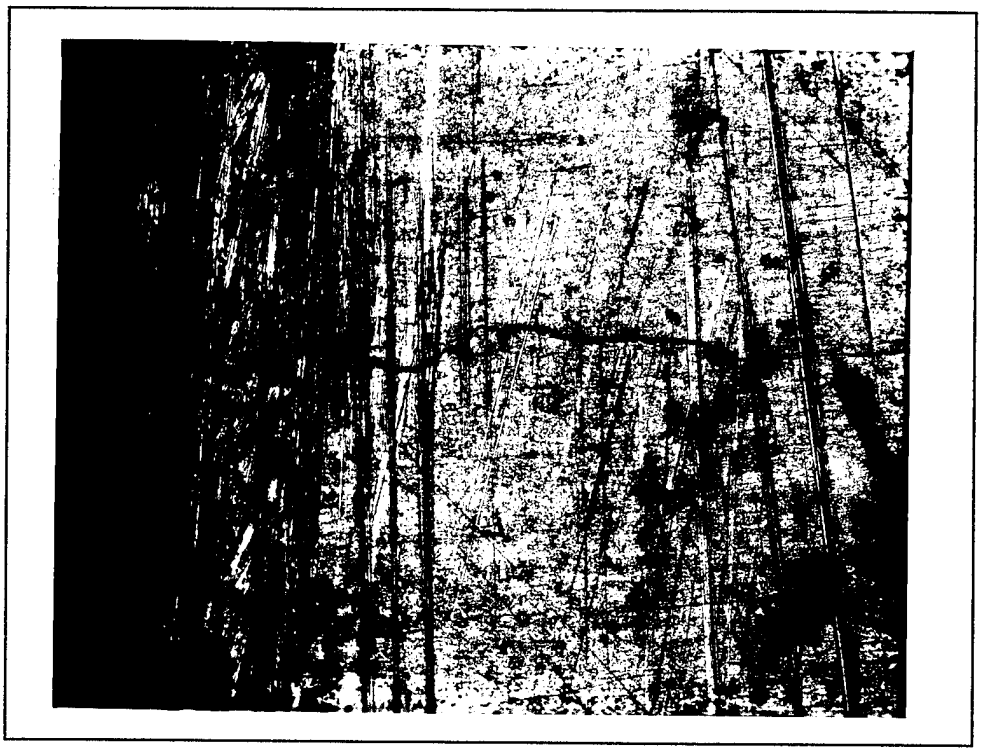

Figure 49. Tension-Tension ($R_\varepsilon = 0.5$) $\varepsilon_{max} = 0.75\%$: Large Specimen Crack (2X)

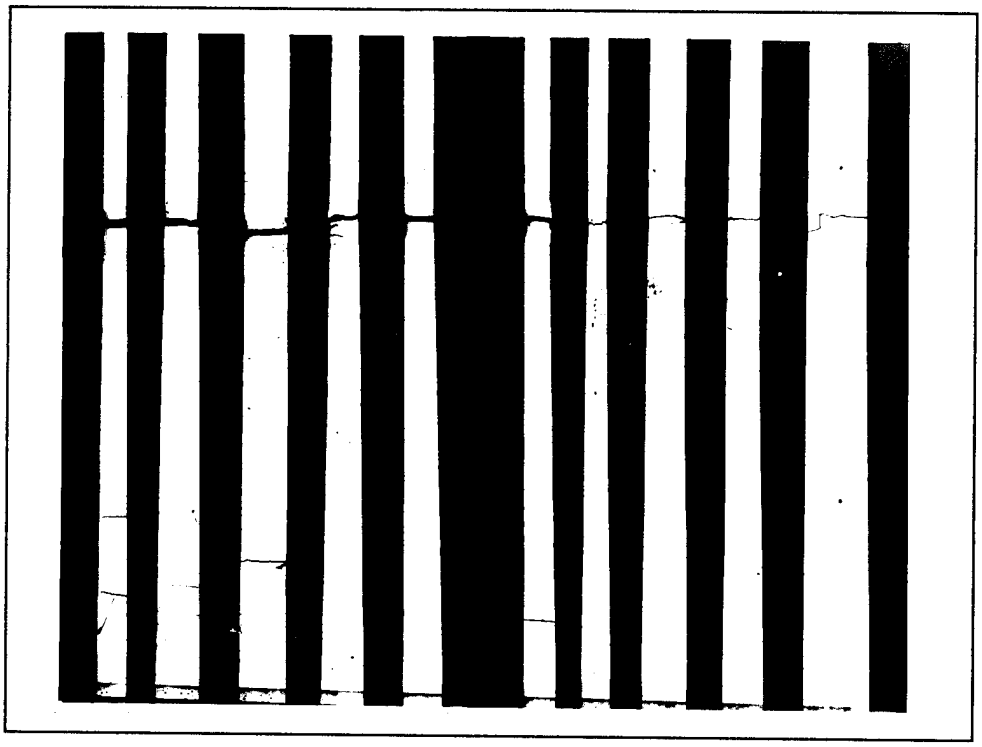

Figure 50. Tension-Tension ($R_\varepsilon = 0.5$) $\varepsilon_{max} = 0.75\%$: Fiber Bridging and Fiber Cracking (50X)

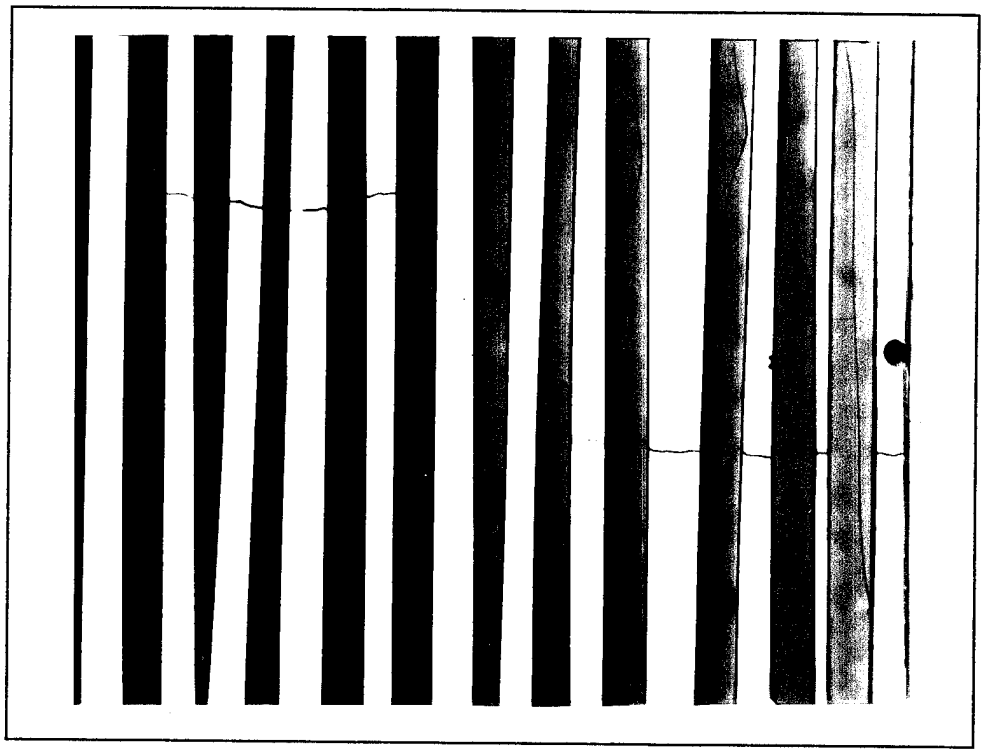

Figure 51. Tension-Tension ($R_\varepsilon = 0.5$) ε_{max} =0.75%: Fiber Bridging and Matrix Cracking (Repeated Test) (50X)

life may also cause the matrix damage for the test conducted at $R_\varepsilon = 0.5$ (see Figure 28). The difference in damage mechanisms between the two strain ratios explains the different modulus trends shown in Figure 24.

4.2.2. Load Control Mode

4.2.2.1 Tension-Tension ($R_\sigma = 0.5$)

The tests conducted at a maximum stress of 1300 MPa and 1150 MPa (Group 1) both exhibited fiber dominated failure. The fracture surfaces for both specimens showed no signs of matrix cracking and consisted of fiber pullout and matrix necking which can be

seen in Figure 52. The sectioned specimens along the longitudinal direction for both tests revealed extensive fiber cracking with no matrix cracks. Figure 53 shows a region of the sectioned specimen for the test conducted at a maximum stress of 1150 MPa. Both sectioned specimens contained a high density of fiber cracks caused by matrix creep. Areas of fiber/matrix debonding are also present in Figure 53. The damage mechanisms (fiber dominated failure) for specimens that comprise Group 1 explain the lack of modulus reduction and constant strain range which are shown in Figures 29 and 33.

The tests conducted at a maximum stress of 1000 MPa and 900 MPa (Group 2) contained a mixture of fiber and matrix failure. Both fracture surfaces showed evidence of matrix cracking, along with fiber pullout. Figure 54 reveals a large flat area for the test conducted at a maximum stress of 1000 MPa where matrix cracking occurred. Figure 55 shows a region on the fracture surface for the test conducted at a maximum stress of 900 MPa where both matrix cracking (flat region) and fiber pullout (leading to matrix necking) are found. The flat portions on the fracture surfaces were also on the same plane as the molyweave, demonstrating that the molyweave is an excellent fiber and matrix crack initiation site.

The sectioned specimens for both tests in Group 2 revealed similar trends. Both specimens contained areas of fiber cracking, along with matrix cracks. A representative region of the 1000 MPa specimen is shown in Figure 56. Fiber bridging was found in both tests and was limited to three or four fibers. The majority of matrix cracks found in these tests initiated from the edge of the specimen; however, some matrix cracks did originate from the fiber/matrix debonded region which can be seen in Figure 56. The matrix

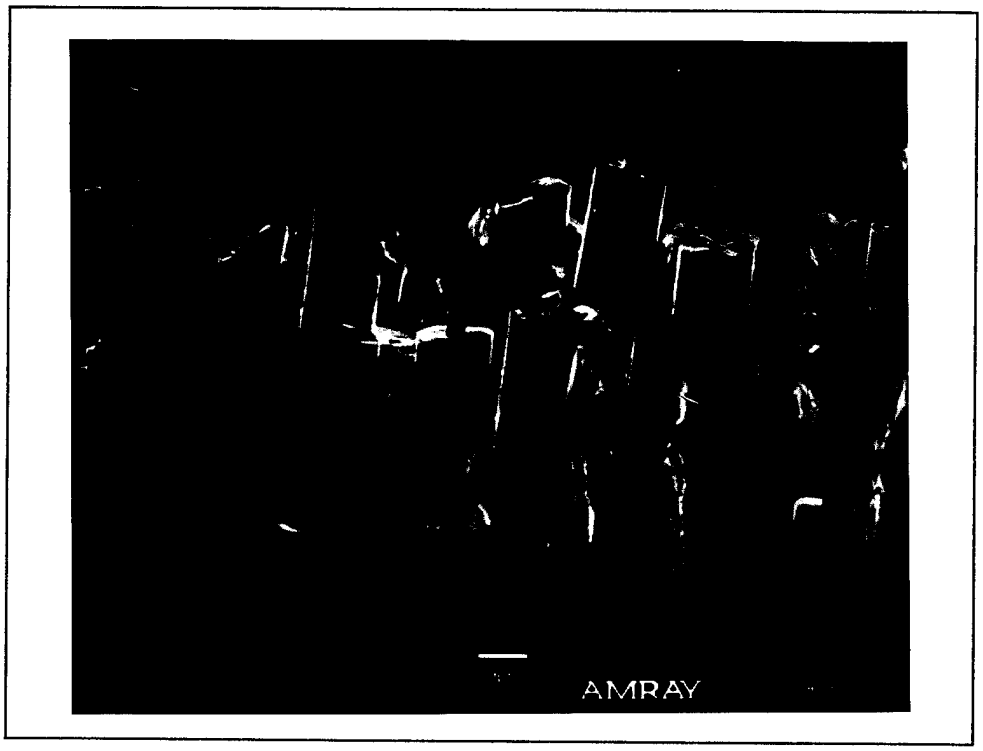

Figure 52. Tension-Tension ($R_\sigma = 0.5$) σ_{max} = 1300 MPa: Fiber Pullout on Fracture Surface

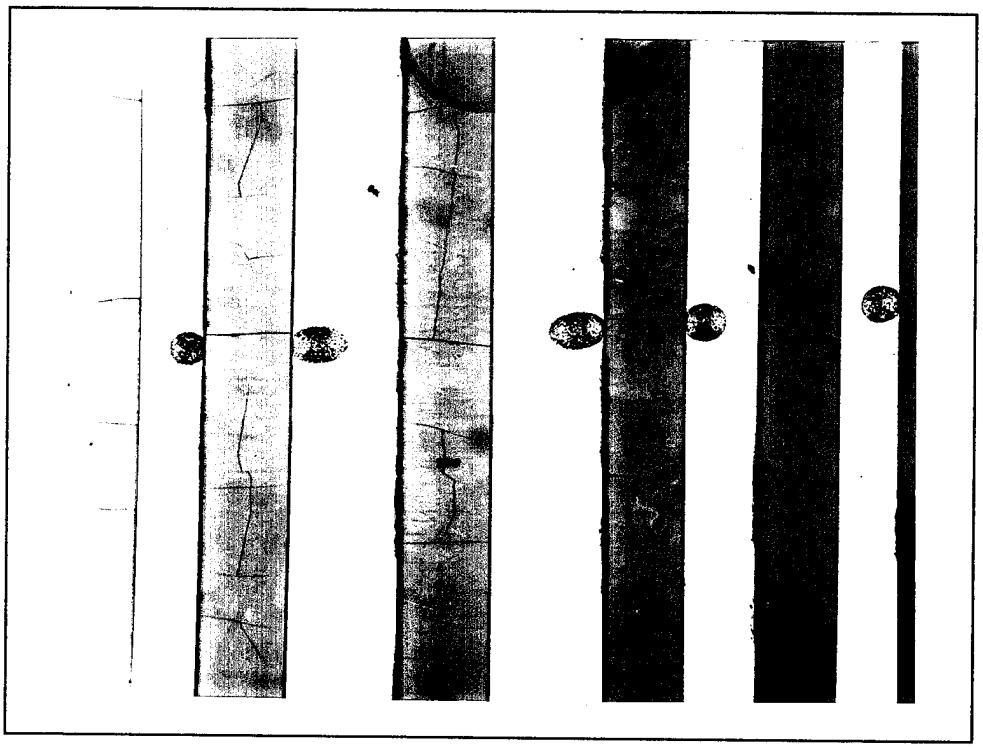

Figure 53. Tension-Tension ($R_\sigma = 0.5$) σ_{max} = 1150 MPa: 0° Fiber Cracks (100X)

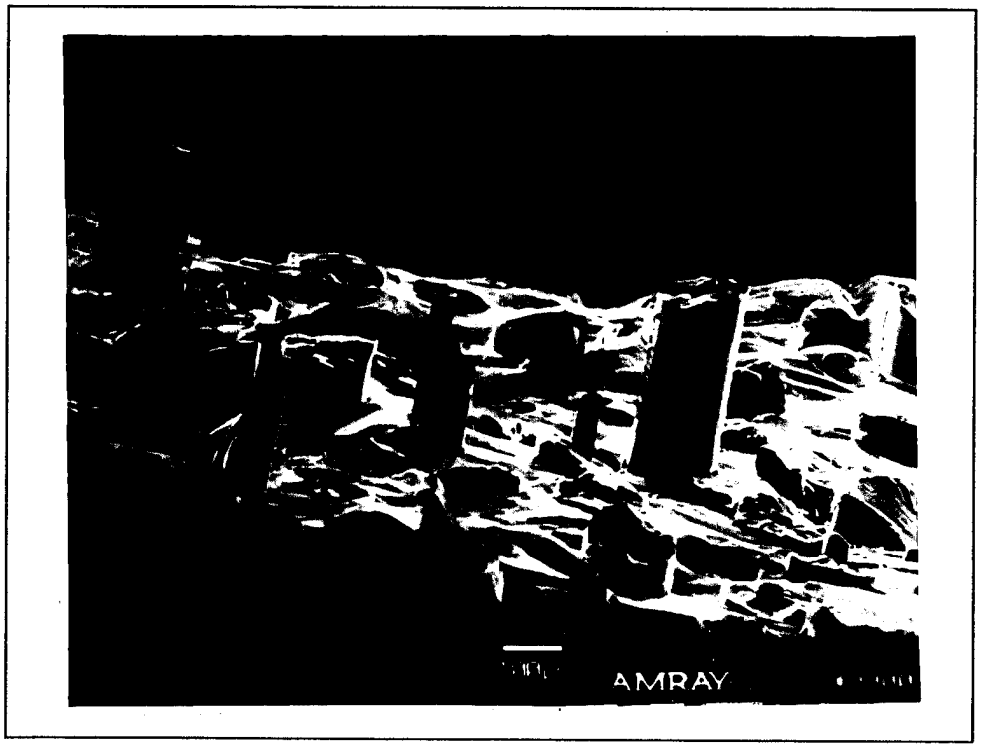

Figure 54. Tension-Tension ($R_\sigma = 0.5$) σ_{max} = 1000 MPa: Flat Portion of Fracture Surface

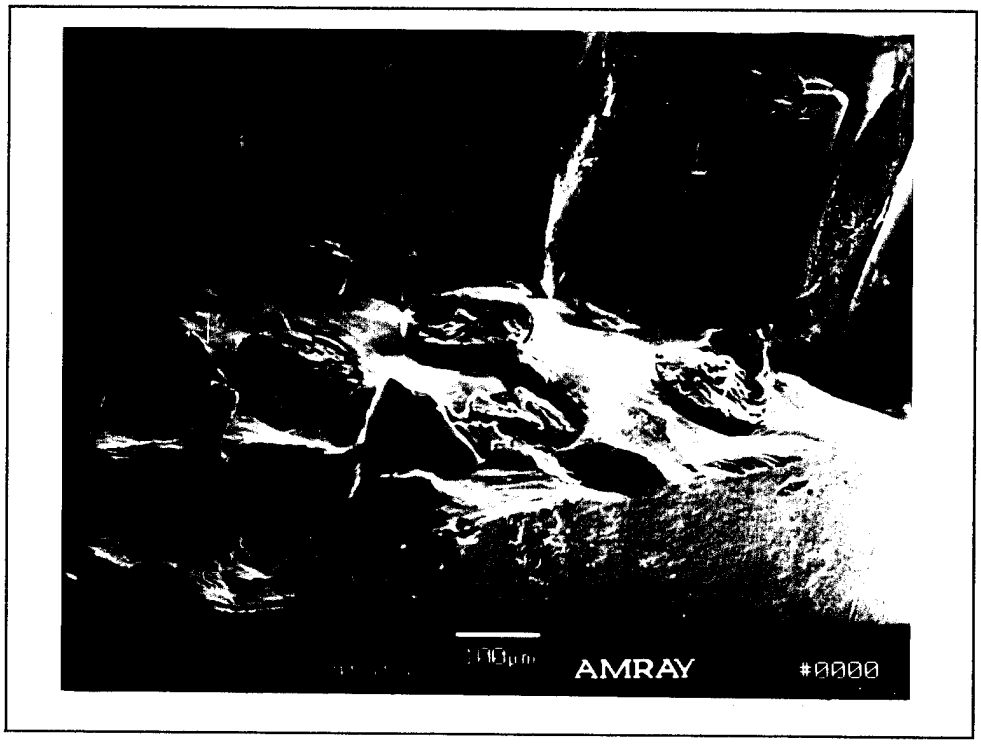

Figure 55. Tension-Tension ($R_\sigma = 0.5$) σ_{max} =900 MPa: Fracture Surface

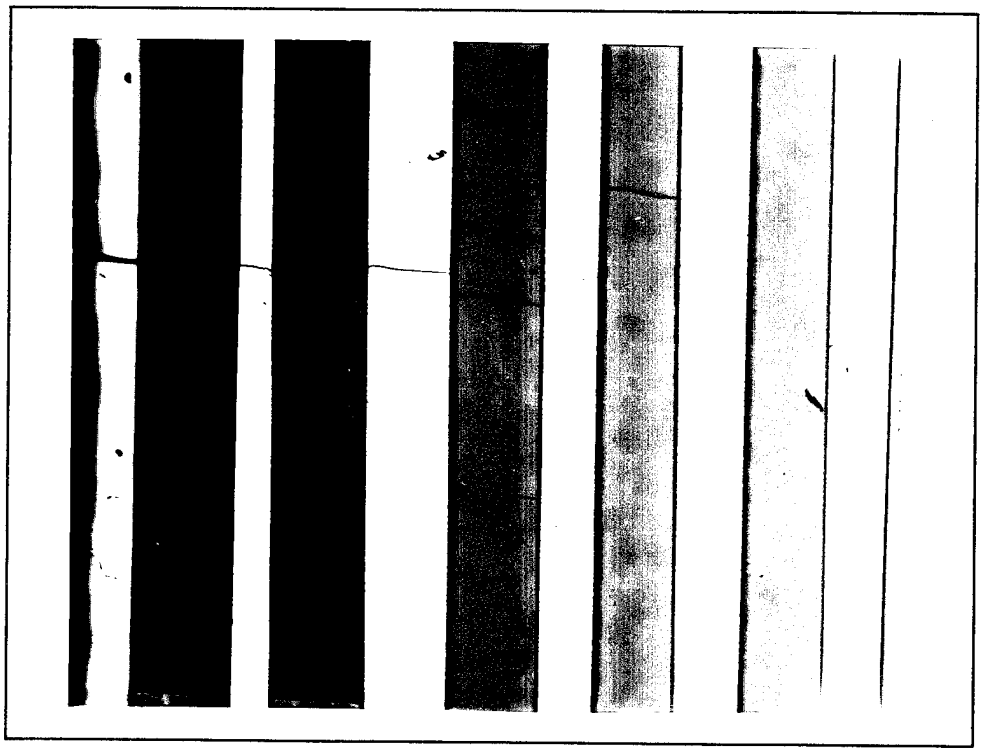

Figure 56. Tension-Tension ($R_\sigma = 0.5$) σ_{max} = 1000 MPa: 0° Fiber and Matrix Cracking (100X)

damage found in the specimens that comprise Group 2 explain the modulus reduction and increase in strain range that is shown in Figures 29 and 33.

A comparison between the tests conducted at 1000 MPa for $R_\sigma = 0.5$ and $R_\sigma = 0.1$ [12] reveal different damage mechanisms. The test conducted at $R_\sigma = 0.5$ contained a mixture of fiber and matrix cracking (see Figure 56) while the test conducted at $R_\sigma = 0.1$ was dominated by fiber failure [12]. The matrix damage for the test conducted at $R_\sigma = 0.5$ is caused by the increased fatigue life when compared to tests conducted at $R_\sigma = 0.1$. The

higher mean matrix stress for the test conducted at $R_\sigma = 0.5$ when compared to the test conducted at $R_\sigma = 0.1$ may also cause the matrix damage. The different damage mechanisms between the two stress ratios explains the different modulus trends shown in Figure 31.

A comparison of the damage mechanisms for strain and load control tests conducted at R = 0.5 reveals how matrix creep affects the damage mechanisms under load control at high stress levels (see Figures 48 and 53). The damage mechanisms for the test conducted at a maximum stress of 1150 MPa (0.3% strain range) when compared with the strain control test conducted at the same strain range ($\varepsilon_{max} = 0.6\%$) are different. The load control test was dominated by fiber failure (see Figure 53) while the strain control tests contained a mixture of fiber and matrix damage (see Figure 48). This indicates that matrix creep occurring under the load control mode causes fiber failure and reduces the fatigue life. The different damage mechanisms between the two control modes explains the different modulus trends shown in Figure 30.

4.3 $[0/90]_{2S}$ Discussion

Three additional tests were conducted under the strain control mode at $R_\varepsilon = 0$ for the cross-ply lay-up. The purpose of these tests was to compare the fatigue response between previous tests completed under the load and strain control mode for the cross-ply lay-up at different stress and strain ratios. This enabled fatigue life comparisons to be

made between the unidirectional and cross-ply lay-ups. These results are presented in Chapter 5.

This study has shown that for tests conducted at $R_\varepsilon = 0$ and $R_\varepsilon = -1$, the failure and damage mechanisms are independent of control mode for the unidirectional lay-up. A comparison of tension-compression tests ($R = -1$) for the cross-ply lay-up under both the load and strain control modes reveals similar damage mechanisms when compared on a strain range basis [1,5]. Based on the trends found for the unidirectional lay-up tested in this study and in previous cross-ply studies conducted at $R = -1$ [1,5], it is expected that the fatigue damage mechanisms that were present in the cross-ply specimens tested in this study, at $R_\varepsilon = 0$, will the same as those found under the load control mode at the same stress ratio [1]. The measured macro-mechanical responses for the three tests are presented in Appendix A.

5. Fatigue Life Discussion and Analysis

The purpose of this chapter is to present and analyze the fatigue life of the MMC tested in this study. The goal of this research was to determine the effects of different stress/strain ratios on fatigue life. The fatigue lives for the tests conducted under the strain control mode will be compared on both a maximum strain and strain range basis. A direct comparison will then be made between the fatigue life for load and strain control modes at the three different stress/strain ratios. Comparisons of the fatigue life for a unidirectional. $[0]_8$,and cross-ply ,$[0/90]_{2S}$, laminates will also be presented. Finally, a Haigh diagram will be presented for the unidirectional lay-up for the tests conducted under both the load and strain control modes.

5.1 Fatigue Life: $[0]_8$

5.1.1 Maximum Strain Basis

Figure 57 shows the maximum strain versus fatigue life (ε-N) relationships for the three different strain ratios (R_ε) tested under the strain control mode. Figure 57 reveals that as R_ε increases the fatigue life increases for a given maximum strain value. For example, at a maximum strain of 0.5% , the fatigue life for the test conducted at $R_\varepsilon = -1$ is 6,995 cycles versus 33,095 for $R_\varepsilon = 0$. When comparing tests conducted at $R_\varepsilon = 0$ and $R_\varepsilon = 0.5$ the same trend is evident. The increase in fatigue life for increasing R_ε can be attributed to a number of different causes which are discussed next.

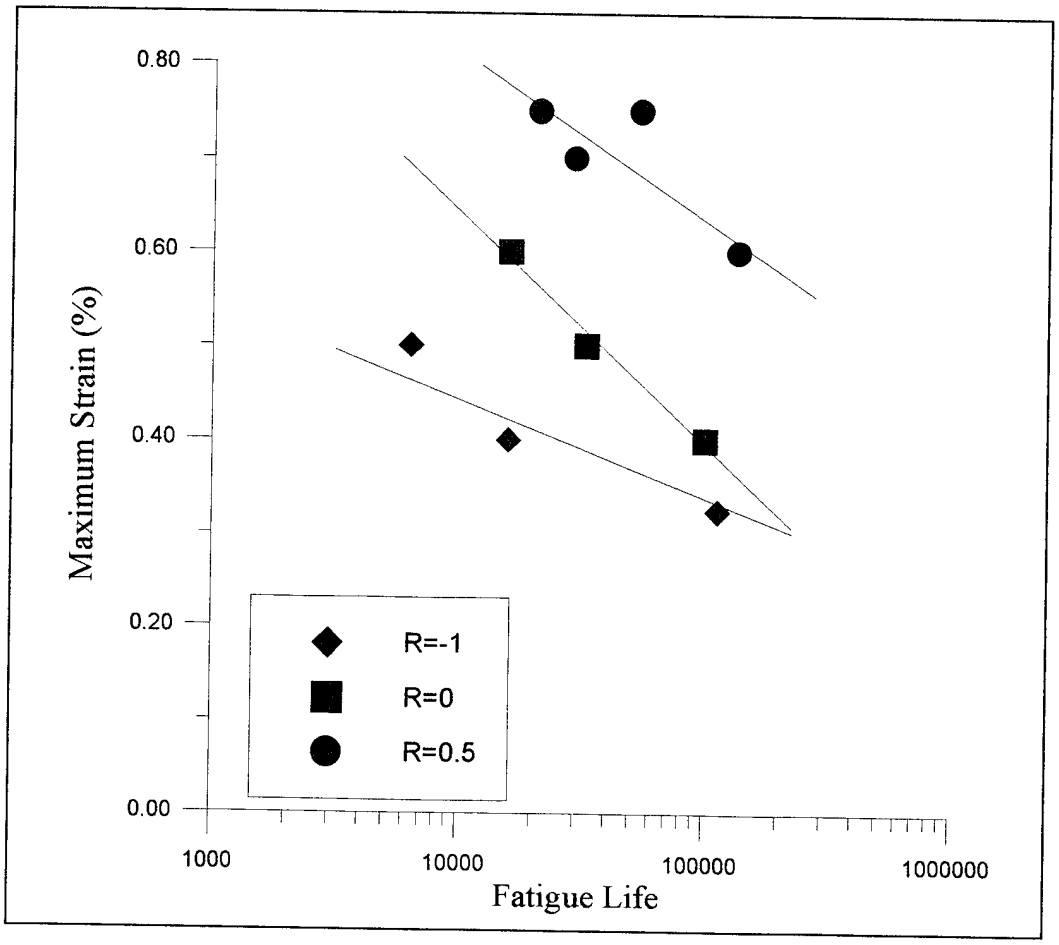

Figure 57. Strain Control Unidirectional Fatigue Life diagram: Maximum Strain

Matrix stress range plays an important role in governing fatigue life of the MMC. The Concentric Cylinder Model (CCM) developed by Sanders [24] and the Laminated composite Inelastic Solver (LISOL) developed by Robertson [22] were used to calculate the matrix stress range for three different strain ratios at a maximum strain of 0.6%. Both analytical models accounted for the residual thermal stresses in the fibers and matrix at 427°C. The analysis showed that the matrix stress range remains constant during fatigue

cycling so the matrix stress range on the first cycle was used. Matrix stress range will decrease if matrix damage occurs, however, these analytical tools do not contain any matrix damage models. Table 7 gives the matrix stress range for the tests conducted at a maximum strain of 0.6% along with the corresponding fatigue life. A test was not conducted at $R_\varepsilon = -1$ at a maximum strain of 0.6%; however, fatigue life data shows that the fatigue life should be less than 6,000 cycles (see Figure 57).

Table 7. $\varepsilon_{max} = 0.6\%$: Matrix Stress Range

Strain Ratio	Matrix Stress Range (MPa)	Fatigue Life
0.5	232	136,137
0	463	16,106
-1	927	<6,000

The results from Table 7 show that the increased matrix stress range as R_ε increases, results in decreased fatigue life at the same maximum strain level.

The fibers and fiber/matrix interface region also affect the fatigue life of the MMC. Gayda et. al. concluded that fibers, along with the fiber/matrix interface govern the fatigue life of the composite [7]. Kantoz and Telesman also found that the fiber/matrix interface region was the controlling factor that influenced fatigue crack propagation [10]. In this study microscopy revealed that the tests conducted at $R_\varepsilon = -1$ contained significant fiber/matrix interface debonding (see Figures 41 and 42) while less fiber/matrix debonding

was present in the tests conducted at $R_\varepsilon = 0$ (see Figures 45 and 46). Fiber/matrix debonded regions act as matrix crack nucleation sites and can reduce the effect of the fibers, negating any of their fatigue life benefits.

Figure 57 showed that as R_ε decreases fatigue life decreases when compared on a maximum strain basis. This decrease in fatigue life can be attributed a number of different causes. The increased matrix stress range as R_ε decreases, causes increased fatigue crack growth rates and decreased fatigue life. Also, the increased fiber/matrix debonding at $R_\varepsilon = -1$ also may attribute to the fatigue life difference between tension-tension and tension-compression testing when compared on a maximum strain basis.

5.1.2 Strain Range Basis

Figure 58 shows the fatigue life diagram for the three strain ratios tested under the strain control mode, and plotted on a strain range basis. Figure 56 reveals that as R_ε increases the slope of the ε-N curve decreases. When the fatigue life diagram is divided into regions based on failure mechanisms (see Figure 5), Region 2 (matrix dominated failure) experiences a decrease in slope. Previous studies have suggested that the fatigue life of the MMC is strain range dependent [1,12]. Therefore, the fatigue lives at all strain ratios should converge at the strain range that defines the fatigue limit of the MMC. The achievable strain range decreases as R_ε increases; therefore, the slope of the fatigue life

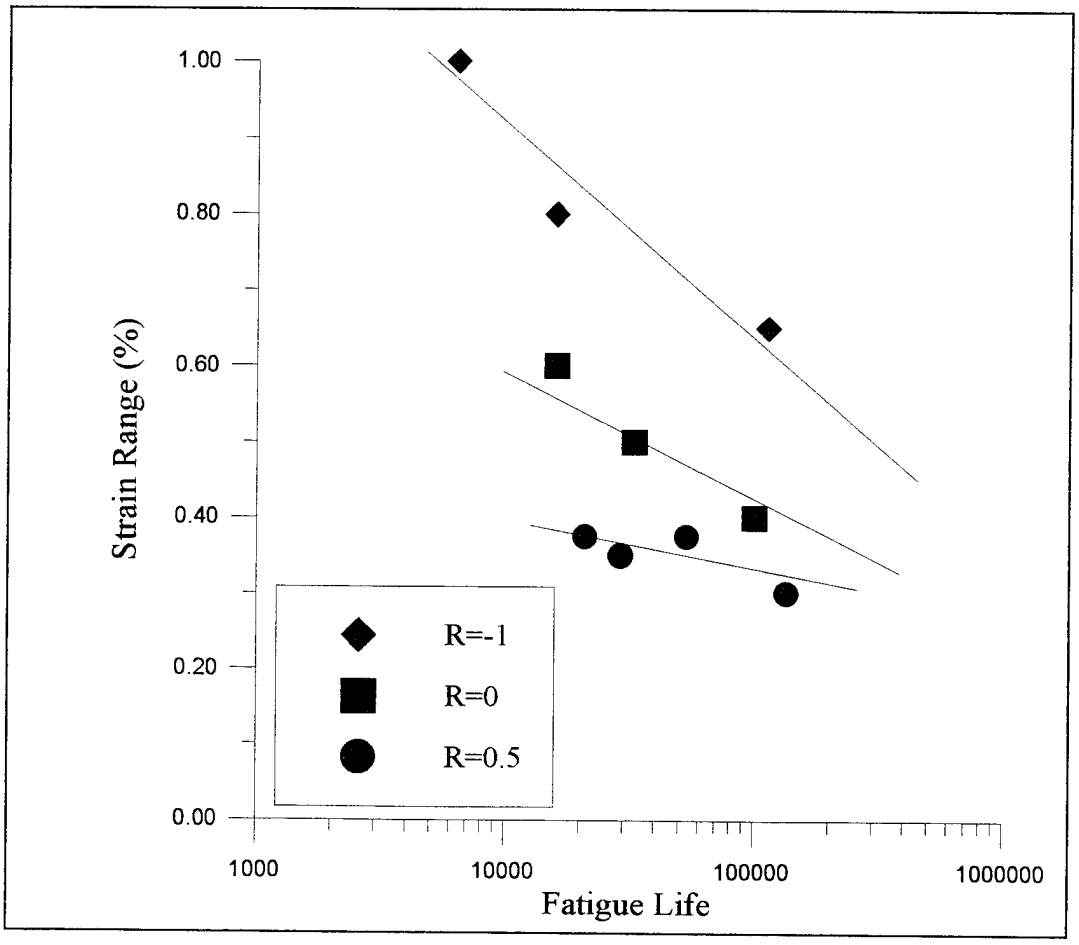

Figure 58. Strain Control Unidirectional Fatigue Life Diagram: Strain Range

curve must decrease as R_ε increases to converge at the strain range fatigue limit of the MMC.

Fatigue life shows opposite trends when compared on a strain range basis versus maximum strain. On a strain range basis the fatigue life decreases as R_ε is increased. For example, the test conducted at $R_\varepsilon = -1$ with a strain range of 0.65% results in a fatigue life of 113,710 cycles, while the test conducted at $R_\varepsilon = 0$ at a strain range of 0.6% results in a

fatigue life of 16,106 cycles. Similar relations exist between the tests conducted at $R_\varepsilon = 0$ and $R_\varepsilon = 0.5$.

The decrease in fatigue life as the strain ratio is increased can be explained by the tensile mean stress/strain in the specimen. With metallic materials, tensile mean stress/strain increases the crack propagation rate and reduces the fatigue life [11]. The tension-compression tests had a mean strain equal to zero while both tension-tension tests had positive mean strains, with the tests conducted at $R_\varepsilon = 0.5$ having the highest mean strains. Therefore, as mean stress/strain increases the fatigue life decreases, as Boyum suggested [1].

5.1.3 Fiber and Matrix Stress Analysis

In this section the fiber and matrix stresses were analyzed for the three strain ratios. Fiber and matrix stresses were determined for each of the three strain ratios and then plotted on an ε-N diagram to determine the fatigue life trends. Sanders' Concentric Cylinder Model (CCM) program [24] was used to compute the first cycle matrix and fiber stresses for the tests conducted at $R_\varepsilon = 0$ and $R_\varepsilon = 0.5$. The CCM program does not analyze tension-compression testing; therefore, the first cycle fiber and matrix stresses for the tests conducted at $R_\varepsilon = -1$ were found using the LISOL program developed by Robertson [22]. Both the CCM and LISOL models accounted for the residual thermal stresses in the fiber and matrix at 427°C.

Figures 59 and 60 show the fatigue life diagrams compared on a fiber and matrix stress range basis. These figures show that the fatigue lives do not collapse onto a single curve, but layer into three distinct curves based on R_ε. This analysis shows that the fiber and matrix stresses can be used to make fatigue life comparisons for the same strain ratio. However, any attempt to collapse different strain ratios onto a single curve must explore the complex interaction between the fiber stresses, matrix stresses and R_ε.

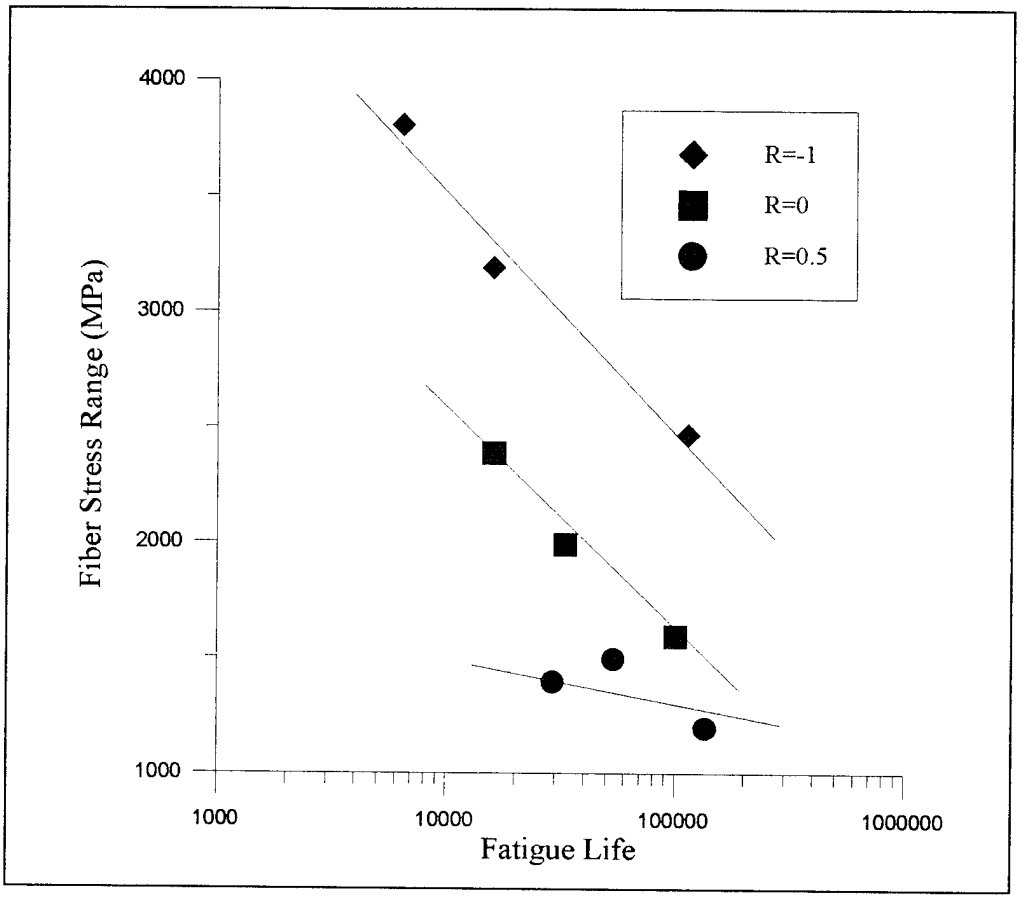

Figure 59. Strain Control Unidirectional Fatigue Life Diagram: Fiber Stress Range

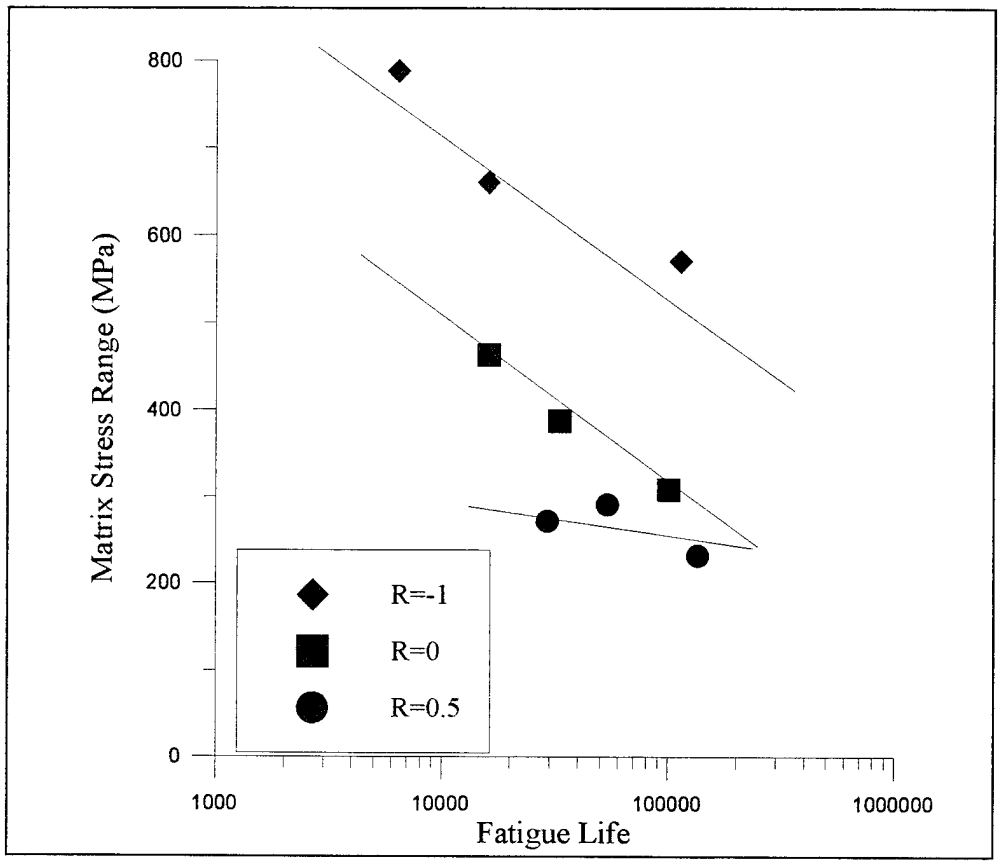

Figure 60. Strain Control Unidirectional Fatigue Life Diagram: Matrix Stress Range

5.1.4 Load Control and Strain Control Comparison

The majority of previous fatigue research conducted for MMCs have employed the load control mode. This research, therefore, allows for a direct comparison between tests conducted under both the load and strain control modes at the three different stress/strain ratios. Load control fatigue life data for the tests conducted at $R_\sigma = 0.1$ and $R_\sigma = -1$ were obtained from previous studies [1,8,12] and were combined to the load control tests conducted at $R_\sigma = 0.5$ in this study. Figures 61 and 62 show the fatigue life trends of the unidirectional lay-up under the load control mode at three different stress ratios. On a

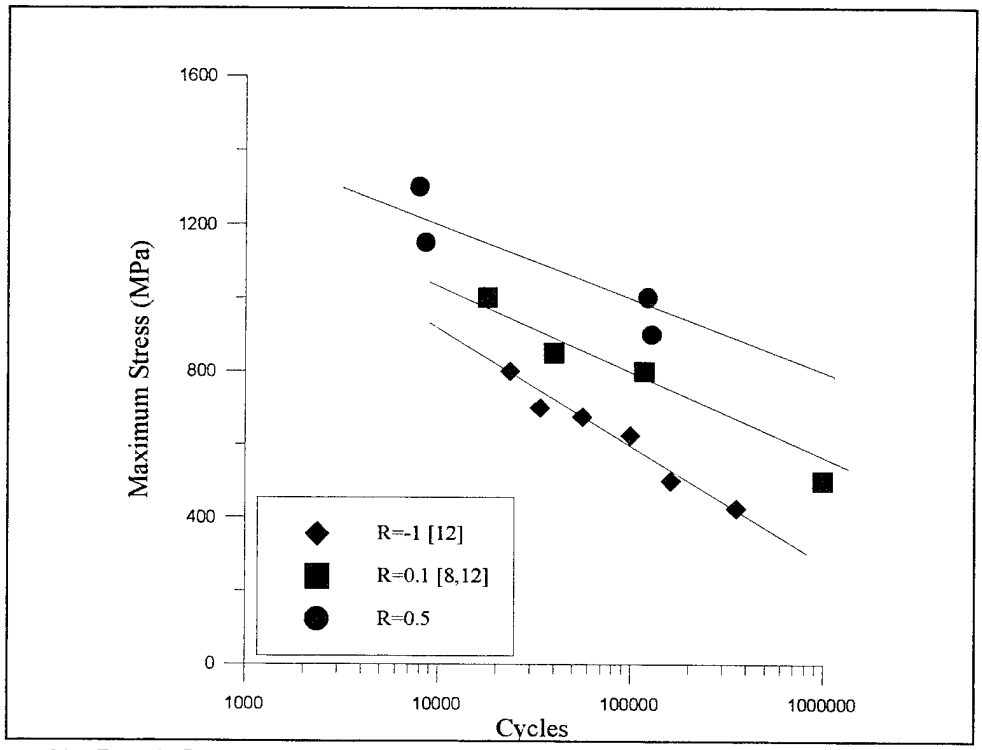

Figure 61. Load Control Unidirectional Fatigue Life Diagram: Maximum Stress

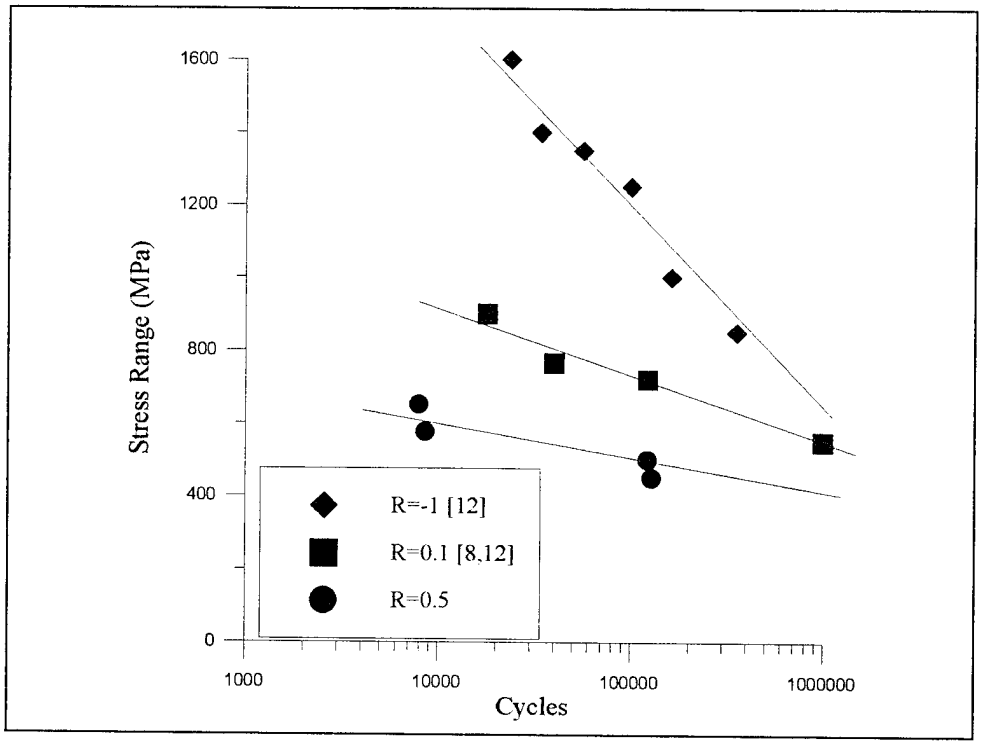

Figure 62. Load Control Unidirectional Fatigue Life Diagram: Stress Range

maximum stress basis, Figure 61, the fatigue life increases as the stress ratio is increased. On a stress range basis, Figure 62, the fatigue life decreases as the stress ratio is increased. This is similar to the effect of strain ratio shown in Figures 55 and 56.

Figure 63 shows a fatigue life comparison between both the load and strain control modes compared on a strain range basis. For the load control fatigue life data, strain range was calculated at the half life of the specimen. Figure 63 shows that the fatigue life of the unidirectional lay-up is independent of control mode for the tests conducted at R = -1 and R = 0. However, at R = 0.5, the tests conducted under the strain control mode have a longer fatigue life than those under the load control mode at the higher strain ranges. This difference in fatigue life is caused by matrix creep in the load control tests. Matrix creep under the load control mode transfers load to the fibers and causes fiber failure. Figure 63 reveals that the fatigue life of the unidirectional lay-up is independent of control mode at R = -1 and R = 0 while matrix creep under the load control mode at $R_\sigma = 0.5$ reduces its fatigue life when compared to tests under the strain control mode at $R_\varepsilon = 0.5$.

5.2 Fatigue life: $[0/90]_{2S}$

Three tests were performed on the $[0/90]_{2S}$ laminate to determine its fatigue life at $R_\varepsilon = 0$ under the strain control mode. Tension-compression fatigue life data for tests conducted under the strain control mode was obtained from a previous study [5]. The

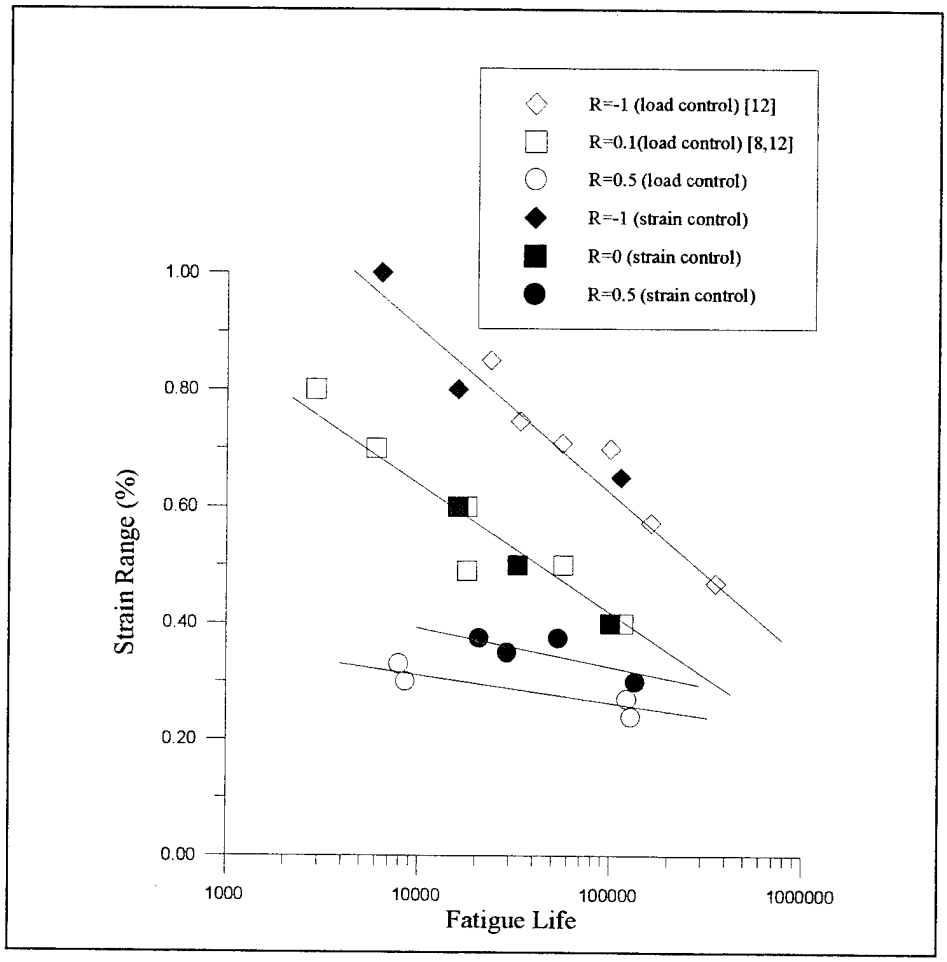

Figure 63. Load Control vs. Strain Control Fatigue Life Diagram: Strain Range

fatigue life data was then used to make fatigue life comparisons between tests conducted at $R_\varepsilon = 0$ and $R_\varepsilon = -1$ for the cross-ply lay-up.

Figures 64 and 65 show the ε-N diagrams plotted on a maximum strain and strain range basis, respectively. Similar to the unidirectional lay-up, fatigue life increases with an increase of R_ε on a maximum strain basis. However, when comparing the two strain ratios on a strain range basis, the fatigue lives begin to collapse together below a strain range of 0.6%. This would indicate that below a strain range of 0.6% the fatigue life is

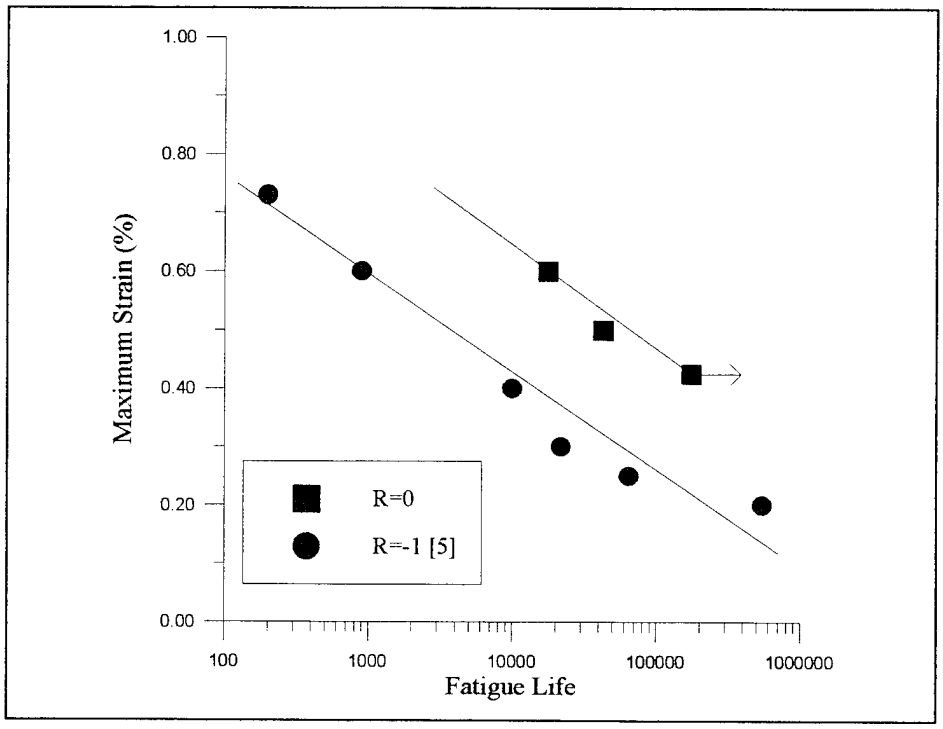

Figure 64. Cross-ply Fatigue Life Diagram: Maximum Strain

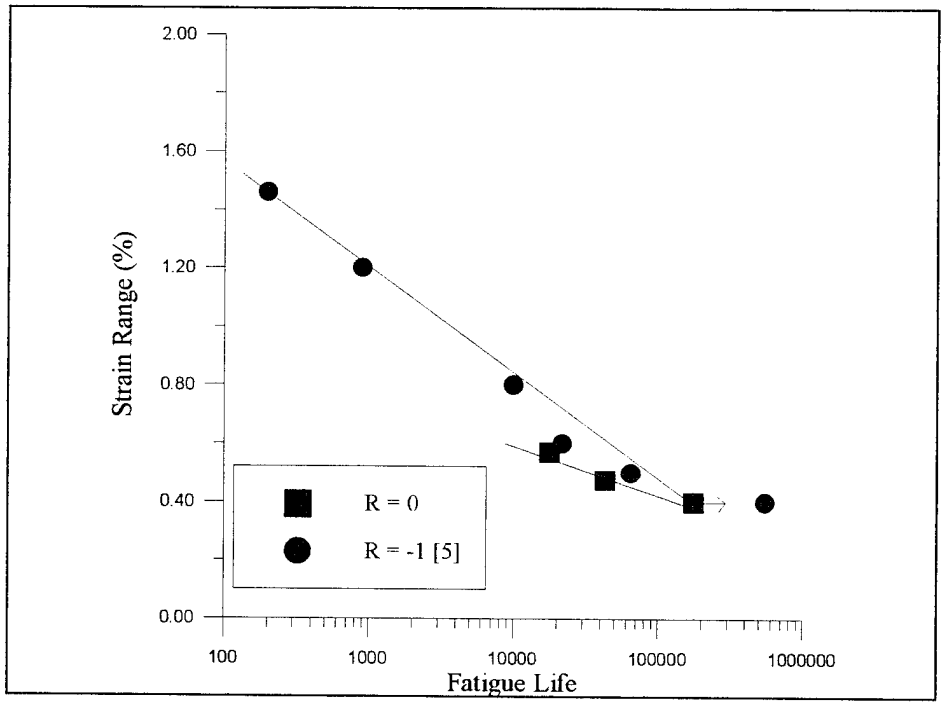

Figure 65. Cross-ply Fatigue Life Diagram: Strain Range

independent of strain ratio and highly dependent on strain range when comparing tests conducted at $R_\varepsilon = -1$ and $R_\varepsilon = 0$. This same trend was not found for the cross-ply lay-up under the load control mode [1]. Before this can be conclusively proven additional testing at both strain ratios should be completed.

5.3 Fatigue Life Comparison of $[0]_8$ and $[0/90]_{2S}$

Figure 66 shows the fatigue life under the strain control mode for both unidirectional and cross-ply lay-ups plotted on strain range basis. The fatigue life data collapses onto three distinct curves for each of the strain ratios. The results suggest that strain range governs the fatigue life of the two lay-ups. This good correlation for the tests conducted under the strain control mode suggests that the 90° plies do not affect fatigue life when compared on a strain range basis.

Figure 67 shows the fatigue life under the load control mode for both lay-ups as a function of stress range. On a stress range basis the fatigue lives do not collapse onto distinct stress ratio curves. The unidirectional lay-up has a much longer fatigue life than the cross-ply lay-up. This shows that the presence of the 90° plies greatly reduces the fatigue life of the cross-ply lay-up when compared on a stress range basis. Previous studies involving the load control mode have shown that the fatigue life of the unidirectional and cross-ply lay-ups for the same stress ratio fall within a narrow band when plotted as a function of stress in the 0° plies [1,5,12,20]. Stress in the 0° ply is simply the laminate stress for the unidirectional lay-up. For the cross-ply lay-up, the 90° plies were assumed

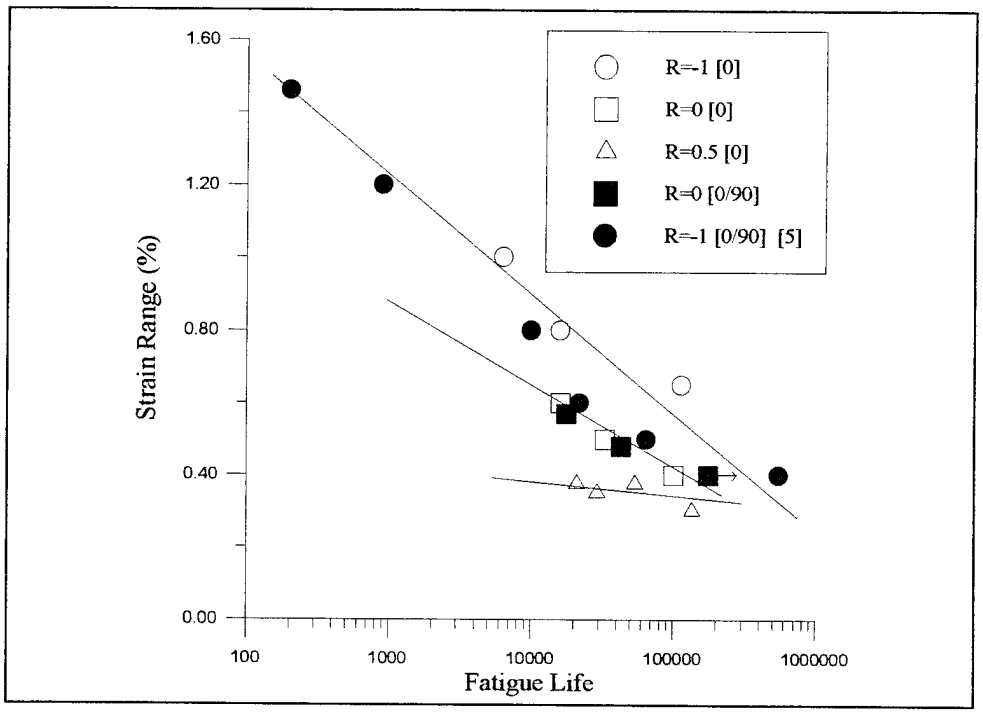

Figure 66. Fatigue Life Diagram for Cross-ply vs. Unidirectional Comparison under Strain Control: Strain Range

to have failed and carry no load. Therefore, the 0° plies carry all of the load. Figure 68 shows the fatigue life comparison for each of the two lay-ups based on stress range in the 0° ply. All of the data collapses onto three curves, one for each stress ratio. This shows that fatigue life for both lay-ups under the load control mode is governed by stress in the 0° plies.

An attempt was also made to collapse all the fatigue life data for both the load and strain control modes onto distinct R ratio curves for both lay-ups. This was only successful for the tension-compression tests. The maximum and minimum stresses under load and strain control for both lay-ups remain relatively constant throughout the fatigue life for tension-compression testing. This allows for a comparison based on maximum

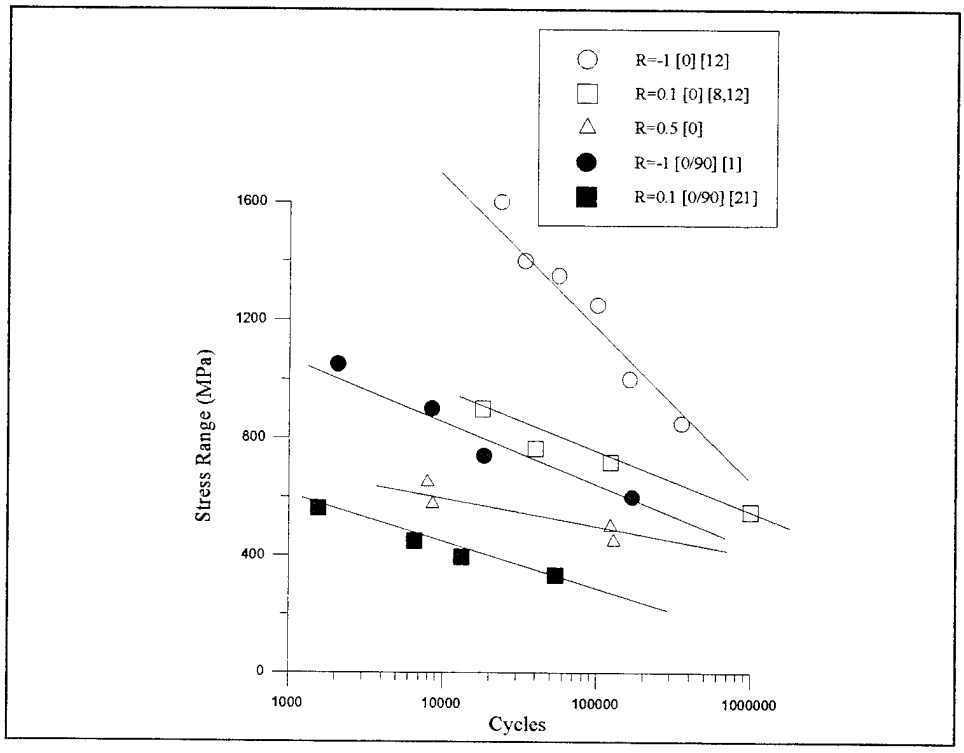

Figure 67. Fatigue Curve for Cross-ply vs. Unidirectional Comparison under Load Control: Stress Range

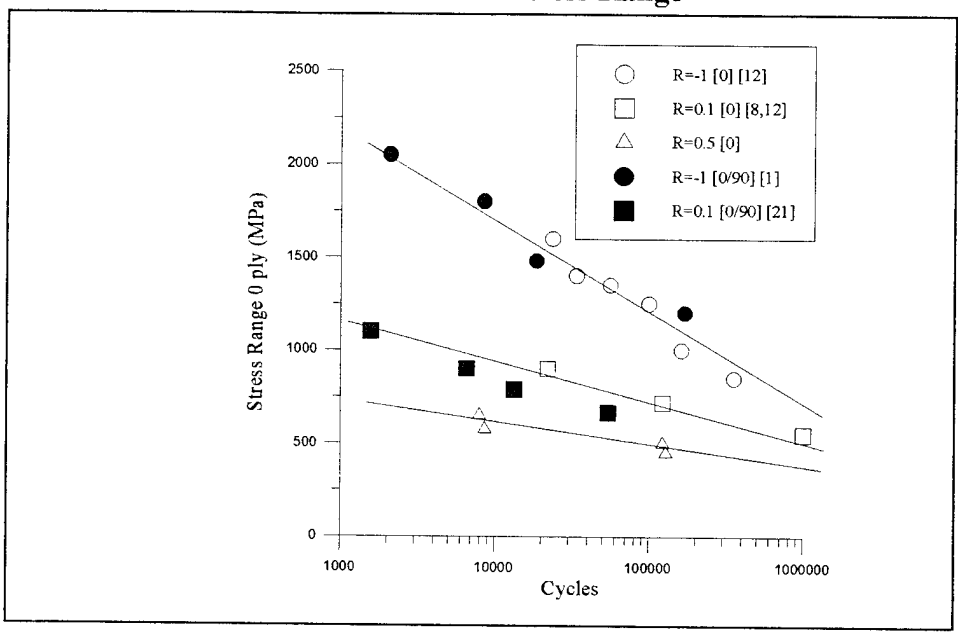

Figure 68. Fatigue Life Diagram for Cross-ply vs. Unidirectional Comparison under Load Control: 0^{o} ply Stress

stress in the 0° plies. Figure 69 shows that the fatigue lives for each of the lay-ups, under both the load and strain control modes, collapse onto one curve when compared against maximum stress in the 0° plies.

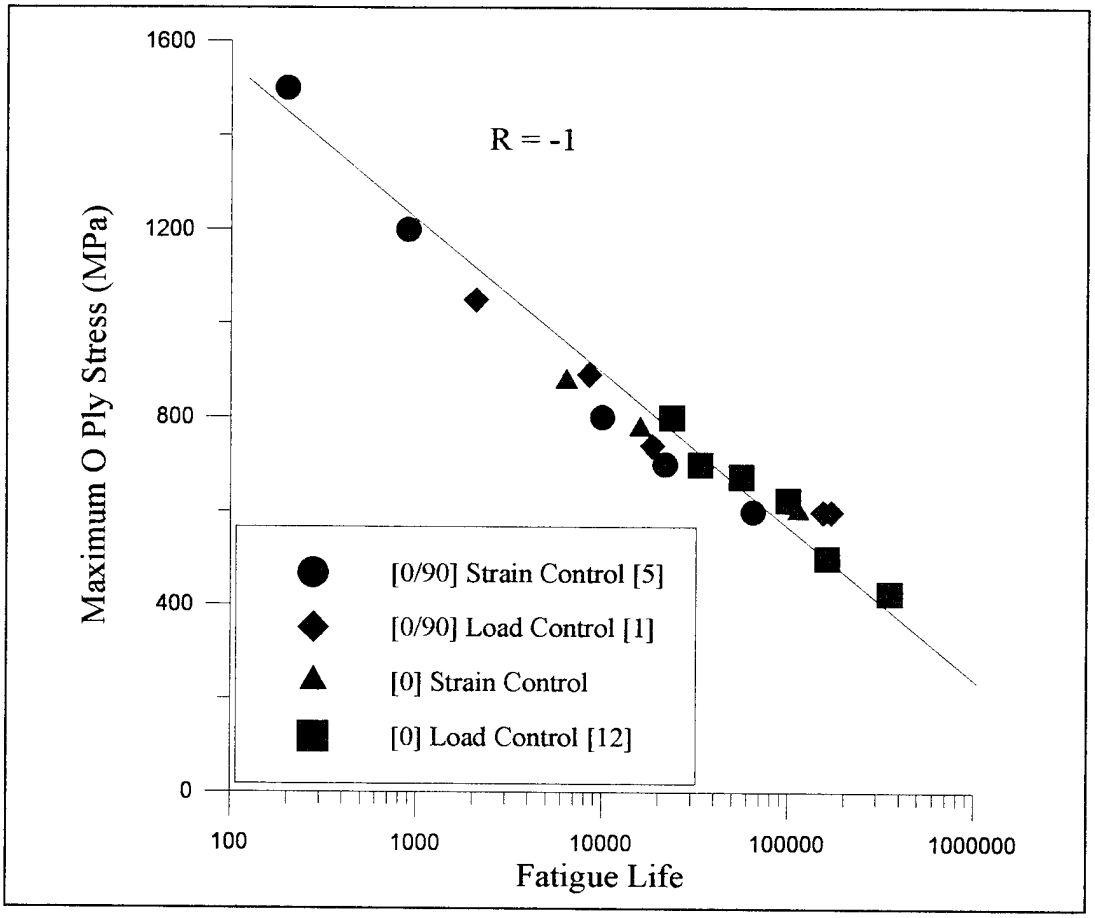

Figure 69. Fatigue Curve under Tension-Compression for Cross-ply and Unidirectional lay-up under Load and Strain Control: Maximum Stress in 0° ply

5.4 Haigh Diagrams

Figures 70 and 71 show Haigh diagrams for the unidirectional lay-up under both the load and strain control mode, respectively. Haigh diagrams were not completed for the cross-ply lay-up since only two stress/strain ratios were available. The Haigh diagram is a plot of mean stress/strain versus alternating stress/strain. Mean stress (σ_m) and alternating stress (σ_a) are defined by the following equations.

$$\sigma_m = (\sigma_{max}+\sigma_{min}) / 2 \qquad (1)$$

$$\sigma_a = (\sigma_{max}-\sigma_{min}) / 2 \qquad (2)$$

The relationships are the same for mean and alternating strain, ε_m and ε_a, respectively. Estimated fatigue life divisions were then added to each of the figures with the limited data available. Each of the fatigue life divisions, shown in Figures 70 and 71, converge at the ultimate strain (1.0%) and stress (1400 MPa) respectively [15]. These lines represent the approximate fatigue life regions for the unidirectional lay-up. Unlike the S-N diagram, the Haigh diagram shows the combined effects of both the alternating and mean stress/strain on the fatigue life of the MMC. More fatigue tests should be completed at different stress/strain ratios to better define the fatigue life divisions on the Haigh diagrams.

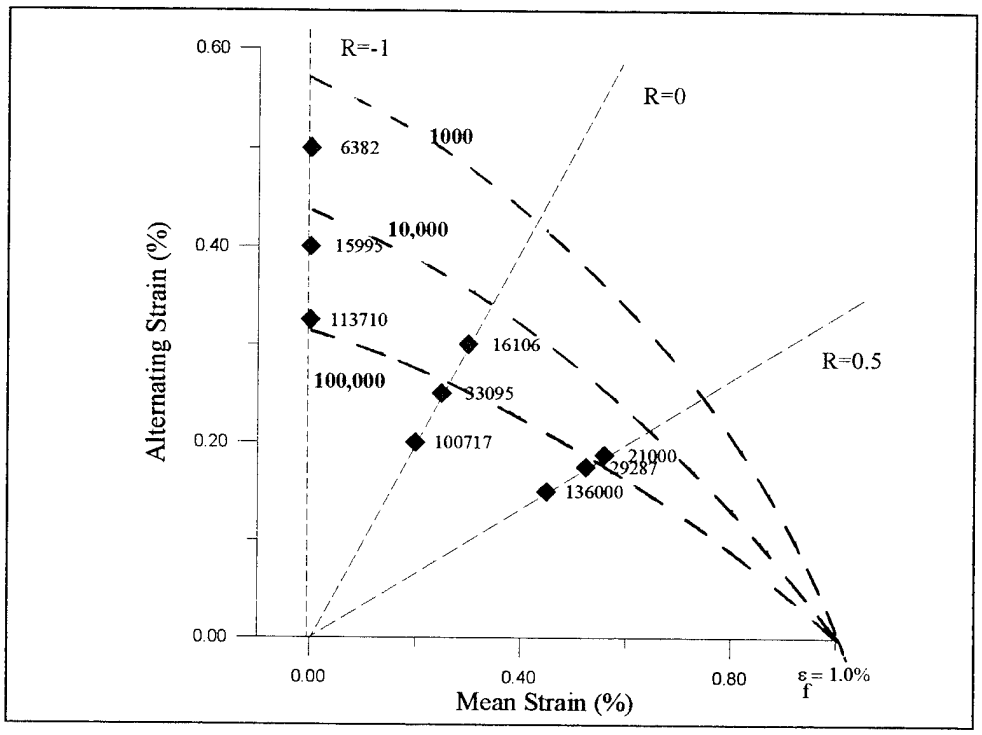

Figure 70. Haigh Diagram for Unidirectional Lay-up Under Strain Control (Numbers with data points represent the fatigue life)

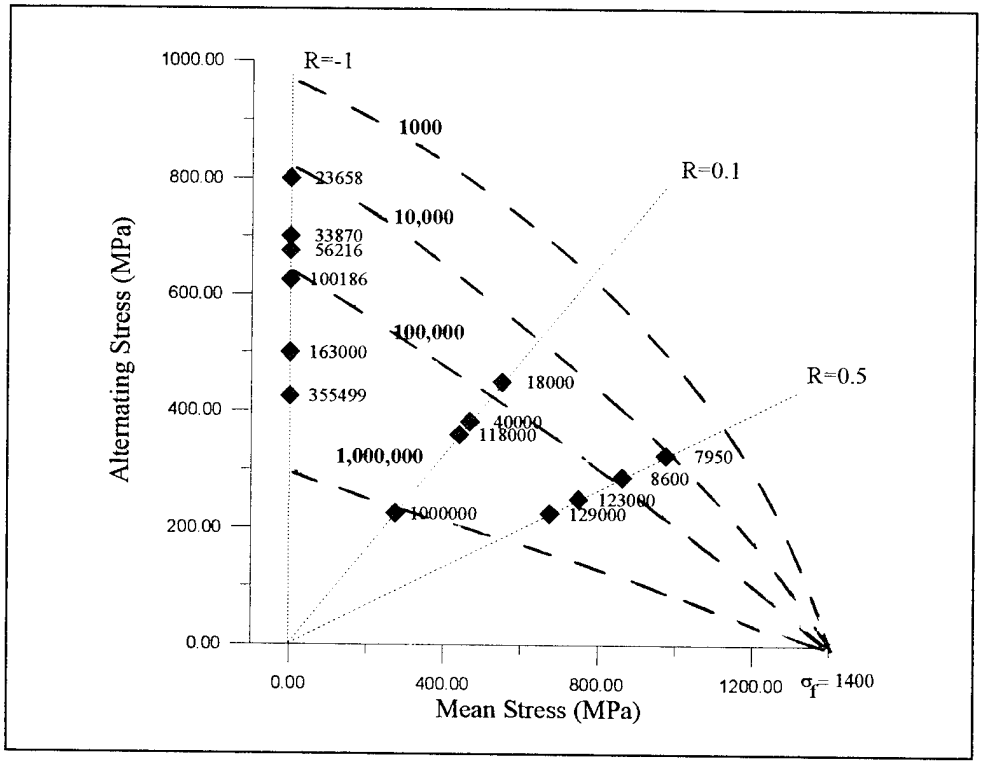

Figure 71. Haigh Diagram for Unidirectional Lay-up Under Load Control (Numbers with data points represent the fatigue life)

6. Conclusions and Recommendations

The purpose of this study was to determine the effects of stress/strain ratios on the fatigue response of a unidirectional, $[0]_8$, SCS-6/Ti-15-3, MMC laminate at 427°C. The fatigue life and damage mechanisms were investigated for stress/strain ratios of -1, 0 and 0.5 under both the load and strain control mode. The fatigue life of a cross-ply, $[0/90]_{2S}$, SCS-6/Ti-15-3, MMC laminate was also investigated under the strain control mode at $R_\varepsilon = 0$ to supplement the results of previous studies with different stress/strain ratios. This allowed for the comparison between the fatigue life of the unidirectional and cross-ply lay-up at different stress/strain ratios.

Similar fatigue damage mechanisms were found in unidirectional laminates under the strain control mode at $R_\varepsilon = -1$ and $R_\varepsilon = 0$. At strain levels greater than 0.5%, failure was fiber dominated. The fracture surfaces exhibited extensive fiber pullout and matrix necking, while the sectioned specimens revealed fiber cracking with little or no matrix cracks. At strain levels below 0.5%, matrix damage occurred and increased as the strain was decreased. The fracture surfaces were flat regions containing fatigue striations, while the sectioned specimens revealed matrix cracking with no fiber cracks. The matrix crack density increased as strain decreased, explaining the larger modulus degradation in the tests conducted at lower strain levels. A comparison with previous tests conducted under the load control mode at similar stress ratios ($R_\sigma = -1$ and $R_\sigma = 0.1$) revealed similar damage mechanisms when compared on a strain range basis [8,12]. This indicates that the damage mechanisms for these two stress/strain ratios are independent of control mode.

Load and strain control tests conducted at R = 0.5 revealed increased matrix damage when compared to tests conducted at the same maximum stress/strain level at R = 0 or R = -1. Matrix damage was found at stress/strain levels that exhibited fiber dominated failure at R=0. This was caused by the increased fatigue life at R = 0.5 when compared to R = 0 and R = -1. The increased fatigue life at R = 0.5 allows matrix cracks to develop and propagate. Fiber and matrix cracks were found in all tests conducted at $R_\varepsilon = 0.5$ under the strain control mode. Matrix creep, resulting in fiber failure, dominated the fatigue response of the load control tests above the level of stress of 1150 MPa with matrix damage occurring below 1150 MPa.

The comparison of fatigue life between the three different strain ratios show that as R_ε increases fatigue life increases when compared on a maximum strain basis. The increase in fatigue life is caused by the increased matrix stress range that is evident as R_ε gets larger . When compared on a strain range basis, fatigue life decreases as R_ε increases. The reduction in fatigue life is caused by the increased mean strain at larger strain ratio. The shape of the ε-N and S-N diagram also changes as R changes. The slope of the fatigue life diagram decreases as R is increased. This is a result of the fatigue life curves at each of the stress/strain ratios converging at the fatigue limit of the lay-up.

Fatigue life comparison between the load and strain control modes for the three stress/strain ratios reveals little difference in fatigue life except at R = 0.5. The load control tests conducted at $R_\sigma = 0.5$ reveal a decreased fatigue life when compared to the tests conducted under strain control. This was caused by matrix creep in the load control

tests. The fatigue life comparison between control modes reveals that the response of the MMC is independent of control mode at R = -1 and R = 0; however, matrix creep reduces the fatigue life at $R_\sigma = 0.5$ when compared to tests conducted at $R_\varepsilon = 0.5$.

Strain controlled fatigue testing was also performed on a cross-ply, $[0/90]_{2S}$, SCS-6/Ti-15-3, MMC at a strain ratio of 0. This was combined with previously published fatigue life data at a strain ratio of -1 [5] to make fatigue life comparisons between strain ratios of. This comparison showed that below a strain range of 0.6% the fatigue lives for the tests conducted at $R_\varepsilon = 0$ and $R_\sigma = -1$ collapse together. This indicates that below a strain range of 0.6% the fatigue life of the cross-ply lay-up is independent of the either strain ratio and strain range dependent. More testing is needed in this area to verify this trend.

Strain range was used to compare fatigue life between the unidirectional and cross-ply lay-ups under the strain control mode. This comparison showed little difference in the fatigue life at the same strain ratio. This suggests that the 90° plies in the cross-ply lay-up do not affect fatigue life when fatigued under the strain control mode. The stress in the 0° plies was used to compare fatigue life between the two lay-ups tested under the load control mode. This comparison revealed little difference in fatigue life at the same stress ratio. This indicates that maximum stress in the 0° plies govern the fatigue life of both lay-ups. The 0° ply stress was also used to collapse the fatigue life for both lay-ups under load and strain control onto a single line for tension-compression testing. Matrix stress relaxation and matrix creep prevented any good correlation between the two control modes at the stress/strain ratios of 0 and 0.5.

In summary, this study investigated the stress/strain ratio effects on the fatigue life of both a unidirectional and cross-ply laminates. It provided fatigue life data for MMCs under the strain control mode and was the first known test to investigate the fatigue response at high stress/strain ratios. However, more experimental and analytical studies are needed to completely understand the fatigue response MMCs. Fatigue testing of the cross-ply lay-up under both the load and strain control modes needs to be accomplished at $R = 0.5$ to determine if the same fatigue life and damage trends are applicable when compared to the unidirectional lay-up. Also, the S-N diagram for all the stress/strain ratios needs to be expanded to determine the fatigue limit of the MMC. New analytical tools that include damage models need to be developed which can accurately predict the response of both the unidirectional and cross-ply lay-up under the strain control mode at different stress/strain ratios.

Appendix A: $[0/90]_{2S}$ Macro-mechanical Results

This Appendix contains the macro-mechanical results for the cross-ply lay-up tested under the strain control mode at $R_\varepsilon = 0$. The maximum strain, strain range, initial modulus and cycles to failure are present in Table 8. The normalized modulus histories and the maximum and minimum stress histories are also presented.

Table 8. $[0/90]_{2S}$ Macro-Mechanical Results

Max Strain (%)	Strain Range (%)	Initial Modulus (GPA)	Cycles to Failure
0.6	0.57	122	17,715
0.5	0.475	122	42,966
0.425	0.4	130	>174,000

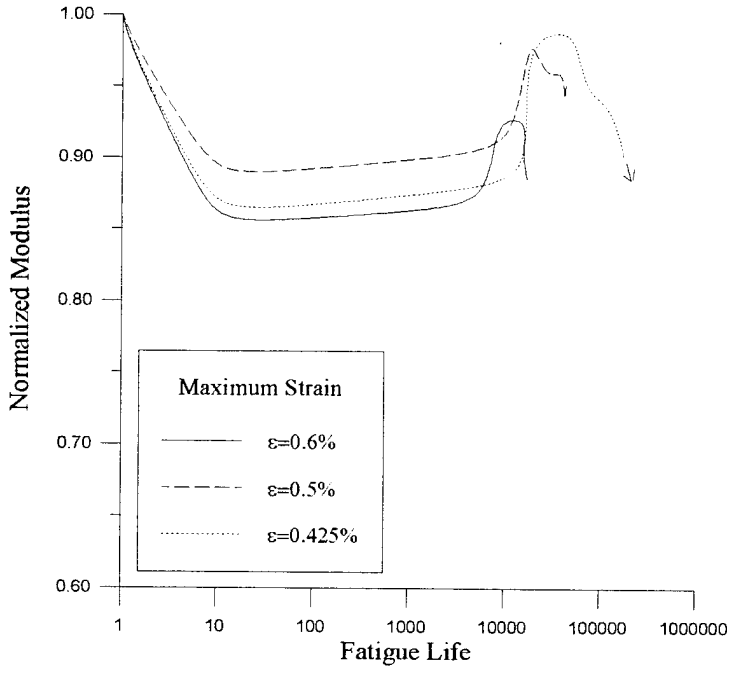

Figure 72. Tension-Tension ($R_\varepsilon = 0$) Modulus Histories (Cross-Ply)

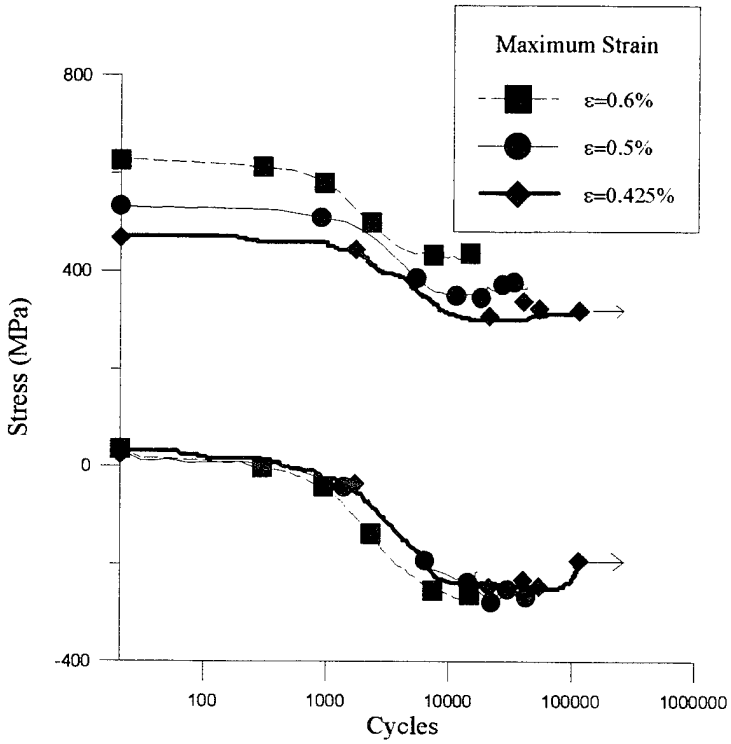

Figure 73. Tension-Tension ($R_\varepsilon = 0$) Stress History (Cross-Ply)

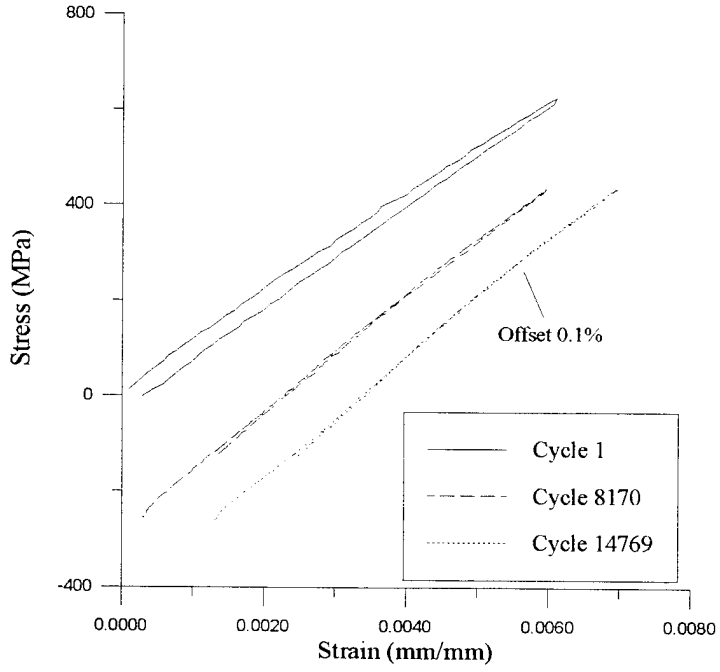

Figure 74. $\varepsilon_{max} = 0.6\%$: Stress/Strain History ($R_\varepsilon = 0$)

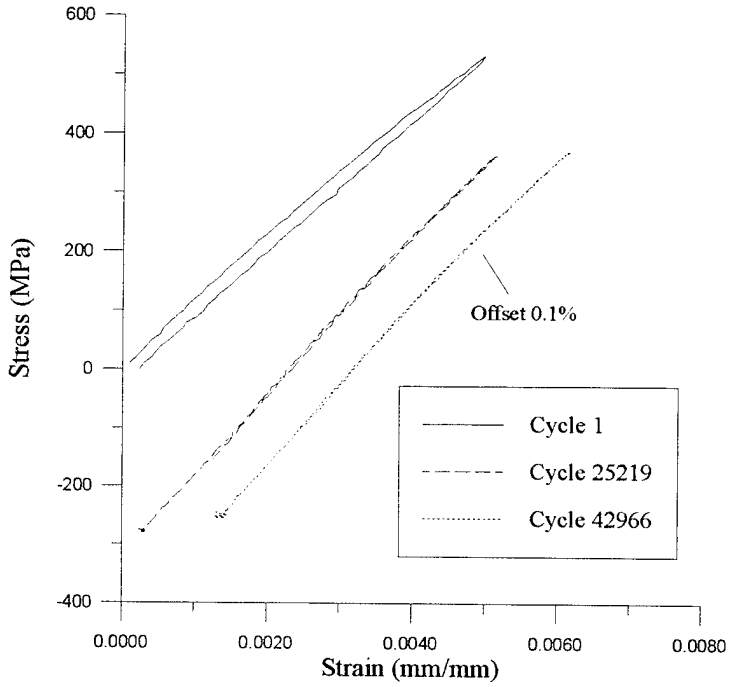

Figure 75. ε_{max} = 0.5%: Stress/Strain History (R_ε = 0)

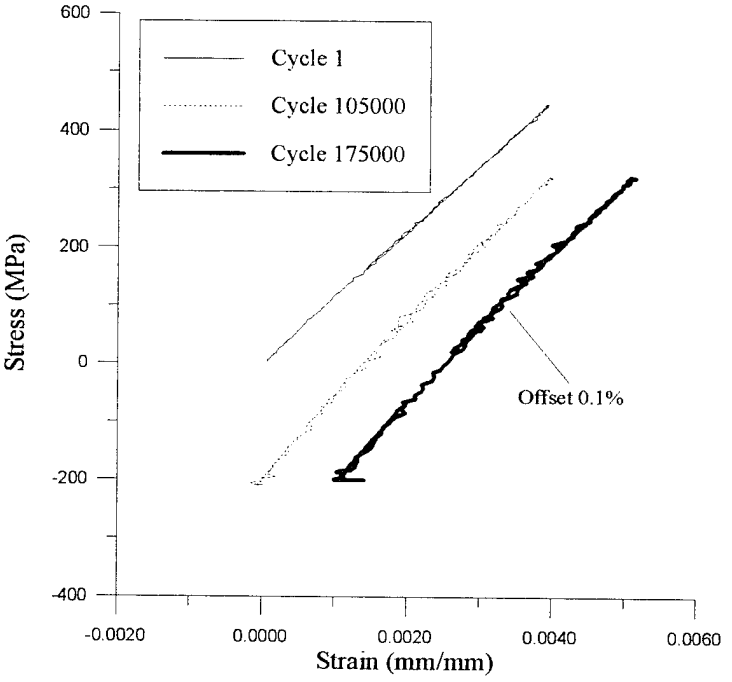

Figure 76. ε_{max} = 0.425%: Stress/Strain History (R_ε = 0)

Appendix B: Additional Unidirectional, $[0]_8$, Data

This appendix contains the stress/strain histories for all of the stress/strain ratios under both the load and strain control mode that were not presented in Chapter 4. Several of the hysteresis loops are offset so that the loops do not all fall together.

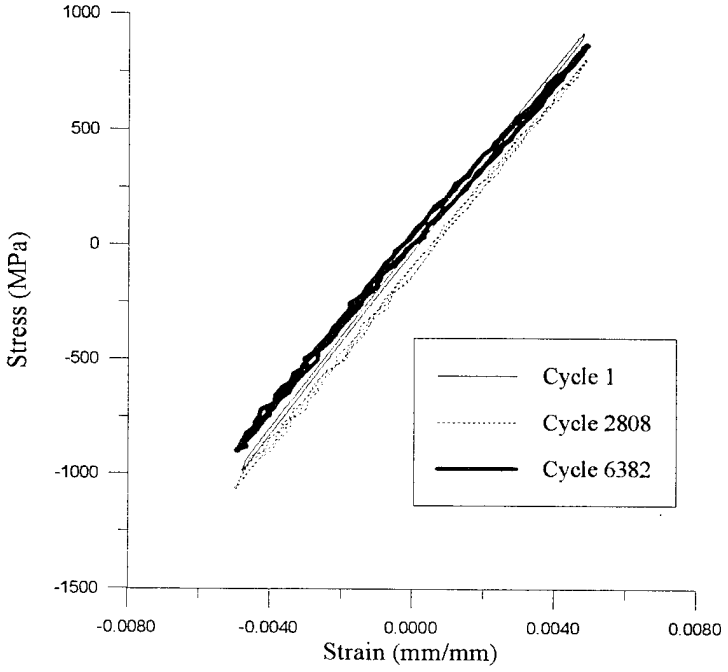

Figure 77. ε_{max} = 0.5%: Stress/Strain History (R_ε = -1)

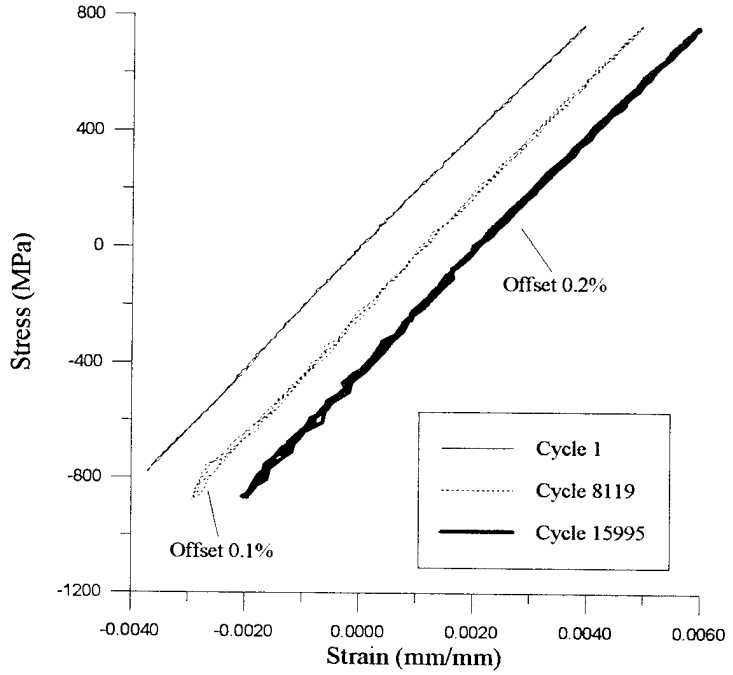

Figure 78. ε_{max} **= 0.4%: Stress/Strain History (**R_ε **= -1)**

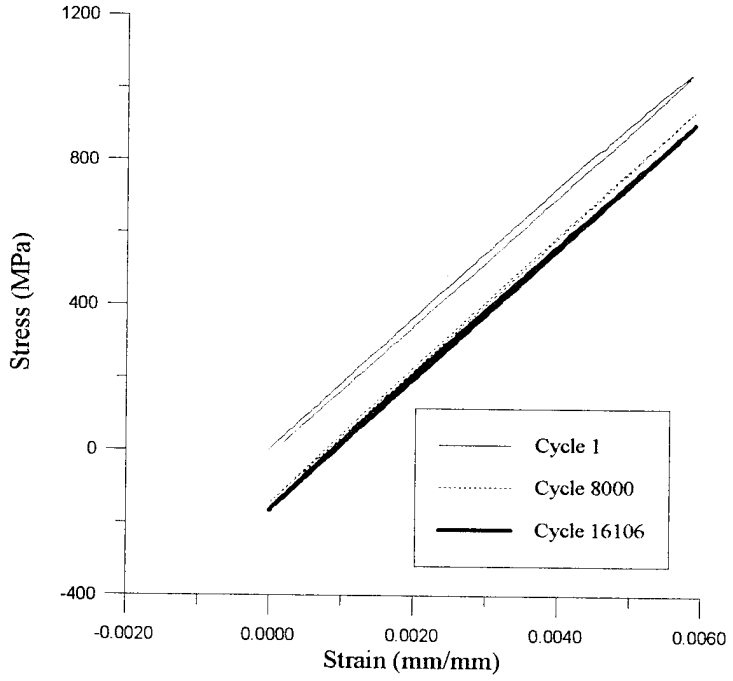

Figure 79. ε_{max} **= 0.6%: Stress/Strain History (**R_ε **= 0)**

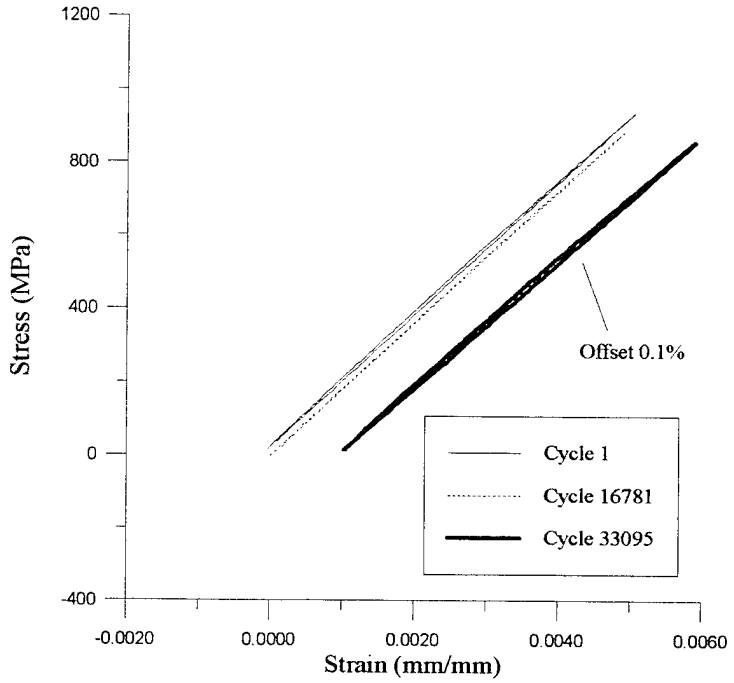

Figure 80. ε_{max} = 0.5%: Stress/Strain History (R_ε = 0)

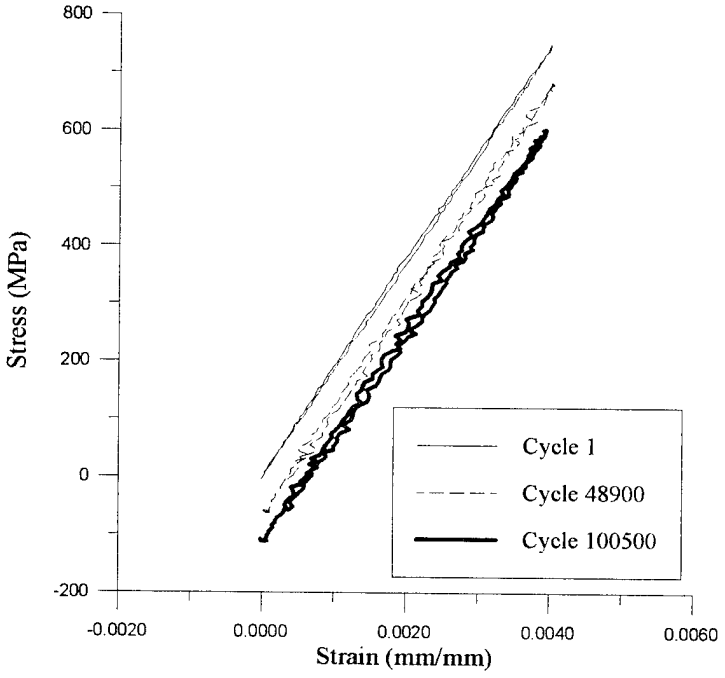

Figure 81. ε_{max} = 0.4%: Stress/Strain History (R_ε = 0)

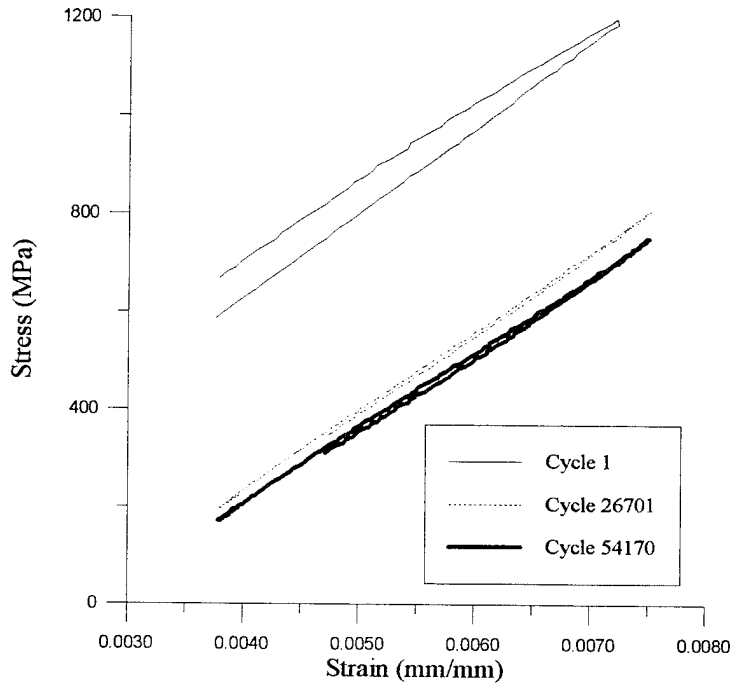

Figure 82. $\varepsilon_{max} = 0.75\%$: **Stress/Strain History** ($R_\varepsilon = 0.5$)

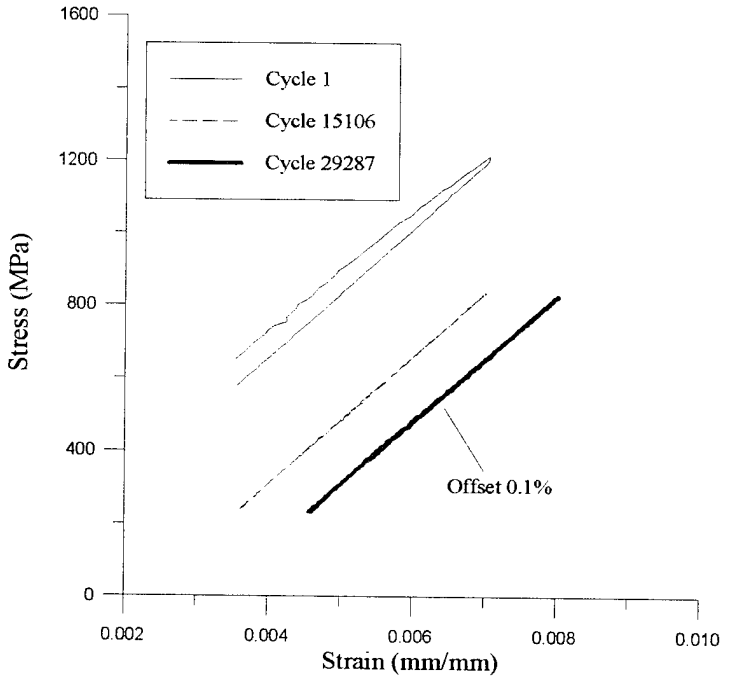

Figure 83. $\varepsilon_{max} = 0.7\%$: **Stress/Strain History** ($R_\varepsilon = 0.5$)

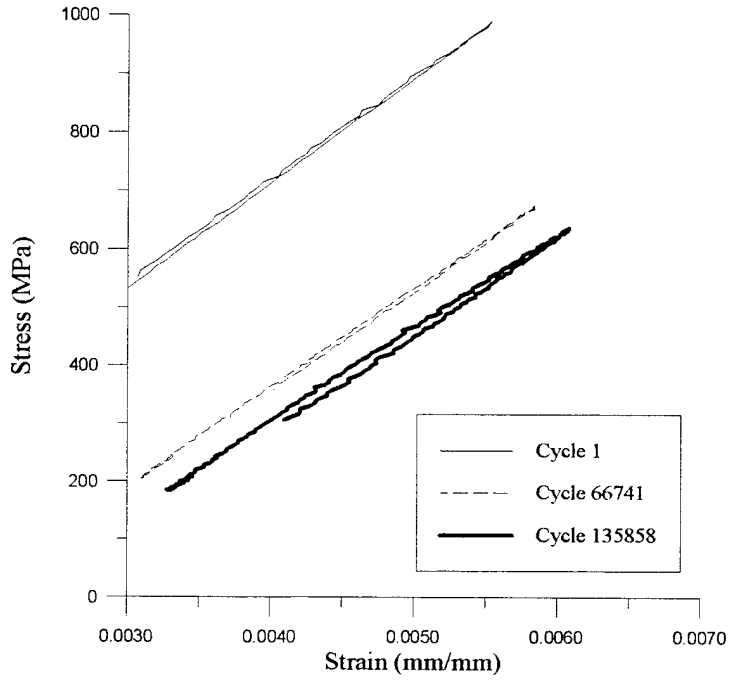

Figure 84. ε_{max} **= 0.6%: Stress/Strain History (**R_ε **= 0.5)**

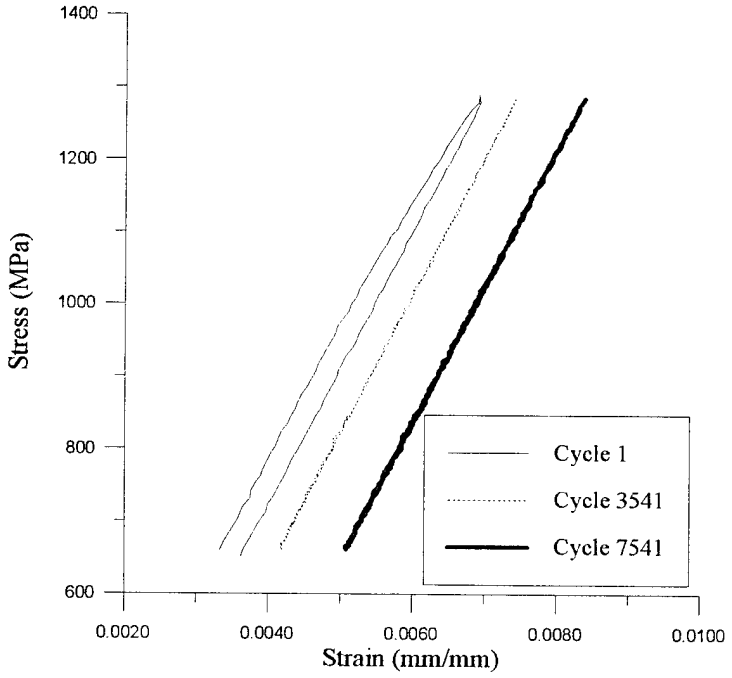

Figure 85. σ_{max} **= 1300 MPa: Stress/Strain History (**R_σ **= 0.5)**

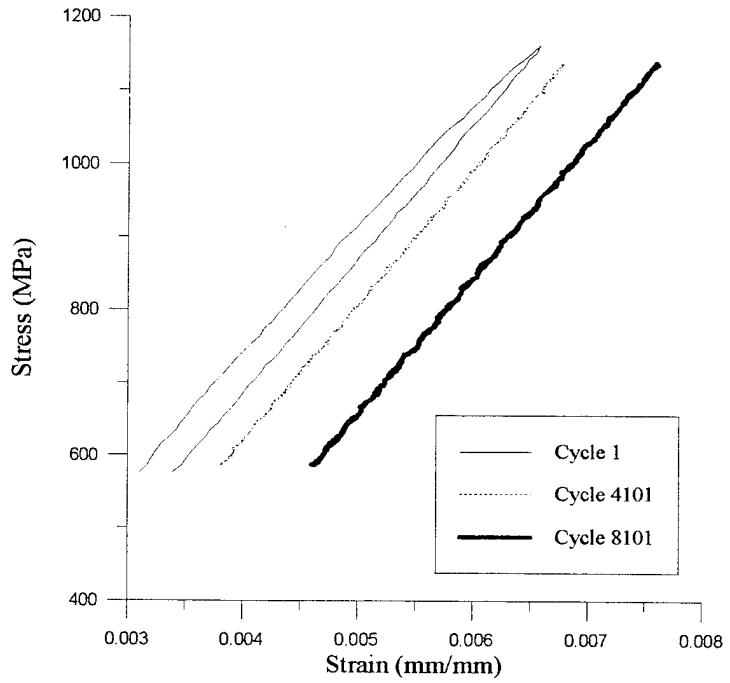

Figure 86. σ_{max} = 1150 MPa: Stress/Strain History (R_σ = 0.5)

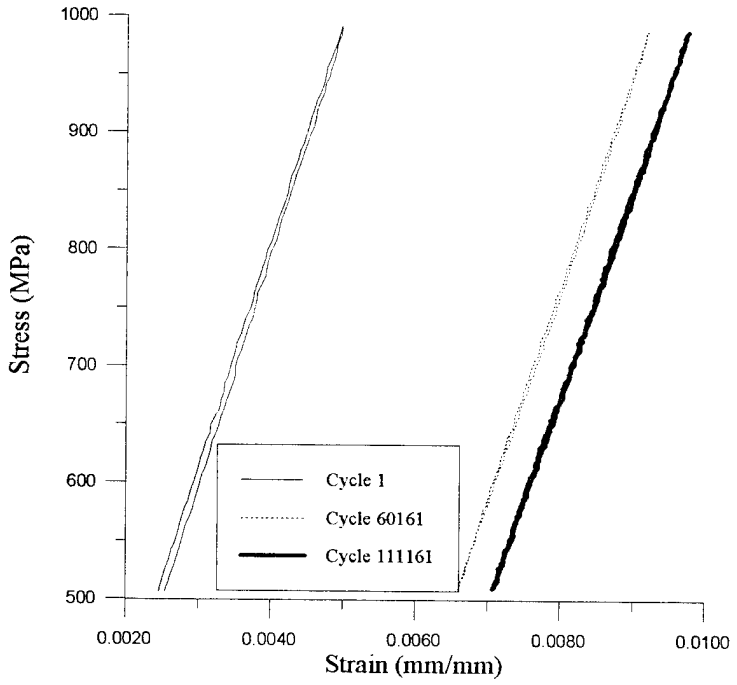

Figure 87. σ_{max} = 1000 MPa: Stress/Strain History (R_σ = 0.5)

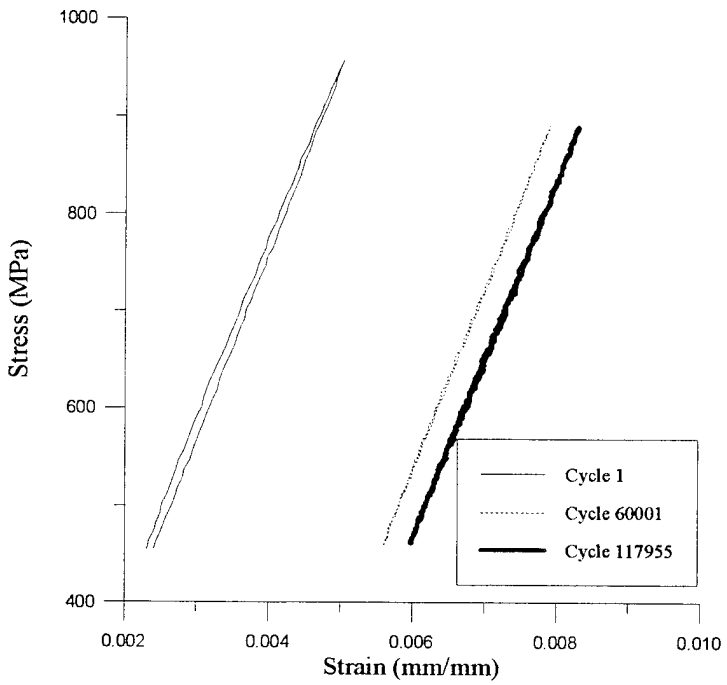

Figure 88. σ_{max} = 900 MPa: Stress/Strain History (R_σ = 0.5)

Bibliography

1. Boyum, E.A., Investigation of Tension-Compression Fatigue Behavior of a Cross-Ply Metal Matrix Composite at Room and Elevated Temperature. MS Thesis, AFIT/GAE//ENY/93D-6. School of Engineering, Air Force Institute of Technology, Wright-Patterson, AFB, OH, December 1993.

2. Broek, D., Elementary Engineering Fracture Mechanics, 4th ed, Boston, Kluwer Academic Publishers, 1991.

3. Castelli, M. G., "Thermomechanical and Isothermal Fatigue Behavior of a $[90]_8$ Titanium Matrix Composite," NASA Contractor Report 191196, Oct 1993.

4. Castelli, M.G., J. R. Ellis and P. A. Bartolotta., "Thermomechanical Testing Techniques for High-Temperature Composites: TMF Behavior of SiC(SCS-6)/Ti-15-3," NASA Technical Memorandum 103171, 1990.

5. Dennis, L.B., Fatigue Behavior of a Cross-Ply Metal Matrix Composite at Elevated Temperature Under Strain Controlled Mode. MS Thesis, AFIT/GAE//ENY/94D-7. School of Engineering, Air Force Institute of Technology, Wright-Patterson, AFB, OH, December 1994.

6. Gabb, T .P, J. Gayda and R.A. Mackay., "Isothermal and Nonisothermal fatigue Behavior of a Metal Matrix Composite," Journal of Composites and Materials, 24: 667-686, June 1990.

7. Gayda, J., T.P. Gabb and A.D. Freed., "The Isothermal Fatigue Behavior Of a Unidirectional SiC/Ti Composite and the Ti Alloy Matrix," NASA Technical Memorandum 101984. NASA Lewis Research Center. Cleveland OH, 1989.

8. Gayda, J. and T.P. Gabb., "Isothermal Fatigue Behavior of a $[90]_8$ SiC/Ti-15-3 Composite at 426°C," NASA Technical Memorandum 103686, January 1991.

9. Gayda, J., T.P. Gabb and G.R. Halford., "The Effect of Matrix Mechanical Properties on $[0]_8$ Unidirectional SiC/Ti Composite Fatigue Resistance," Scripta Metallurgica et Metallurgica, 25: 2879-1884, Pergamon Press (1991).

10. Kantzos, P. and J. Telesman., "Fatigue Crack Growth Study of SCS-6/Ti-15-3 Composite," NASA Technical Memorandum 102332, Lewis Research Center, 1989.

11. Klesnil, M. and P. Lukas., Fatigue of Metallic Materials, New York, Esdevier Scientific Publishing Company, 1980.

12. Kraabel, D., Investigation of Tension-Compression Fatigue Behavior of a Unidirectional Metal Matrix Composite at Elevated Temperature, MS Thesis, AFIT/GAE//ENY/94D-6. School of Engineering, Air Force Institute of Technology, Wright-Patterson, AFB, OH, December 1994.

13. Lerch, B.A., M.J. Verrilli and G.R. Halford., "Fully-Reversed Fatigue of a Ti-MMC," Conf. Proceedings of the 17th Annual Conference on Composites, Materials and Structures, Cocoa, Beach, Fl, January 1993.

14. Lerch, B. A., "Matrix Plasticity in SiC/Ti-15-3 Composite", NASA Technical Memorandum 103760, July 1991.

15. Lerch, B.A. and J.F. Saltsman., "Tensile Deformation of SiC/Ti-15-3 Laminates", ASTM Symposium on Composite Materials, Indianapolis, Indiana, May 1991.

16. Majumdar,B.S. and B.A. Lerch., "Fatigue Mechanisms in a Ti-Based Fiber-Reinforced MMC and Approaches to Life Prediction." Submitted to Titanium Matrix Composites Workshop, La Jolla, California, June 1993.

17. Majumadar, B.S. and G.M. Newaz., "Isothermal Fatigue Mechanisms in Ti-Based Metal Matrix Composites," NASA Contractor Report 191181, Columbus, Ohio, 1993.

18. Nichols T. and J. Ahmad., "Modeling Fiber Breakage in a Metal Matrix Composite", submitted for publication, Composite Science and Technology, 1994.

19. Pernot, J. J., Crack Growth Rate Modeling of a Titanium Aluminide Alloy Under Thermal Mechanical Cycling. PhD Dissertation, AFIT/DS/AA/91-3, School of Engineering, Air Force Institute of Technology, Wright-Patterson, AFB, OH, December 1991.

20. Pollock, W.D. and W.S. Johnson., "Characterization of Unnotched SCS-6-Ti-15-3 Metal Matrix Composites at 650°C," NASA Technical Memorandum 102699, Langley Research Center, 1990.

21. Portner, B.D., Investigation of Fatigue Damage Mechanisms in a Metal Matrix Composite Under Elevated Temperature. MS Thesis, AFIT/GAE//ENY/90D-20. School of Engineering, Air Force Institute of Technology, Wright-Patterson, AFB, OH, December 1990.

22. Robertson, D., LISOL Users Manual, Air Force Institute of Technology, Jan 1995.

23. Russ S.M. and T. Nicholas., "Isothermal and Thermomechanical Fatigue of Cross-Ply SCS-6/TIMETAL 21S," Science and Engineering of Composite Materials, 3:, 177-189, 1994.

24. Sanders, B.P., Characterization of Fatigue Damage in a Metal Matrix Composite (SCS-6/Ti-15-3) at Elevated Temperature. PhD Dissertation, AFIT/DS/AA/93-4. School of Engineering, Air Force Institute of Technology, Wright-Patterson, AFB, OH, December 1993.

25. Sanders, B.P and S. Mall., "Longitudinal Fatigue Response of a Metal Matrix Composite Under Strain Controlled Mode at Elevated Temperature," Journal of Composite Research, 16:, Oct 1994.

26. Sanders, B.P., S. Mall and B.A. Lerch., Fatigue Response of the Unidirectional and Cross-Ply SCS-6/Ti-15-3 MMC, Air Force Institute of Technology, 1995.

27. Schubbe, J.J., Investigation of Damage Mechanisms in a Cross-Ply Metal Matrix Composite Under Thermo-Mechanical Loading. MS Thesis, AFIT/GAE//ENY/90D-26. School of Engineering, Air Force Institute of Technology, Wright-Patterson, AFB, OH, December 1990.

28. Talreja, R., Fatigue of Composite Materials, Lancaster, Technomic Publishing Company, 1987.

29. Taya, M. and R.J. Arsenault., Metal Matrix Composites Thermomechanical Behavior, New York, Pergamon Press, 1989.

30. Verrilli, M.J. and T.P. Gabb., "High-Temperature Tension-Compression Fatigue Behavior of a Unidirectional Tungsten Copper Composite," Composite Materials:Fatigue and Fracture, Fourth Volume: ASTM STP 1156, 1993.

Vita

Captain Sean C. Jackson was born September 17, 1968 in Kansas City, Missouri. He graduated from Leavenworth High School in Leavenworth, Kansas, in 1986 and entered the University of Kansas that fall. In 1991, Captain Jackson graduated with a Bachelor of Science in Aerospace Engineering and was commissioned a Second Lieutenant in the United States Air Force. He then served as a stability and control engineer in the F-16 Systems Program Office, Wright-Patterson AFB, until entering the School of Engineering, Air Force Institute of Technology in May 1994.

Permanent Address: RR#2 Box 2310
Hermitage, Missouri 65668

REPORT DOCUMENTATION PAGE

Form Approved
OMB No. 0704-0188

1. AGENCY USE ONLY (Leave blank)	2. REPORT DATE	3. REPORT TYPE AND DATES COVERED
	December 1995	Master's Thesis

4. TITLE AND SUBTITLE
STRESS/STRAIN RATIO EFFECTS ON THE FATIGUE RESPONSE OF A SCS-6/Ti-15-3 METAL MATRIX COMPOSITE AT ELEVATED TEMPERATURE

5. FUNDING NUMBERS

6. AUTHOR(S)
Capt Sean C. Jackson

7. PERFORMING ORGANIZATION NAME(S) AND ADDRESS(ES)
Air Force Institute of Technology
Wright-Patterson AFB, OH 45433-6583

8. PERFORMING ORGANIZATION REPORT NUMBER
AFIT/GAE/ENY/95D-14

9. SPONSORING/MONITORING AGENCY NAME(S) AND ADDRESS(ES)
Dr. Walter Jones
AFOSR/NA
Bolling AFB, DC 20322-6448

10. SPONSORING/MONITORING AGENCY REPORT NUMBER

11. SUPPLEMENTARY NOTES

12a. DISTRIBUTION/AVAILABILITY STATEMENT
Approved for Public Release; distribution unlimited

12b. DISTRIBUTION CODE

13. ABSTRACT *(Maximum 200 words)*

This study investigated the fatigue life and damage mechanisms of a $[0]_8$, SCS-6/Ti-15-3, metal matrix composite at 427°C for three different stress/strain ratios, R = -1, 0 and 0.5. Fatigue life and damage mechanism comparisons were made for the varying R ratios and between the load and strain control modes. Fatigue life comparisons show that on a maximum stress/strain basis as R is increased fatigue life increases while on a stress/strain range basis as R increases fatigue life decreases. Similar damage mechanisms were found between the R = -1 and R = 0 tests conducted at the same maximum stress/strain level. However, comparisons between R = 0 or R = -1 and R = 0.5 show that the decreased stress/strain range at R = 0.5 results in increased fatigue life and the onset of matrix damage at the same maximum stress/strain level.

14. SUBJECT TERMS
metal matrix composite, MMC, SCS-6/Ti-15-3, Strain Ratio
strain control

15. NUMBER OF PAGES
123

16. PRICE CODE

17. SECURITY CLASSIFICATION OF REPORT	18. SECURITY CLASSIFICATION OF THIS PAGE	19. SECURITY CLASSIFICATION OF ABSTRACT	20. LIMITATION OF ABSTRACT
Unclassified	Unclassified	Unclassified	UL

GENERAL INSTRUCTIONS FOR COMPLETING SF 298

The Report Documentation Page (RDP) is used in announcing and cataloging reports. It is important that this information be consistent with the rest of the report, particularly the cover and title page. Instructions for filling in each block of the form follow. It is important to ***stay within the lines*** to meet ***optical scanning requirements***.

Block 1. Agency Use Only *(Leave blank)*.

Block 2. Report Date. Full publication date including day, month, and year, if available (e.g. 1 Jan 88). Must cite at least the year.

Block 3. Type of Report and Dates Covered. State whether report is interim, final, etc. If applicable, enter inclusive report dates (e.g. 10 Jun 87 - 30 Jun 88).

Block 4. Title and Subtitle. A title is taken from the part of the report that provides the most meaningful and complete information. When a report is prepared in more than one volume, repeat the primary title, add volume number, and include subtitle for the specific volume. On classified documents enter the title classification in parentheses.

Block 5. Funding Numbers. To include contract and grant numbers; may include program element number(s), project number(s), task number(s), and work unit number(s). Use the following labels:

C	- Contract	**PR**	- Project
G	- Grant	**TA**	- Task
PE	- Program Element	**WU**	- Work Unit Accession No.

Block 6. Author(s). Name(s) of person(s) responsible for writing the report, performing the research, or credited with the content of the report. If editor or compiler, this should follow the name(s).

Block 7. Performing Organization Name(s) and Address(es). Self-explanatory.

Block 8. Performing Organization Report Number. Enter the unique alphanumeric report number(s) assigned by the organization performing the report.

Block 9. Sponsoring/Monitoring Agency Name(s) and Address(es). Self-explanatory.

Block 10. Sponsoring/Monitoring Agency Report Number. *(If known)*

Block 11. Supplementary Notes. Enter information not included elsewhere such as: Prepared in cooperation with...; Trans. of...; To be published in.... When a report is revised, include a statement whether the new report supersedes or supplements the older report.

Block 12a. Distribution/Availability Statement. Denotes public availability or limitations. Cite any availability to the public. Enter additional limitations or special markings in all capitals (e.g. NOFORN, REL, ITAR).

- **DOD** - See DoDD 5230.24, "Distribution Statements on Technical Documents."
- **DOE** - See authorities.
- **NASA** - See Handbook NHB 2200.2.
- **NTIS** - Leave blank.

Block 12b. Distribution Code.

- **DOD** - Leave blank.
- **DOE** - Enter DOE distribution categories from the Standard Distribution for Unclassified Scientific and Technical Reports.
- **NASA** - Leave blank.
- **NTIS** - Leave blank.

Block 13. Abstract. Include a brief *(Maximum 200 words)* factual summary of the most significant information contained in the report.

Block 14. Subject Terms. Keywords or phrases identifying major subjects in the report.

Block 15. Number of Pages. Enter the total number of pages.

Block 16. Price Code. Enter appropriate price code *(NTIS only)*.

Blocks 17. - 19. Security Classifications. Self-explanatory. Enter U.S. Security Classification in accordance with U.S. Security Regulations (i.e., UNCLASSIFIED). If form contains classified information, stamp classification on the top and bottom of the page.

Block 20. Limitation of Abstract. This block must be completed to assign a limitation to the abstract. Enter either UL (unlimited) or SAR (same as report). An entry in this block is necessary if the abstract is to be limited. If blank, the abstract is assumed to be unlimited.

★U.S.GPO:1993-0-336-043